



FOURIER TRANSFORM RAMAN SPECTROSCOPY AND ITS APPLICATION FOR THE ANALYSIS OF POLYMERIC MATERIALS

GI XUE

Department of Polymer Science and Engineering, Nanjing University, Nanjing 210093, People's Republic of China

CONTENTS

1. Introduction	314
2. Fourier transform Raman spectroscopy	318
2.1. Principle of interferometry	318
2.1.1. Obtaining the interferogram	318
2.1.2. The Fourier transform	320
2.1.3. Resolution	321
2.1.4. Apodization	322
2.1.5. Beam divergence	323
2.1.6. Phase correction	324
2.2. Data processing in FT interferometers	325
2.2.1. Data processing	325
2.2.2. Spectral subtraction	327
2.3. Some essential elements of an FT Raman spectrometer	328
2.3.1. Nd: YAG laser source	328
2.3.2. The use of pulsed lasers in near-IR Raman	329
2.3.3. Detectors and filters	332
2.3.4. Laser safety	336
2.4. Fiber optic probes and microprobes	336
3. The analysis of polymeric materials using FT Raman spectroscopy	339
3.1. General analysis	339
3.1.1. Raman and IR studies of polymers	339
3.1.2. Sampling procedures for polymeric materials	342
3.1.3. Resonance Raman spectroscopy	346
3.2. Crystals and tacticity studies	348
3.3. Liquid crystalline polymer studies	350
3.4. Conjugated conducting polymers	353
3.5. Engineering polymers and composites	357
3.5.1. Nylons	357
3.5.2. Poly(aryl ether ketone) and poly(aryl ether ether ketone)	360
3.5.3. Poly(aryl ether ether sulfone) and poly(aryl ether sulfone)	362
3.6. Elastomers	363
3.6.1. Raw rubbers	364
3.6.2. Sulphur cured elastomers	365
3.6.3. The effect of fillers	366
3.6.4. Raman studies of stretched rubber	367

3.7. Paints	368
3.8. The study of gels	369
3.9. Thin polymer films	369
3.10. Polymerization kinetics studies	372
4. FT Raman spectra of biological materials	373
4.1. Polypeptides and proteins	374
4.1.1. Polypeptides	374
4.1.2. Keratin	375
4.1.3. Photosynthetic proteins	376
4.2. Plant materials	378
4.2.1. Wood tissues	378
4.2.2. Cotton	381
4.3. Membranes	382
4.4. Biomedical applications	383
4.4.1. Bone tissue	383
4.4.2. Teeth	384
4.4.3. Ocular lenses	385
4.4.4. Skin	387
4.4.5. Arteries	388
4.5. Biodegradable polymers	389
4.6. Foodstuffs	389
5. FT surface-enhanced Raman scattering (SERS)	391
5.1. SERS spectra of polymers	391
5.2. Near-infrared FT Raman SERS studies	397
6. Concluding remarks	401
Acknowledgements	401
References	401

1. INTRODUCTION

Raman and infra-red spectroscopy have steadily become increasingly important techniques for characterization of the chemical and physical nature of polymeric materials. Until the 1960s, almost all investigations on polymers were based on information derived from infrared spectra alone. Since the introduction of visible laser sources, Raman spectroscopy has increasingly contributed to the elucidation of polymeric structure.^{1,2} Samples that are pure, transparent and colorless are indeed simple to study and hence relatively economical to investigate. However, polymers that are colored or fluorescent cause real problems and, in many cases, hours of work can be wasted. Although many polymers are not considered to be fluorescent materials, when irradiated with a visible laser, the spectra do show a sufficiently intense level of fluorescence masking the Raman signal. Impure materials and a vast array of pure inorganic and organic materials are fluorescent enough to prevent Raman studies. As a result, even well established laboratories report very low success rates (often less than 20% of the polymer samples submitted). Sample purification can sometimes improve spectral quality. Hence, to an academic laboratory interested in the fundamental aspects of the spectroscopic behavior of polymers, studies can be restricted to carefully purified compounds. However, for intrinsically fluorescent or colored materials, purification is futile, and for the industrial analyst, purification is rarely a viable option. During the 1970s and 1980s other spectroscopic methods such as Fourier transform nuclear magnetic resonance spectroscopy (NMR) and mass

spectrometry joined Fourier transform infra-red spectroscopy as standard techniques for both qualitative and quantitative analysis. Thus it became clear that while visible laser Raman spectroscopy is useful in specialized areas, it is not attractive as a routine analytical method.

In 1964, Chantry, *et al.*³ demonstrated that it was possible to record near infra-red (near-IR) excited Raman spectra by using a Michelson interferometer. However, because of the experimental limitations of the day, this initial paper failed to attract interest. It was not until 1986 that Chase and Hirschfeld published the second paper on this subject.⁴ Laser, interferometer, detector and computer technology had all improved enormously, making it possible to produce good quality Fourier transform (FT) Raman spectra. Several papers then appeared presenting experimental results and discussing the value of near-IR excited FT Raman methods.⁵⁻⁹ These papers presented good FT Raman spectra for a variety of polymers. The use of interferometry and Fourier transform methods enabled data to be collected rapidly and Raman light to be processed more efficiently, enabling high-resolution studies similar to those undertaken with FT IR spectrometers.

The most common excitation frequency for FT Raman spectroscopy is the near-IR Nd:YAG laser source at $1.064\text{ }\mu\text{m}$ (939.8 cm^{-1}). Laser excitation in the near-IR region generally precludes electronic absorptions, thus leading to a nearly complete elimination of photolytic sample decomposition and fluorescence interference. In addition, the use of a Michelson interferometer for performing Raman spectroscopy offers the benefits of superior spectral resolution, frequency accuracy and relatively high throughput compared with a dispersion-based spectrometer. These developments lifted the experimental restrictions which had hindered Raman spectroscopy for so long, and FT Raman was set to join FT IR as a truly complementary analytical technique.

Most industrial polymer samples exhibit very strong fluorescence, and so vibrational analysis has been confined to IR spectroscopy. The greatest achievement of FT Raman spectroscopy is the removal of this fluorescence. In some cases, the effects are quite dramatic. The Raman spectra of a highly fluorescing dye shown in Fig. 1 were recorded with conventional Raman using different

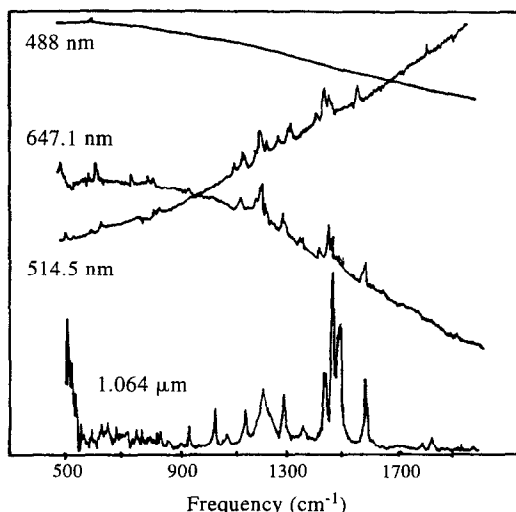


Fig. 1. Raman spectra of a cyanine dye recorded at different wavelengths throughout the visible and into the near-IR region.¹⁰

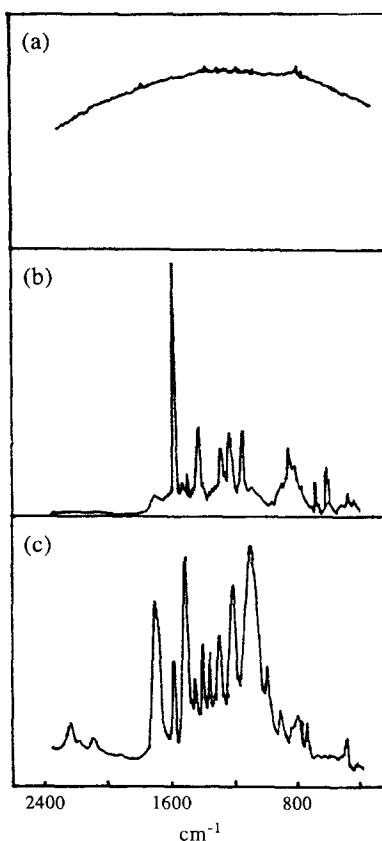


Fig. 2. (a) Normal Raman spectrum of polyurethane elastomer. (b) FT Raman spectrum of polyurethane elastomer. (c) FT IR spectrum of a polyurethane elastomer.¹⁷

exciting sources and with FT Raman spectroscopy.¹⁰ The resulting spectra suggest that the effort required to remove the fluorescence from the Raman scattering is rewarding. To date, good-quality FT Raman spectra have been reported for fluorescent dyes,^{10–12} industrial polymers,^{13,14} photolabile organometallic compounds¹⁵ and some biological molecules.^{13,16} However, potential applications of this newly developed technique for the non-destructive analysis of various polymeric materials remain largely unexplored.

The advantages of the FT Raman technique as applied to polymer samples are well illustrated by the Raman and IR spectra of a polyurethane elastomer, as shown in Fig. 2.¹⁷ The fluorescent background observable in the conventional Raman spectrum due to the presence of an impurity resulting from the synthetic procedure completely obscures any Raman bands. Figure 2(b) shows the FT Raman spectrum of the polyurethane, which required a collection time of 20 min. Figure 2(c) shows the IR spectrum of the same material, this spectrum being run as a thin film cast from a melt of the sample. Polyurethane elastomer shows very strong fluorescence under visible excitation in Fig. 2(a). But there is no evidence of fluorescence under near-IR excitation. In most cases the goal of fluorescence minimization is achieved. But it is still far from true to say that FT Raman is entirely fluorescence-free for every polymer sample.

Figure 3 shows the comparison of an FT Raman spectrum and an FT IR spectrum recorded

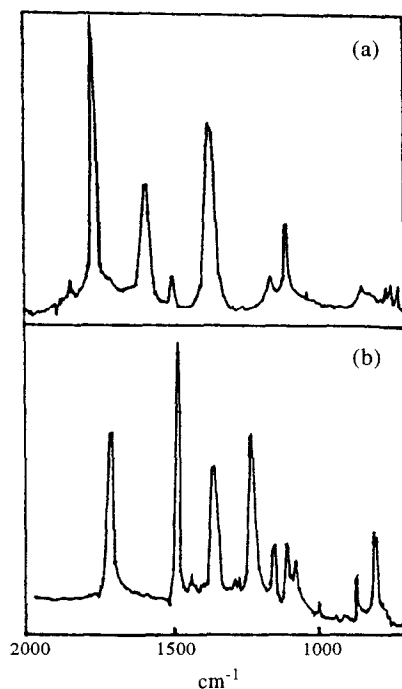
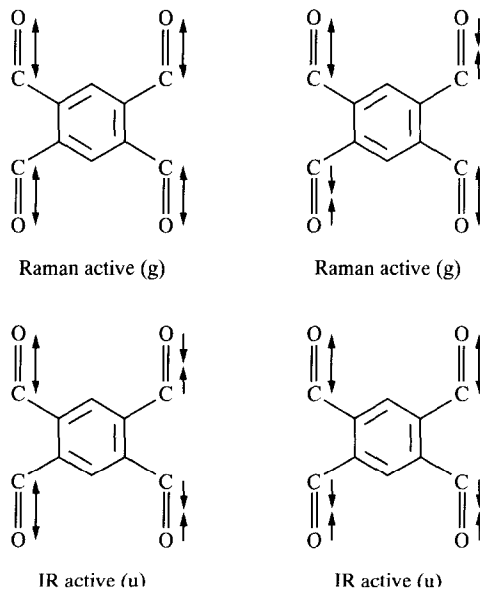


Fig. 3. (a) FT Raman spectrum of a polyimide polymer. (b) FT IR spectrum of apolyimide polymer.¹⁷

for a piece of polyimide-based polymer.¹⁷ This example highlights the complementary information given by the two FT techniques. As there are four carbonyl groups, one might expect to see four separate bands of C=O stretching modes. In this case, the four carbonyls are grouped around a center of symmetry (the benzene ring). The Raman- and IR-active modes of these C=O are illustrated schematically as follows:



One can observe bands due to antisymmetric (u) modes in the IR spectrum and bands due to symmetric (g) vibrations in the Raman spectrum.

It has become clear that FT Raman spectroscopy is extremely versatile and can tackle a diverse range of analytical problems. Many multinational instrument manufacturers now offer FT Raman products. Since FT Raman and infra-red spectrometers share the same basic interferometer, some commercial instruments offer both spectroscopies on a combined bench. In the future, there will be a massive expansion of the applications of the Raman method for the analysis of polymeric materials.

2. FOURIER TRANSFORM RAMAN SPECTROSCOPY

2.1. *Principle of interferometry*

2.1.1. *Obtaining the interferogram*

Figure 4 shows a schematic diagram of an FT Raman spectrometer and a simple Michelson interferometer which is the heart of an FT Raman spectrometer. The Michelson interferometer, as shown in Fig. 4(b), consists mainly of a beam splitter, two mirrors (**M1** and **M2**) and a means of altering the distance between one of the mirrors, **M1**, and the beam splitter. The radiation which enters the interferometer is split by the beam splitter into two beams of equal intensity (ideally). One beam is transmitted to mirror **M1** and the other beam is reflected to mirror **M2**. After reflection at **M1** and **M2**, the two beams are recombined at the beam splitter; again, half of the light is reflected and half is transmitted. The overall effect is that half the light reaches the detector. Thus, the theoretical maximum efficiency of an ideal interferogram is 50%.

When the two mirrors, **M1** and **M2**, are at equal distances from the beam splitter, the path of the light beams are identical. Under these conditions, all wavelengths of radiation striking the beam splitter after reflection combine to produce a maximum flux at the detector, and generate a center burst. If **M1** is moved a distance of one-fourth of the wavelength ($\lambda/4$) of the incident light, then the ray of light that is reflected from **M1** travels an extra distance of $\lambda/4$ in each direction. Hence, on arrival back at the beam splitter, the ray has traveled an additional $\lambda/2$. Thus, the rays from **M1** and **M2** are 180° out of phase; they recombine destructively and no light reaches the detector. This will be true for all values of $n\lambda/4$ (n is odd). At all other distances the two rays are not out of phase and signals will be observed at the detector. The energy $I(\delta)$ reaching the detector is:

$$I(\delta) = 2\epsilon I_0 [1 + \cos(2\pi\delta\bar{\nu})] \quad (1)$$

where I_0 is the intensity of incident light, δ is the path difference and $\bar{\nu}$ is the wavenumber. At the detector this would be registered as a constant (d.c.) component [the first term of eqn (1)], and a modulated (a.c.) component [the second term of eqn (1)]. Only the latter contains useful spectroscopic information and is known as the interferogram. When an ideal monochromatic source passes through the interferometer and the optical delays varied, the signal detected is a cosine wave, as shown in Fig. 5(a). Now consider the signal obtained when two ideally monochromatic sources of different wavelength pass through the interferometer. The signal

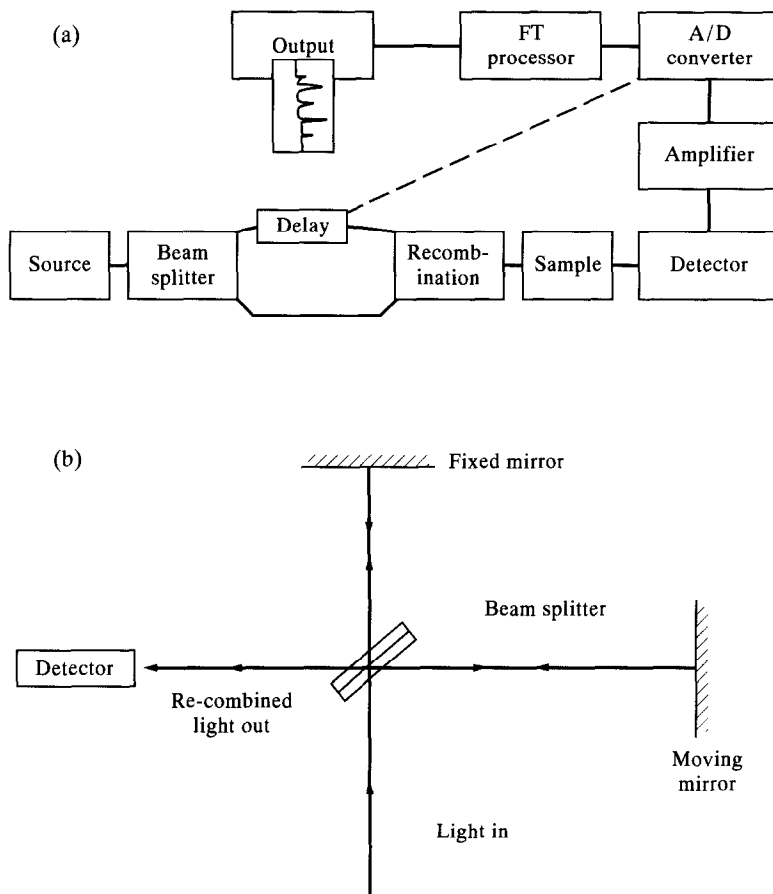


Fig. 4. (a) Schematic diagram of FT Raman spectrometer; (b) Simple Michelson interferometer.

is the sum of the signal that would be obtained for the two sources if they were analyzed separately, as shown in Fig. 5(b). As the source becomes increasingly polychromatic, the beat frequency becomes longer and longer. Thus, when a polychromatic source illuminates the interferometer, the beat frequency is also long and we observe only a single characteristic burst, as shown in Fig. 5(c). This trace is an interferogram and the point of maximum intensity is known as the "center burst". This occurs when the optical path difference is zero.

In the general case where the source is a continuum, each frequency contributes a term of the type in eqn (1), hence the total intensity of interest at the detector is given by:

$$I(\delta) = \int_{-\infty}^{+\infty} C(\bar{\nu}) \cos(2\pi\delta\bar{\nu}) d\bar{\nu}, \quad (2)$$

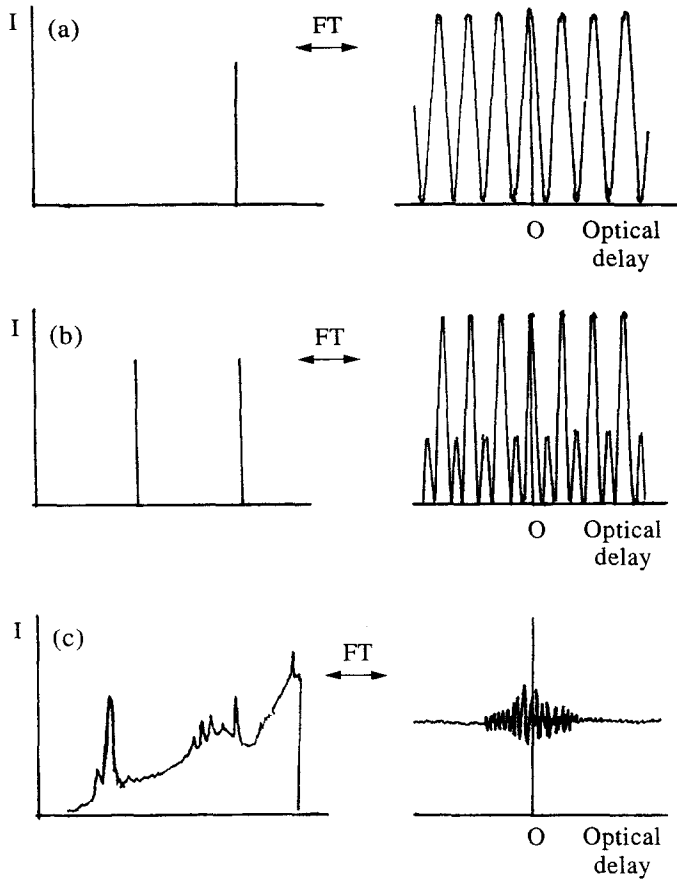


Fig. 5. Interferogram produced by (a) a monochromatic source; (b) two monochromatic sources; (c) a polychromatic source.

with $C(\bar{\nu})$ defined as

$$C(\bar{\nu}) = 0.5R(\bar{\nu})I(\bar{\nu}), \quad (3)$$

where $R(\bar{\nu})$ is the frequency-dependent response of the interferometer. This is a composite of a number of factors, but is primarily determined by the beam splitter, the detector and the electronics. $I(\bar{\nu})$ is the intensity at each frequency, hence $C(\bar{\nu})$ is the observed spectrum. The problem is to obtain $C(\bar{\nu})$ from $I(\delta)$.

2.1.2. The Fourier transform

Equation (1) is an example of the general type:

$$F(x) = \int_{-\infty}^{+\infty} G(\bar{\nu}) \cos(2\pi\bar{\nu}x) d\bar{\nu} \quad (4)$$

where $F(x)$ is defined as the cosine Fourier transform of $G(\bar{\nu})$. Similarly:

$$G(\bar{\nu}) = \int_{-\infty}^{+\infty} F(x) \cos(2\pi\delta\bar{\nu}) dx, \quad (5)$$

and $F(x)$ and $G(\bar{\nu})$ are said to form a cosine Fourier-transform pair. A comparison of eqns (1) and (4) shows that $I(\delta)$ and $C(\bar{\nu})$ also form a cosine Fourier-transform pair, hence:

$$C(\bar{\nu}) = \int_{-\infty}^{+\infty} I(\delta) \cos(2\pi\delta\bar{\nu}) d\bar{\nu}. \quad (6)$$

This means that the spectral distribution (the spectrum, $C(\bar{\nu})$) can be obtained from the a.c. signal at the detector by a cosine Fourier transform. Equation (6) is an important result because it forms the basis of interferometric spectroscopy. The reasons for this may be seen by considering what is stated in eqns (1) and (6); every point in the interferogram $I(\delta)$ contains information about every frequency in the spectrum. This is the origin of the multiplex advantage of Fourier transform spectroscopy.¹⁸

The overall effect of the Fourier transform is to obtain a wavelength-dispersed spectrum without having to physically disperse the light. The absence of slits or gratings leads to a throughput advantage of interferometers over dispersive instruments. Together, the two factors give a major improvement in the signal-to-noise ratio over that obtainable from a dispersive instrument under equivalent conditions, i.e. the same laser power at the sample, detector, measurement time, resolution and collection efficiency of scattered light.

2.1.3. Resolution

Equation (6) in its present form has a number of implications. Firstly, the limits of integration are from $-\infty$ to $+\infty$. But in practice the mirror is moved from a position $-L$ to $+L$. This has important consequences for the resolution of the instrument. Secondly, eqn (6) is symmetric about $\delta = 0$; in reality, this is not usually the case. Given that the moving mirror is only translated between $\pm L$, eqn (6) could be rewritten with the limits of integration as $-L$ to $+L$. It is more convenient to define a function $A(\delta)$ such that:

$$A(\delta) = \begin{cases} 1 & (-L \leq \delta \leq +L) \\ 0 & \text{elsewhere} \end{cases} \quad (7)$$

Hence eqn (6) becomes:

$$C(\bar{\nu}) = \int_{-\infty}^{+\infty} I(\delta)A(\delta) \cos(2\pi\delta\bar{\nu}) d\bar{\nu}. \quad (8)$$

The resolution ($\Delta\bar{\nu}$ in cm^{-1}) of the interferometer depends inversely on the distance that the moving mirror is translated:

$$\Delta\bar{\nu} = 1/L. \quad (9)$$

The critical parameter is the “relative resolution” defined as:

$$\frac{\text{instrument resolution}}{\text{full width at half height of the band}}$$

The effects of measuring a band with different values of relative resolution are shown in Fig. 6 for a synthetic 100% Lorentzian band. At small values of the relative resolution, the band is

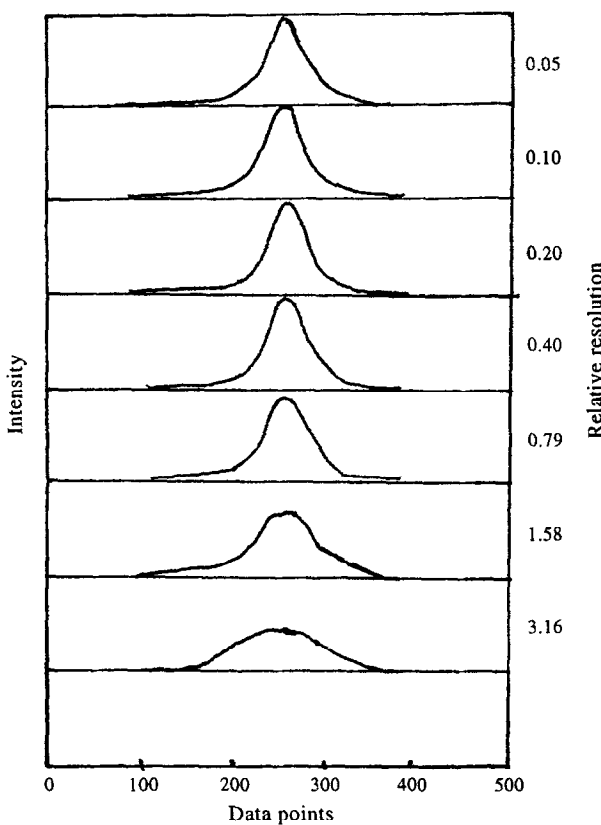


Fig. 6. Effect of boxcar apodization and different values of relative resolution on the shape of a pure Lorentzian line.

accurately represented in terms of its width, height and shape. At larger values, it becomes progressively more distorted until, at sufficiently large values, the shape is determined by the instrument lineshape.

2.1.4. Apodization

An important consequence of eqn (8) is $A(\delta)$, the function that is introduced into the expression for the interferogram. By choosing a different form for $A(\delta)$, it is possible to change the instrument lineshape. Many different functions could be used to replace $A(\delta)$ in eqn (8). For mid-IR FT spectroscopy, the effect of the choice of the apodization function on the amplitude of the sidelobes, the width of the bands, and the bandshape have all been considered by a number of authors.¹⁹⁻²¹ The commonly used apodization functions are boxcar, triangular, Happ–Genzel, cosine, Norton–Beer and Blackman–Harris.²² The effects of finite resolution and apodization on FT Raman spectra should be very similar to those seen for FT IR spectra. An experimental study of the ν_1 band of KMnO_4 as a function of relative

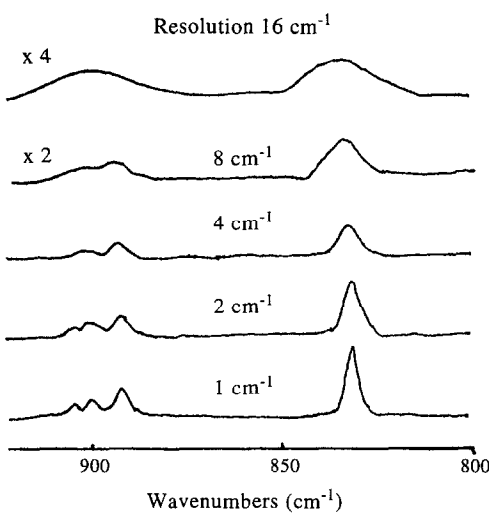


Fig. 7. The effect of finite resolution and Norton-Beer apodization on the $\nu/7$ and $\nu/3$ bands of KMnO_4 .²²

resolution has confirmed that this is the case.²³ Practical implications are illustrated in Fig. 7 for the case of the Norton-Beer apodization function. In the solid state, the threefold degeneracy of the 914 cm^{-1} (ν_3) band of KMnO_4 is lifted by the site symmetry.²⁴ It can be seen that as the resolution is degraded (numerically larger), the triplet structure of the band is progressively lost as the bands broaden. At relative resolution values greater than 3, the triplet has merged into a single peak. In fact, curve fitting of the top spectrum in Fig. 7 is best carried out by treating the composite envelope as a single band even though it is in reality a triplet.

2.1.5. Beam divergence

Up to now it has been implicitly assumed that the light beam through the interferometer is perfectly collimated. However, it is only possible to obtain a perfectly collimated light beam from a point source; thus, the beam from any real source exhibits some divergence. The reason why this is important may be seen by considering a diverging beam in the interferometer. The central light ray and the light ray from the edge of the beam will travel different distances inside the interferometer. The different distances traveled will result in the rays having a slightly different phase and this will generate interference when the two rays are recombined at the beam splitter, with a consequent reduction in the amplitude of the signal. The beam divergence can be controlled by placing an aperture at an image of the source inside the interferometer.²⁵

The necessity to control beam divergence has the important consequence that, as the resolution is increased (numerically smaller), the throughput of the spectrometer is reduced and hence the signal-to-noise ratio per unit time is also reduced. The effect of throughput and resolution has been discussed previously.²⁶

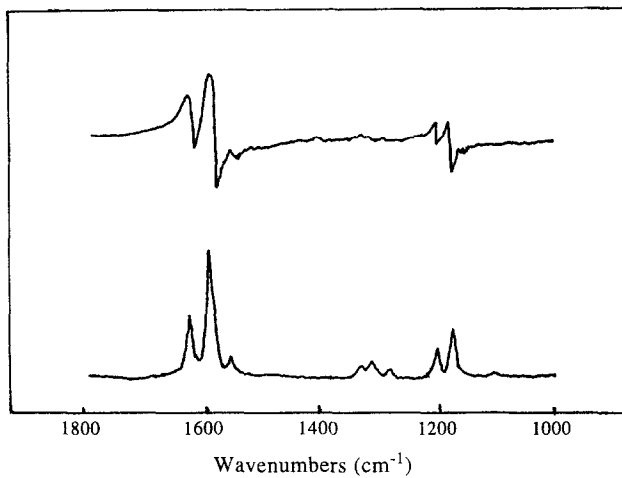


Fig. 8. Effect of phase correction in the FT Raman spectrum of 1,4-bis(2-methylstyryl) benzene. Top: spectrum computed without phase correction; bottom: phase corrected spectrum.²²

2.1.6. Phase correction

Equation (6) is symmetric about $\delta = 0$. In practice this is rarely, if ever, true. There are three reasons for this. Firstly, none of the points where the interferogram was sampled may have coincided exactly with the point of zero path difference. Secondly, the interferogram may be intrinsically asymmetric because of wavenumber-dependent phase delays in the detection system or the high-frequency electronic filters. Thirdly, only a single-sided interferogram may be collected. An additional term has to be introduced into eqn (2):

$$I(\delta) = \int_{-\infty}^{+\infty} C(\bar{\nu}) \cos[2\pi\delta - \phi(\bar{\nu})] d\bar{\nu}, \quad (10)$$

where $\phi(\bar{\nu})$ is the wavenumber-dependent phase delay introduced by any of the factors. The effect of the phase delays is to introduce sine terms into the interferogram. Equation (10) may be rewritten as:

$$I(\delta) = \int_{-\infty}^{+\infty} C(\bar{\nu}) \exp(2\pi\delta\bar{\nu}) d\bar{\nu}. \quad (11)$$

Equation (11) is half of a complex Fourier-transform pair; $C(\bar{\nu})$ may be obtained from $I(\delta)$ by the inverse Fourier transform:

$$C(\delta) = \int_{-\infty}^{+\infty} I(\delta) \exp(-2\pi i\delta\bar{\nu}) d\bar{\nu}. \quad (12)$$

The spectrum that results from eqn (12) displays phase errors which give the bands a derivative-like appearance; an example is shown in Fig. 8. The phase errors have caused the spectrum to lie in the complex plane, rather than along the real axis. A phase correction is applied in order to rotate it back to the real axis. This may be done in a number of ways. One

method is to ignore the phase error altogether. This can be done if the interferogram is symmetric. This method has the virtue of simplicity, but it has a number of drawbacks.²²

The true spectrum $S(\bar{\nu})$ and the complex spectrum $C(\bar{\nu})$ are related by the phase angle $\phi(\bar{\nu})$:

$$C(\bar{\nu}) = S(\bar{\nu}) \exp[i\phi(\bar{\nu})]. \quad (13)$$

Rearranging eqn (13) gives:

$$S(\bar{\nu}) = Re(\bar{\nu}) \cos \phi(\bar{\nu}) + Im(\bar{\nu}) \sin \phi(\bar{\nu}). \quad (14)$$

It may be shown that the phase angle $\phi(\bar{\nu})$ is given by:²⁷

$$\phi(\bar{\nu}) = \arctan[Re(\bar{\nu})/Im(\bar{\nu})]. \quad (15)$$

Equation (15) provides a way of obtaining the phase angle as a function of $\bar{\nu}$. This forms the starting point for two major phase correction algorithms developed by Mertz²⁸ and Forman *et al.*²⁹ The two techniques differ in that the phase correction is carried out in the frequency domain in the Mertz method and in the Fourier transform domain in the Forman method. In essence, the Mertz method calculates $S(\bar{\nu})$ from eqn (14). The Forman method is based on the generation of a phase-corrected interferogram, $P(\delta)$:

$$P(\delta) = \int_{-\infty}^{+\infty} I(\delta') \phi(\delta - \delta') d\delta. \quad (16)$$

A cosine Fourier transform is then sufficient to generate the true spectrum. The process of phase correction is discussed in mathematical detail elsewhere.³⁰

The problem with FT Raman spectra is that both of these methods require the determination of $\phi(\bar{\nu})$ by the extraction of a symmetrical interferogram from the total interferogram. The problem is circumvented in one of two ways: either magnitude spectra are calculated or a spectrum is recorded using a white light source. The phase correction determined from it (using either the Mertz or Forman method) is stored and subsequently used to phase-correct the FT Raman spectra.

2.2. Data processing in FT interferometers

2.2.1. Data processing

The mathematical process which is used to turn the interferogram (in the time domain) into the spectrogram (in the frequency domain) is called the Fourier transform. Thus, the interferogram and stick spectra shown in Fig. 5 are in fact Fourier transforms of each other. This process is carried out by using a computer algorithm. For n data points, the number of calculations required varies as n^2 . In 1965, Cooley and Tukey developed an algorithm such that the number of calculations required varies as $n \log(n)$.³¹ This results in a large reduction in computation time at realistic values of n , and is known as fast Fourier transformation (FFT); it is used on all commercial instruments.^{32,33}

Radiation entering the interferometer is analyzed by recording the intensity trace versus optical delay, digitizing and transforming the spectrogram from the interferogram. The interferogram is sampled at regular intervals and digitized by an analog-to-digital (A/D) converter. The number of data points recorded is related to the length of the interferogram and the periodicity of data sampling which is triggered by the use of a reference laser. Two

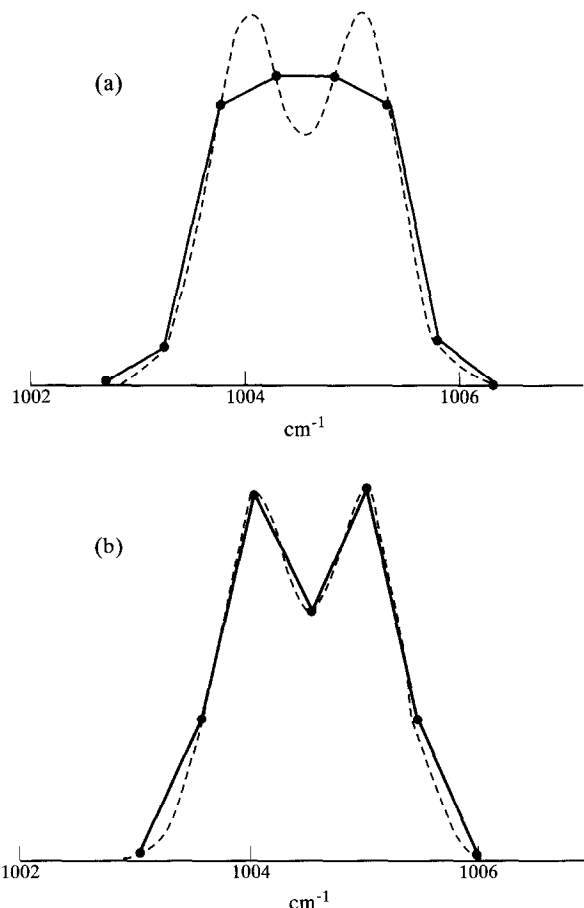


Fig. 9. Two overlapping bands showing the effect of data-point position. In both (a) and (b) the dashed line shows the true profile and the solid line shows the digitized spectrum.

data points in the main interferogram are collected for every cycle of the reference laser interferogram. The wavelength of the reference He-Ne laser is 632.8 nm, so that for every centimetre of optical path difference an instrument can collect 31 606 data points if it samples two data points per cycle of the reference laser interferogram.

The FT process cannot yield more data points than those input. In practice, the number of data points in the spectrogram is half that in the interferogram. Thus, unlike a conventional dispersive instrument, the spectrum obtained is discrete rather than continuous. Interferometer-based spectrometers produce a finite data-point density in the computed spectrogram. In the previous example, there would be 15 803 data points in the spectrogram. For a 4000 cm^{-1} spectral range, this corresponds to 4 data points per wavenumber. The spectrum produced is actually a histogram with straight lines drawn between the data points. For most purposes this is not a problem but, when small regions of a spectrum are expanded, the

discrete nature of the data becomes obvious, particularly at coarse data point pitching, as shown in Fig. 9. Figure 9 shows two overlapping bands separated by 1 cm^{-1} . To resolve this profile, a bare minimum of two data points per wavenumber is required, if they happen to fall in the right place. Thus it is clear that many more data points per wavenumber are needed to define band profiles adequately. This then brings us to frequency accuracy. The shape of the calculated interferogram is dependent on the alignment of the radiation and the He–Ne laser as they pass through the interferometer. As the radiation is moved off-axis, these two beams will no longer follow exactly the same path, and will experience slightly different optical delays. This results in the frequency of spectral bands shifting in the spectrogram by as much as 2 cm^{-1} in most commercial instruments. If the user records IR absorption spectra, and never varies the manufacturer's alignment, then there should be no frequency errors. FT Raman instruments may suffer from absolute frequency inaccuracies, but because any displacement will be consistent across the spectrum, the frequency shifts measured should be correct.

The peak-picking routines which have been built into the software of many spectrometers list the frequencies of spectral bands. For each band, these quote the frequency of the data point which has the greatest intensity. They then display this "peak" frequency with quite good precision. In a well aligned interferometer the frequency of the data points is known very accurately. However, as seen in Fig. 9, unless this data point coincides exactly with the real band head, the accuracy of the "peak" frequency quoted is meaningless. Thus, peak-picking routines are a useful indication of band position, but it must always be remembered that it is the data point rather than the band position that is being quoted. When it is desired to measure small band shifts it is, therefore, essential to have high density of data points in the spectrogram. There are several methods of increasing the data-point density, such as scanning the movable mirror further and collecting more data points in the interferogram, and zero filling techniques.³³

The interferogram, in theory, continues out to an infinite distance on either side of the center burst. Therefore, in a practical spectrometer, the interferogram must be truncated. The problem associated with the truncation of the interferogram is the accurate representation of both the intense center burst and the much weaker side features [see Fig. 5(c)]. In order that both can be recorded meaningfully, high-resolution A/D conversion is essential. Usually, 16-bit systems are used, so that the center burst can be up to almost 33 000 times greater than the weakest feature digitized, whilst still accurately depicting both.³⁴

2.2.2. Spectral subtraction

Since the spectral data can be stored on a computer data station in an FT Raman spectrometer, the manipulation and analysis of spectra are considerably simplified. This improvement facilitates spectral subtraction and the ready comparison of Raman and IR data. Figure 10 illustrates FT Raman spectra of undyed and dyed synthetic fibers, and their subtraction. The difference spectrum indicates clearly a dye.

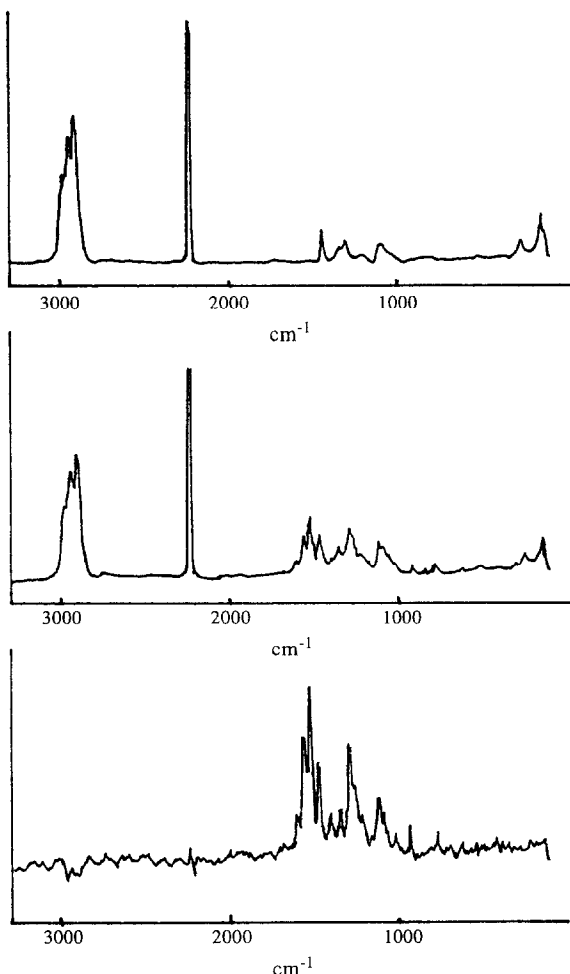


Fig. 10. FT Raman spectra of synthetic fibers. Top: not dyed; middle: dyed red; bottom: subtraction showing dye. 100 scans, resolution 4 cm^{-1} , 500 mW. (from Bruker FT-IR)

2.3. Some essential elements of an FT Raman spectrometer

2.3.1. Nd:YAG laser source

A laser source, detector and filter are the basic components of an FT Raman spectrometer. Presently, almost all of the commercial FT Raman instruments use Nd:YAG laser sources. The stability of the laser source is important in order to get a low-noise spectrum. The effect of a variation in source intensity is to multiply the interferogram by a completely random noise function. This then transforms to give spikes and increased noise in the spectra. Fortunately, the instability occurs at the same frequency of the main electricity supply and its first few harmonics. This is a much lower frequency than the beat of the Raman interferogram, and

fortunately most of the spurious effects of laser instability appear outside the FT Raman range in the frequency domain. However, if the interferometer scanning speed and hence the data acquisition rate are reduced, laser instability can be far more problematic. In present FT Raman spectrometers, the quality of the spectra obtained is constrained by the inherent noise of the detection system. As detectors are improved, another element of the spectrometer will limit its performance, and this is most likely to be the stability of the laser source. The fluctuation in the output of diode-pumped Nd:YAG lasers is very much less than that of their discharge-lamp-pumped predecessors, often better than 0.1% RMS. These devices are much smaller than the lasers traditionally used and they do not require water cooling or bulky power supplies.

The xenon discharge lamps used to pump current Nd:YAG lasers produce a series of emission lines in the FT Raman range. The sample under study will either reflect or Raleigh scatter these emissions, and spurious lines will be produced in the spectrum which can easily be mistaken for real Raman bands. For this reason it is essential to modulate the output from the laser by using either a laser premonochromator or a notch filter. Similar near-IR lines are also emitted by the He-Ne laser used to frequency-calibrate FT Raman instruments. Unless a stable filter is placed in front of the He-Ne laser, massive spikes can appear in the FT Raman spectra. Sharp emission lines will also produce sidelobes, and the very sharp bands found in the FT Raman spectra of gases will inevitably cause the same problem.

2.3.2. *The use of pulsed lasers in near-IR Raman*

It has been estimated that, using near-IR excitation, industrial laboratories can routinely record spectra from 90% of samples using the technique of FT Raman spectroscopy. Of the remaining 10% of samples, a few are strongly fluorescent, some absorb the exciting radiation which is strongly re-radiated as heat, and the remainder tend to degrade due to their thermal sensitivities and/or photo sensitivities. The use of Q-switched pulsed lasers in near-IR FT Raman spectroscopy can give significant increases in signal-to-noise ratios over continuous-wave measurements made using the same average laser power. It is also shown that when a thermal background is present, the use of pulsed excitation can greatly reduce its effects and, under certain circumstances, can allow it to be subtracted completely.

The principle behind the pulsed FT Raman experiment was recently described by Cutler *et al.*³⁵ In the pulsed mode, the excitation laser only operates while the instrument is scanning and is triggered immediately prior to the A/D converter sampling the detector signal. A sample without background will produce a detector signal consisting only of a set of narrow pulses broadened by the response time of the detector system. By adjusting the A/D converter sampling point to coincide with the maxima of the Raman signal, a digitized interferogram is produced whose envelope is the same as that recorded using continuous wave (CW) excitation. However, in the case of pulsed excitation, the amplitude of the interferogram of the Raman emission is inversely proportional to the time constant of the detector system. Hence, for short pulses, the contribution of the Raman signal to the entire interferogram, and hence to the spectrum, can be significantly enhanced.

In order to demonstrate the signal-to-noise ratio advantage arising from the use of pulse excitation, the laser power was reduced until a single CW scan of a poly(ethylene terephthalate) sample contained no reliable spectral features. The spectrum is shown in Fig. 11(a), recorded with 7 mW of a CW 1.064 μm Nd:YAG near-IR laser. The spectrum in Fig. 11(b) is

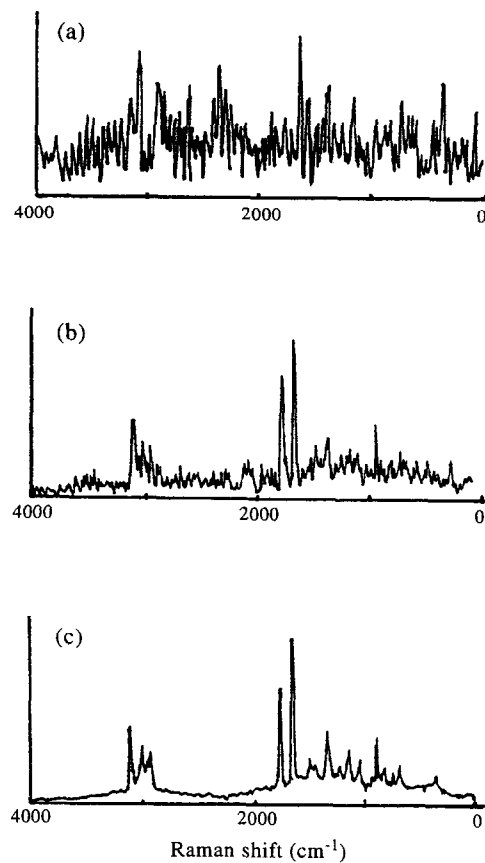


Fig. 11. Raman spectra of poly(ethylene terephthalate) sheet showing the SNR enhancement obtained when using pulsed excitation. The spectra were recorded using a Ge detector at 77 K, 16 cm^{-1} resolution and (a) one scan with 7 mW of CW $1.064\text{ }\mu\text{m}$ Nd:YAG, (b) and (c) one scan and 64 scans, respectively, with 7 mW excitation Q-switched at 3 kHz.³⁵

a single scan of the same sample at equivalent laser power but recorded with the excitation Q-switched, the other conditions remaining the same. The improvement in the signal-to-noise ratio is striking. For comparison, Fig. 11(c) demonstrates that more scans can further enhance the signal-to-noise ratio.

The improvement in the signal-to-noise ratio is of great benefit in cases where there is no strong background present. To illustrate this point, suppose the A/D converter is sampling at 5 kHz and that the Raman signal from the detector-preamplifier combination is 2 ms wide. If in each case the sample receives the same number of photons, per integration period, the peak level of the Raman signal from the pulsed experiment will be potentially 100 times larger than that using CW excitation. Any constant or slowly changing background signal is not enhanced. But, in order to cope with the faster signals arising from pulsed operation, the detector system must have an increased bandwidth. Unfortunately, this increases noise ten-

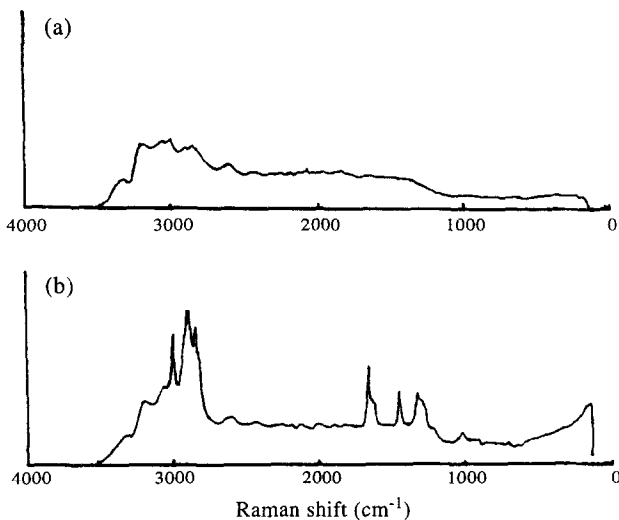


Fig. 12. Simulated spectra of a hot sample of a brown plastic foam using CW (a) and pulsed excitation (b) with the Q-switched laser at 3 kHz.³⁵

fold. So, in this example, operating in the pulse near-IR mode would give an overall tenfold enhancement in the signal-to-noise ratio over the continuous wave mode. In cases of strong background, it can be reduced or even completely removed.

There is a great potential to reject strong background using pulsed laser FT Raman. To illustrate this point, a brown plastic foam was placed at the sample position of the instrument

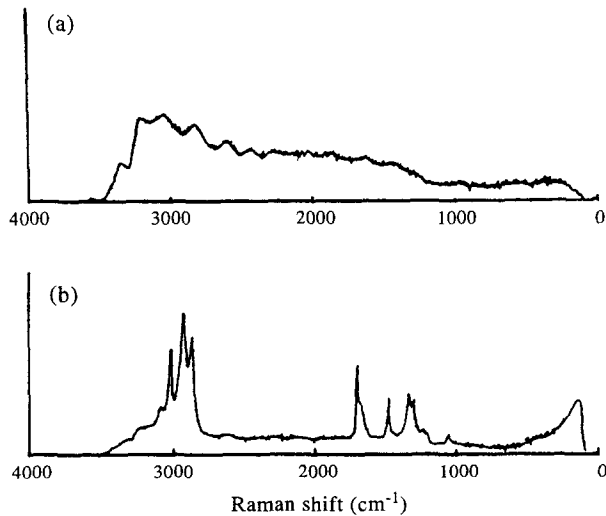


Fig. 13. (a) Spectrum recorded using the condition in Fig. 46(b) but with the ADC sampling time delayed until after the Raman pulsed had decayed; (b) spectrum obtained by subtracting Fig. 47(a) from Fig. 46(b).³⁵

and a small amount of light from a torch was allowed to enter the interferometer, inducing a thermal background. Figure 12 shows the Raman spectrum of the plastic foam recorded with both CW and pulsed excitation. In the former case, the Raman bands are present only as small features in the background. In the latter spectrum, the enhancement of the Raman lines is clearly evident.

If the A/D converter sampling is delayed until after the Raman pulse has ended, it becomes possible to obtain a spectrum of the background. This can then be subtracted from the normal pulsed spectrum to give Raman lines free from the background interference. The Raman spectrum shown in Fig. 13(a) was recorded using the same sample and with the same conditions as in Fig. 12(b), but with the sampling time delayed until after the Raman pulse had ended; it shows just the thermal emission. The spectrum shown in Fig. 13(b) was obtained by subtracting Fig. 13(a) from Fig. 12(b) and is essentially identical to that recorded from the plastic foam with the torch turned off. Clearly, this method of background subtracting seems to be effective.

2.3.3. Detectors and filters

The performance characteristics of two kinds of detector are illustrated in Fig. 14. The InGaAs detector operates to slightly longer wavelengths than the cooled Ge device, but it is noisier.

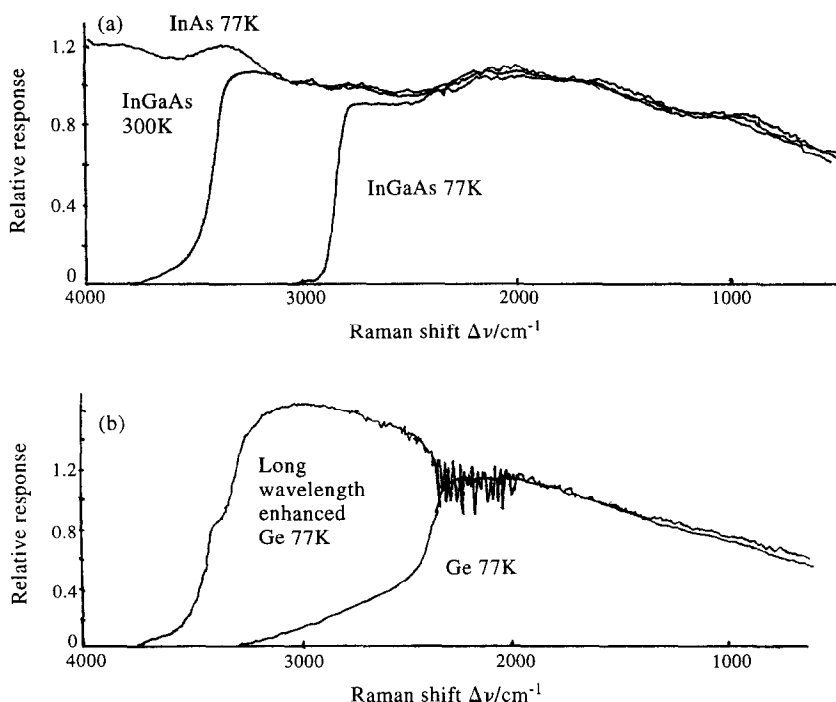


Fig. 14. Characteristics of different detectors suitable for FT Raman spectroscopy: (a) InAs at 77 K, InGaAs at 77 K; (b) an extended-range Ge detector at 77 K compared with a Judson Ge detector at 77 K. Detector responses normalized to 1.3 m.⁴⁶

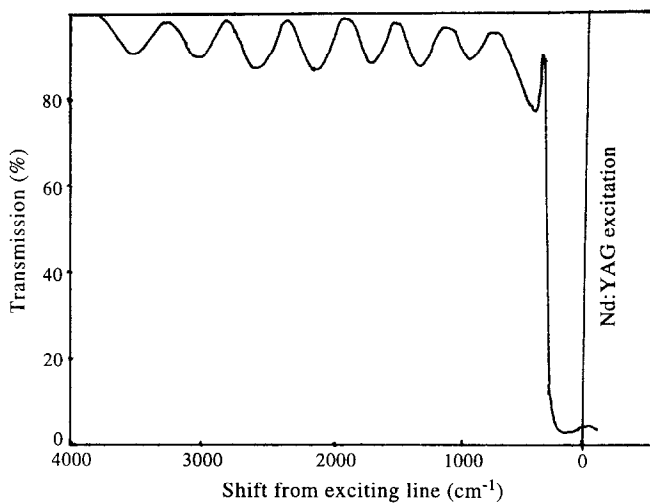


Fig. 15. Transmission characteristics of a Barr Associates multilayer rejection filter as a function of wavenumber shift from Nd:YAG excitation line.

In the mid 1980s, in Chase's instrument, the collected light was almost entirely composed of elastically reflected and scattered radiation at $1.064\text{ }\mu\text{m}$. The Raman contribution was small. To remove the laser radiation, there must be efficient rejection at that frequency. The filter system must "cut in" as steeply as possible to allow the user to approach the laser

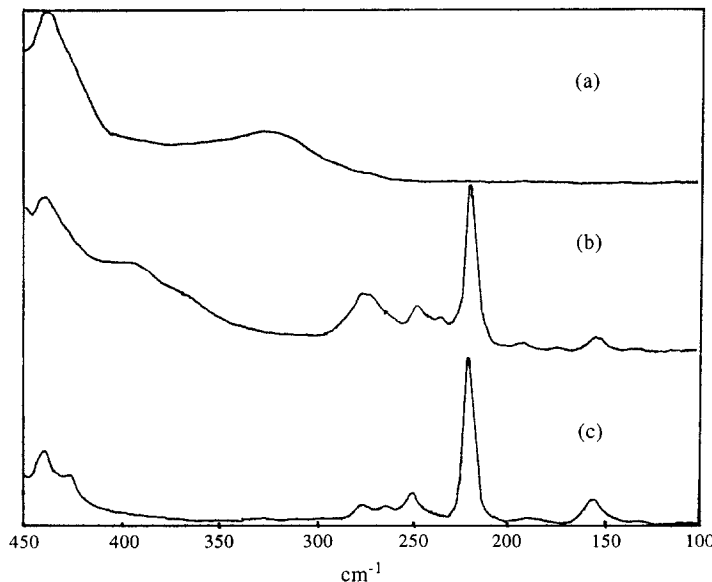


Fig. 16. FT Raman spectra of sulphur recorded with the rejection filters tilted with respect to the optical axis at (a) 0° , (b) 6° , (c) 13° . Uncorrected data.³⁴

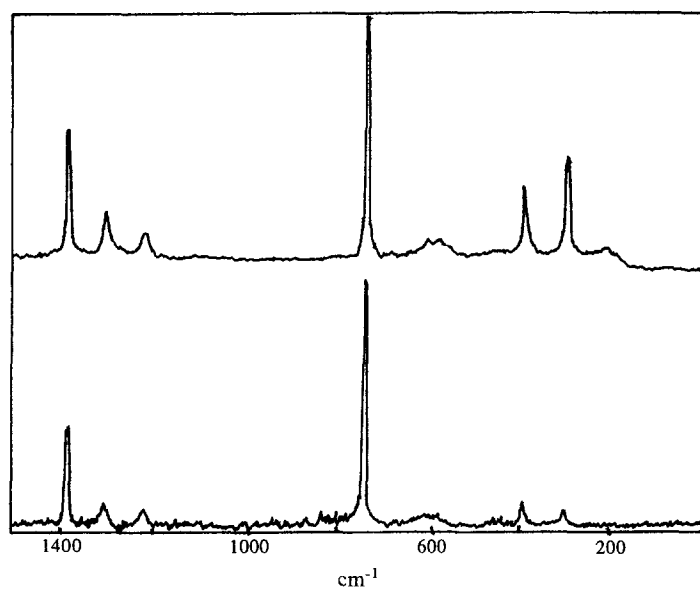


Fig. 17. Uncorrected FT Raman spectra on PTFE (polytetrafluoroethylene) recorded by different instruments using different detectors and filters.³⁴

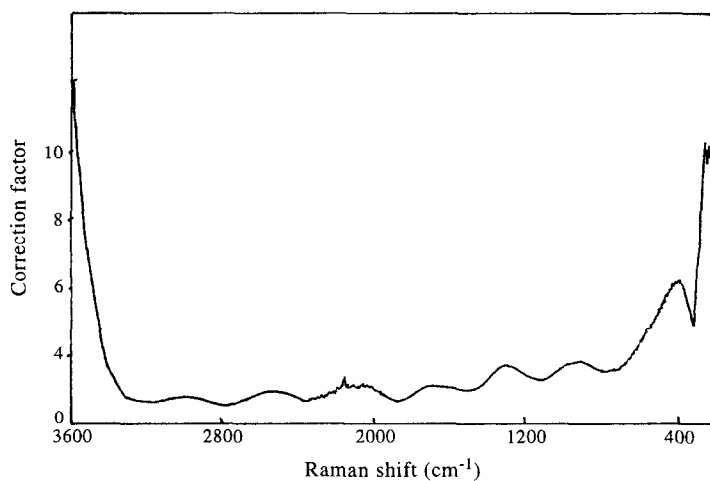


Fig. 18. Typical correction function used to compensate for the instrumental sensitivity curve.

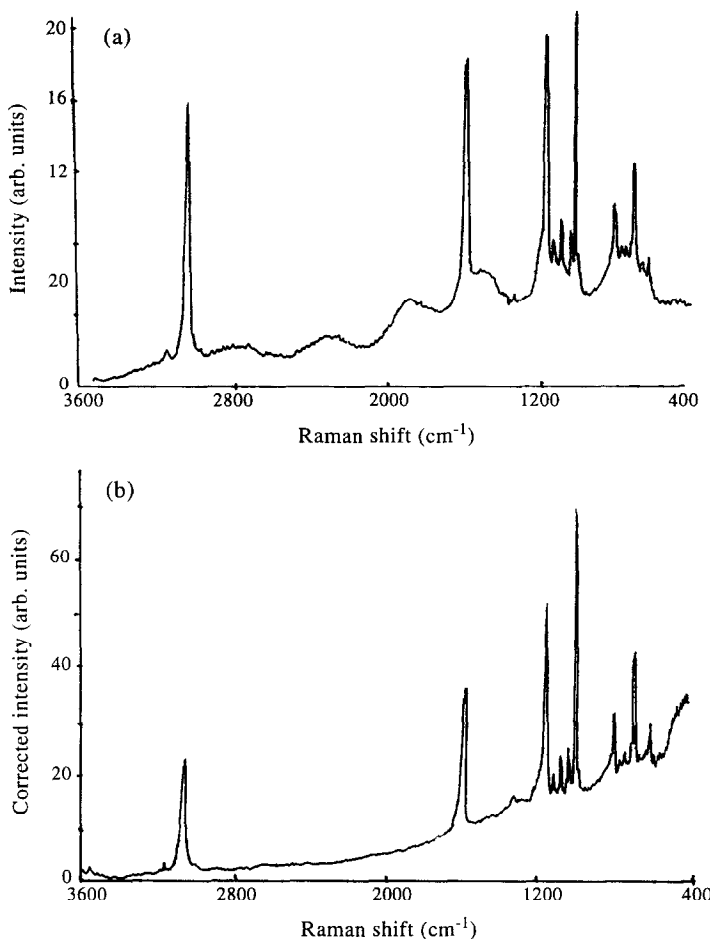


Fig. 19. (a) Raw uncorrected FT Raman spectrum of PEES/PESES copolymer showing oscillations due to filter characteristics. (b) The same spectrum after multiplication by the correction curve.³⁶

line and hence see Raman bands at small shifts. Figure 15 shows the transmission properties of a modern transmission filter suitable for Raman work. This is much superior to those previously available. Filters change their characteristics if they are tilted with respect to the optical axis. An example of the successful use of filter tilting to observe lower frequency Raman bands is shown in Fig. 16.

The filter and detector combinations in FT Raman spectrometers give rise to an oscillating sensitivity profile, so the spectra recorded are distorted. Different filters and detectors have markedly different sensitivity characteristics, and thus the overall sensitivity profile can vary from instrument to instrument. Figure 17 shows raw FT Raman spectra for polytetrafluoroethylene (PTFE). It can be seen that the relative band intensities are very dissimilar. A

correction function, shown in Fig. 18, is produced to compensate for the filter and detector characteristics.³⁶ Multiplying raw data by this curve will adjust relative band intensities and remove artificial oscillations in fluorescent backgrounds of a spectrum of PEES/PESES copolymer (Fig. 19). Similarly, Fig. 19 shows how the relative band intensities change in the corrected spectrum of the PEES/PESES copolymer. Since the correction curve varies across the spectral range, the noise level in different regions of corrected spectra will not be the same.³⁶

2.3.4. *Laser safety*

Unlike conventional Raman spectrometers, commercial FT Raman instruments have been designed to operate in a normal analytical laboratory alongside other equipment. In all cases, the sample area is enclosed with a totally opaque lid fitted with more than one microswitch wired in series and interlocked to the laser power supply. The purpose of these is to switch off the laser if the sample lid is opened for any reason. It must be remembered, however, that the Nd:YAG laser found in an FT Raman spectrometer produces a high-power invisible beam. Thus it is potentially very dangerous if proper safety precautions are not taken. It is recommended that the instrument should be prominently labelled to show that a powerful invisible laser is inside.

2.4. *Fiber optic probes and microprobes*

Since the laser wavelength used to obtain the Raman spectrum lies in the visible and infra-red regions in most cases, it is feasible to focus the laser beam on one end of a length of fiber optic and place the other end such that the emerging laser beam impinges on the sample to be analyzed using a microscope objective lens. It is also possible to collect the back-scattered Raman photons using a bundle of fiber optics placed around the fiber carrying the laser beam.

The use of fiber optics opens up the possibility of analyzing samples situated remotely from the Raman spectrometer. From the point of view of polymer analysis, this has the advantage that polymer samples of any size or shape can be analyzed in situations where they would not normally be amenable to study.³⁷ A Raman spectrum can be readily obtained of a sample under stress in a tensometer, and in this way changes in orientation, crystallinity and strain can be monitored. Similarly, polymer samples under conditions of high pressures or high temperatures can be examined without danger. Polymerization reactions under high pressures or in solutions can be followed *in situ* by inserting the end of the fiber optic probe into the reaction vessel. Spectra may be obtained from polymers during processing, and this affords the opportunity of using Raman-based techniques for on-line monitoring and for process control.

The development of the Raman microscope or microprobe is one of the most significant advances in the area of sample handling in recent years. The Raman microprobe, in its simplest form, comprises a conventional optical microscope connected to the monochromator of the Raman spectrometer. The laser radiation is focused on the sample to be analyzed through the microscope objective and the back-scattering of the Raman signal is collected also via the objective lens and passed into the monochromator. Such a system gives the

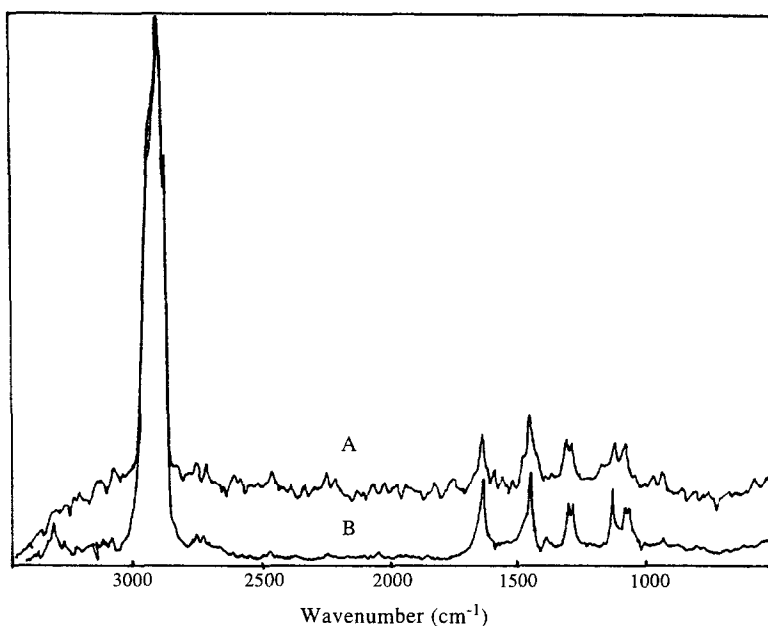


Fig. 20. Raman spectra of Nylon fibers. Resolution: 8 cm^{-1} ; laser power: 100 mW. Spectrum A was recorded by using a macroprobe with scan time 60 min. Spectrum B was recorded by using a microprobe with scan time 3 min (spectra were provided by Bruker Instruments Ltd, 1993).

capability of examining very small particles ($1 \mu\text{m}$) or specific parts of the samples that may be of particular interest. In the structural analysis of polymers, especially the analysis of commercial samples, this type of microprobe has proved to be extremely useful.³⁸ Figure 20 shows a comparison of Raman spectra of a Nylon film recorded by macro- and microprobes respectively. The two spectra are clearly identical to each other, but there are some details worth noting. Despite the fact that both spectra were recorded with the same power of incident radiation at the sample, there is a clear difference in the signal-to-noise ratio. Although the scan time for the microprobe measurement was much shorter than that for the macroprobe, the spectrum recorded by microprobe shows higher quality in terms of the signal-to-noise ratio. The estimated ratio for the spectrum recorded with the macro optics is approximately 5:1. This value has been derived by dividing the 1720 cm^{-1} peak intensity of the C=O stretching mode by the peak-to-peak noise between 1800 and 2500 cm^{-1} . For the case of the microscope, the signal-to-noise ratio is closer to 20:1.

The use of an FT Raman microprobe and fiber optic system opens up the possibility of analyzing samples situated remotely from the spectrometer. From the point of view of polymer analysis, this affords the advantage that polymer samples of any size or shape can be analyzed in situations where they are not normally amenable for investigation. For example, by using the FT Raman microprobe, a subtraction Raman spectrum can be readily obtained of a tiny piece of inked paper, which resembles the spectrum of plain

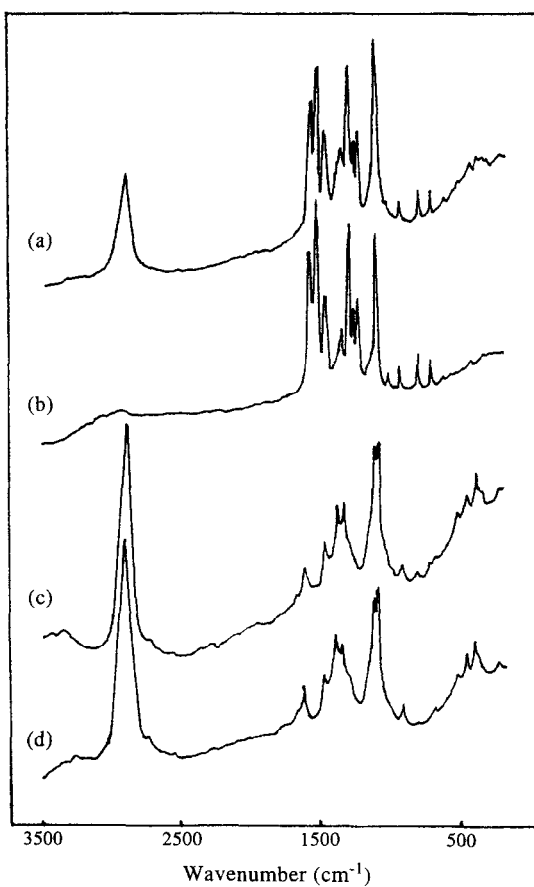


Fig. 21. Spectral subtraction and microanalysis with FT Raman spectroscopy. (a) FT Raman spectrum of a piece of inked paper; (b) FT Raman spectrum of ink on KBr; (c) difference spectrum (a - b) showing paper; (d) FT Raman spectrum of plain paper. (a),(b) Measurement time: 3 min; laser power: 215 mW. (d) Measurement time: 30 s; laser power 215 mW. (Spectra provided by Bruker Instruments Ltd, 1993).

paper, as shown in Fig. 21. The FT Raman microprobe is also particularly useful in the analysis of polymer "sandwiches" where two or more different polymers are pressed together to form a sheet with overlapping layers of the individual polymers which may be only a few micrometres in thickness. As shown in Fig. 22, FT IR meets with difficulties in performing spectral work for this kind of sample. However, the FT Raman microprobe can be used to identify the individual components of such a "sandwich" by scanning across the edges of the sample and looking at each layer in turn. The FT Raman spectra are shown in Fig. 23. The individual components of the "sandwich" were identified to be polyethylene, polyisobutylene, Nylon, poly(vinylidene chloride) and poly(ethylene terephthalate), respectively.

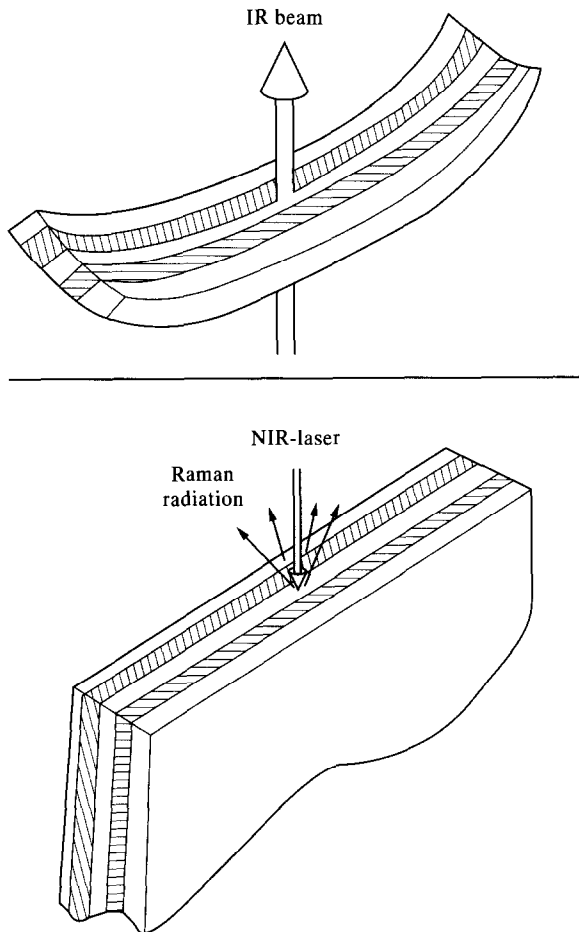


Fig. 22. Schematic diagram of Raman radiation scattered from a "sandwich" sample consisting of 5 polymer films.

3. THE ANALYSIS OF POLYMERIC MATERIALS USING FT RAMAN SPECTROSCOPY

3.1. General analysis

3.1.1. Raman and IR studies of polymers

Since the first Raman spectrum of a polymer—polystyrene—was published by Signer and Weiler in 1932,³⁹ there have been several reviews which have summarized the application of Raman spectroscopy for the analysis of polymers.^{2,40–42}

In principle, Raman and IR spectra provide qualitative and quantitative information about

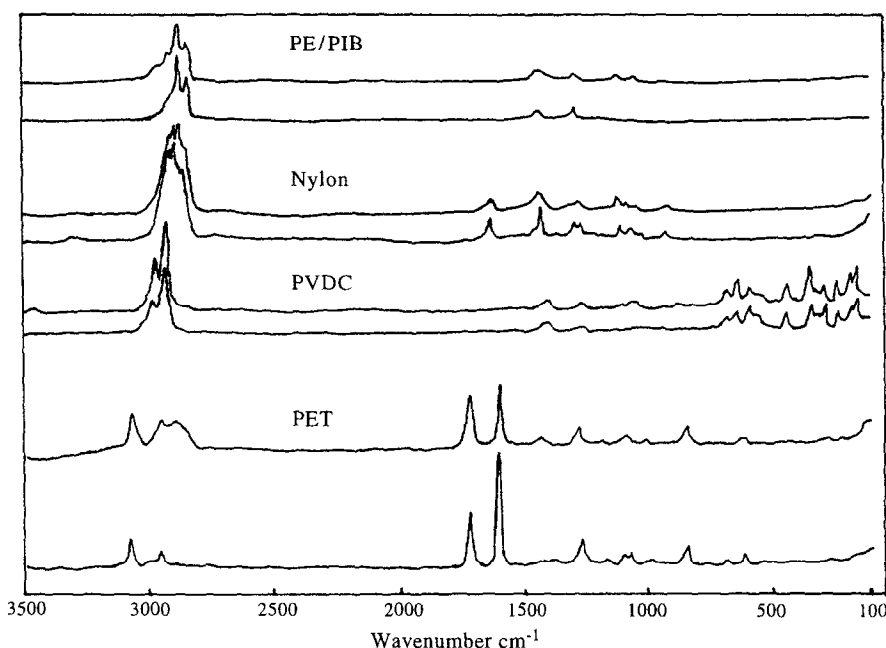


Fig. 23. FT Raman spectra of the components of a “sandwich” composite shown in Fig. 22 (from Bruker FT-IR).

the following structural details of polymeric materials under examination.

1. Chemical structure and composition: structural units, end groups, type and degree of branching, additives.
2. Stereo-order: *cis-trans* isomerism and stereoregularity.
3. Conformational order: physical arrangement of polymer chains both in the solid and in the melt states, e.g. planar zigzag or helix conformations.
4. State of order: crystalline, mesomorphous and amorphous phases; intermolecular forces; lamellar thickness.
5. Orientation: Raman depolarization and infra-red dichroism of preferential polymer chains and side-group alignments in anisotropic polymers.
6. Surface and interface structures.

Due to the sensitivity of Raman and IR spectroscopy to changes in the polarizability and dipole moment, respectively, of vibrating molecules under examination, Raman spectroscopy is especially helpful for the characterization of homonuclear polymers whereas IR spectroscopy generally yields more useful information for the identification of polar groups. Vibrations that are active in Raman may be inactive in the IR range, and vice versa. The complementary nature of Raman and IR analyses is of particular importance for the characterization of macromolecular structures.

In about the last 20 years, Raman spectroscopy has made phenomenal progress owing to

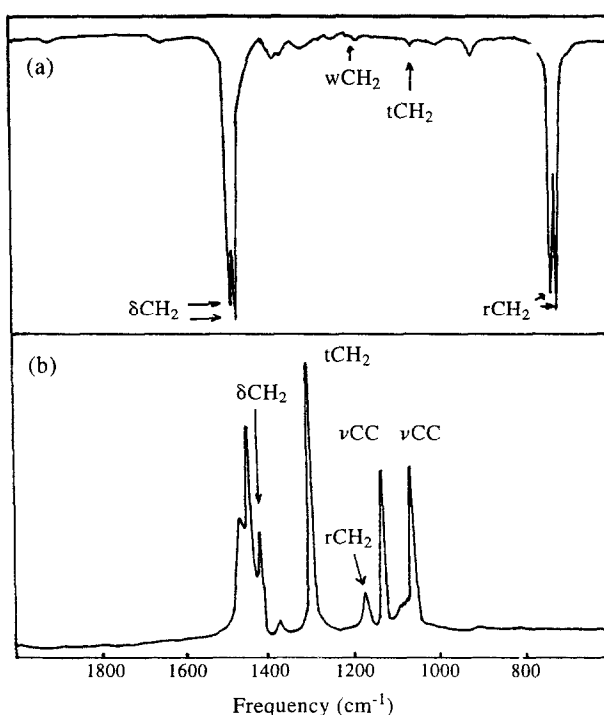


Fig. 24. (a) IR and (b) Raman spectra of linear polyethylene.⁵

technological innovations in lasers, detectors, electronics and computers. Fourier transform Raman, resonance Raman and surface-enhanced Raman spectroscopy are the most notable examples. Today, the application of Raman spectroscopy spreads over large areas of science and technology. Besides its complementary nature to IR, Raman spectroscopy has some notable advantages over IR for the study of polymers.

The Raman effect is produced by the exchange of energy between incident photons and the vibrational energy levels of the molecule. In many instances, the magnitudes of the Raman shifts in frequency correspond exactly to those of IR absorptions. But some vibrational modes appear only in the Raman spectrum. The differences in the vibrational patterns of Raman and IR spectroscopy can be used to great advantage in the measurement of the structure of molecules, and these differences are probably the prime reasons for interest in Raman spectroscopy. Generally, the more symmetric the molecule is, the greater the differences will be between Raman and IR spectra. In chain-like polymer molecules, vibrations of the carbon chain are easily studied by using Raman spectroscopy while the vibrations of side groups can often be characterized by using IR spectroscopy.

These differences between Raman and IR spectroscopy for polymeric materials can be illustrated. Figure 24 shows both Raman and IR spectra for linear polyethylene (PE).^{1,2} The PE molecule has a center of symmetry, and Raman and IR spectra should exhibit entirely different vibrational modes. The C-C modes can be clearly observed in the Raman spectrum, but the CH₂ modes dominate the IR spectra.

Because water is a highly polar molecule, it is a strong IR absorber. However, it is a weak Raman scatterer. Therefore the Raman effect can be used to study aqueous solutions, and this fact has been beneficial in the biological field and for studies of water-soluble polymers such as surfactants.

Compared with the IR technique, Raman spectroscopy has many advantages, and these are:

1. Raman spectroscopy is a scattering process, and it does not have the problems associated with the requirement of light transmission. So samples of any size or shape can be examined.
2. Aqueous solutions can be analyzed.
3. Fiber optics can be used for remote sampling.
4. The low frequency ($10\text{--}500\text{ cm}^{-1}$) region is available on the same instrument.

The major limitation of the Raman technique for polymer studies is that of fluorescence, and spectra of good quality cannot be obtained for many polymeric samples by the use of conventional Raman instruments due to this fluorescence. Even when fluorescence arises from an impurity which is present at the level of parts per million, 10 fluorescent photons will generally be produced for each Raman photon. In the visible excitation region, most polymers are not amenable to Raman analysis directly because of unquenchable fluorescence.

By their very nature, polymers are impure and in their applications they are usually combined with antioxidants and other additives which tend to exacerbate the fluorescence problem. Techniques capable of reducing this fluorescence (extraction, recrystallization and burning out the fluorescence by exposure to the exciting beam) are time-consuming and tend to make the technique uneconomical. In addition, many of the additives and pigments used in polymer technology are deeply colored and may absorb the visible laser excitation, causing sample heating which may well obliterate the Raman signal and even destroy the sample.

The recent advent of near-IR excited FT Raman spectroscopy has allowed a re-evaluation of the Raman technique for the routine analysis of polymeric materials. The lower proton energy used does not excite the same levels of fluorescence as for visible Raman spectroscopy. This has allowed a massive expansion of the number of samples that are measurable. The availability of analytical-grade FT spectrometers also allows for the rapid acquisition of data. Thus commercial polymers, copolymers and polymer blends can be examined, allowing properties such as composition or crystallinity to be monitored at different stages in a manufacturing process, even when the sample is contaminated with reinforcing agents or dyes.⁴³

The Raman effect affords advantages for the determination of polymer structure besides its complementary nature to IR. Ideally, a spectroscopist would like to have both the FT IR and FT Raman spectra of a sample in order to look at its structure in detail.

The following descriptions of applications of FT Raman spectroscopy serve not to summarize the total field but to illustrate the usefulness of the technique to the analyst.

3.1.2. *Sampling procedures for polymeric materials*

3.1.2.1. *Solid polymers* – Polymeric materials may be examined in a variety of physical forms: powders, pellets, pieces of sheet and thin films pose no problems. Solid powders are usually compacted into cells consisting of a 3 mm hole drilled through a brass cylinder, into which a reflective metal rod is placed to compress the powder. The cell filling procedure for

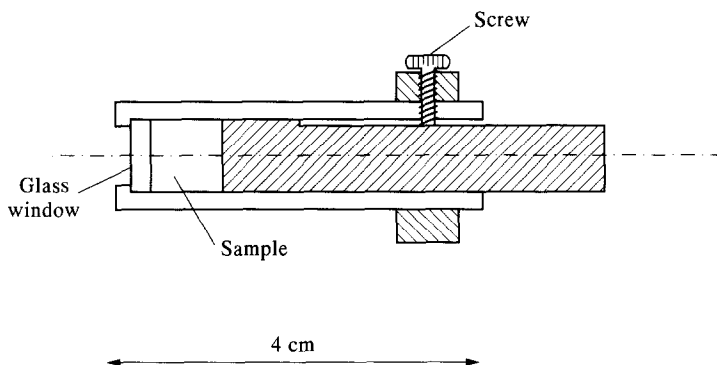


Fig. 25. Sample cell for polymers in fiber form, used in Dr Patrick Hendra's laboratory at Southampton University.⁴⁵

powders and pellets is self-evident. Circular pieces of the appropriate diameter may be punched from polymers in sheet form, and thin films are rolled into cylinders and inserted end-on into the cavity. The Raman intensity observed is related to the thickness of the sample, but does not increase once the sample depth exceeds 2 mm. Micro solid cells have been made with 0.7 mm diameter holes from which spectra of 0.006 mg of a strong Raman scatterer have been recorded. When toxic or air-sensitive materials are studied, a glass-fronted cell can be used. Here, there can be an 11% drop in performance owing to reflection losses off the glass.⁴⁴

This type of cell is not ideally suited for the examination of fibers because they cannot be compressed tightly into the cavity. Figure 25 shows the cell that has proved very satisfactory for fibers developed by Hendra's group at Southampton University. The polymeric fibers are compressed between a glass window and an adjustable concentric metal rod, which is located with a screw fitting.⁴⁵ This arrangement ensures that unwanted voids are not present in the sample area, and that a high density of sample is intercepted by the laser beam.

3.1.2.2. Polymer solutions – Generally, spectra from liquids are recorded by using silvered spherical glass cells or glass cuvettes, sometimes with the back surface silvered. The spherical cells act as reflective integrating spheres and, when their radius is optimized (about 7 mm), they are around five times better than unsilvered cuvettes.⁴⁶ However, they do not work well with solutions that absorb Raman light, where it is important that Raman light passes through only a short pathlength of liquid. Very acceptable spectra can also be recorded by using half-silvered 8 mm sample bottles which are cheap enough to be disposable.

3.1.2.3. Measurements at elevated temperatures – Measurements at elevated temperatures are somewhat less straightforward than for the case of dispersive Raman spectroscopy using an exciting line in the visible spectral region. There is appreciable near-IR thermal emission from the hot cell, and the higher the temperature, the more intense it becomes, obscuring the Raman signal. Williams and Mason have suggested a ceiling temperature of about 140°C in practice.⁴⁷ The size of the problem is also a function of the cell design; if the amount of heated

metalwork is small and the cell walls are relatively cool, measurements are possible up to about 200°C. This suffices for most polymer studies.

3.1.2.4. Microscope accessories – Conventional Raman spectrometers have often been fitted with a microscope attachment. This allows the Raman spectrum of a very small area of the sample to be collected. Not only does this permit the use of very small samples, but it also makes it possible to investigate variations in the structure of a sample with fine spatial resolution. Microscope accessories for use with dispersive Raman spectrometers have proved very useful for a range of polymer studies, e.g. single fibers, very small samples and small inclusions *in situ*.² Not surprisingly, microscopes for use with FT Raman spectrometers have yet to reach the same degree of efficiency, but encouraging progress is being made. By using a computer-controlled sample stage, it is possible to produce an “image” of the sample by plotting the frequency of intensity of a Raman band as a function of position.^{2,48}

Several commercial microscope accessories are available. The one offered by Bruker is somewhat dated and this is reflected in its performance.²

3.1.2.5. Electrochemical measurements – The electrochemical cells consist of a working electrode mounted in a KelF cylinder surrounded by a platinum-wire counter-electrode. A reference electrode with its attendant capillary enters from the side of the cell. The application of electrochemical cells in surface-enhanced Raman scattering studies will be described in a later section.

3.1.2.6. Adsorbed species – Pyrex cells used for the study of adsorption processes are almost trivially simple, consisting of a horizontal tube ending with an optical flat 15 mm in diameter. The tube is fitted with a PTFE grease-free vacuum tap, to allow it to be connected to a vacuum system. The tap stopper is removable so that bulk catalyst can be placed in the tube. The complete cell will easily hold 1 g of sample and has a total mass of about 70 g. Adsorption processes are thus simple to follow gravimetrically with a conventional balance. Details of operation are given elsewhere.³⁴

3.1.2.7. Quantitative measurements – The quantification of Raman scattering involves an absolute intensity measurement, and this poses considerable problems. It is very difficult to obtain successive spectra of the same sample, or spectra of different samples in succession, for which the reproducibility of intensities is acceptable.

Two methods have been used with dispersive Raman spectrometers to overcome this problem sufficiently to permit quantitative analysis in more favorable cases. The first is the use of an internal standard. The second, more favored approach is to use the ratio of the intensities of two Raman lines, preferably not too widely separated on the frequency shift scale.⁴⁹

It has been shown recently that Raman intensity measurements are more easily made with an FT Raman instrument. One important factor making this possible is the ease with which samples may be located reproducibly in the spectrometer, coupled with a negligible effect on the scattering intensity for a small sample displacement.

If intensity measurements made on different spectrometers are to be compared, or measurements on a given instrument over a period of time are to be related, it is necessary to

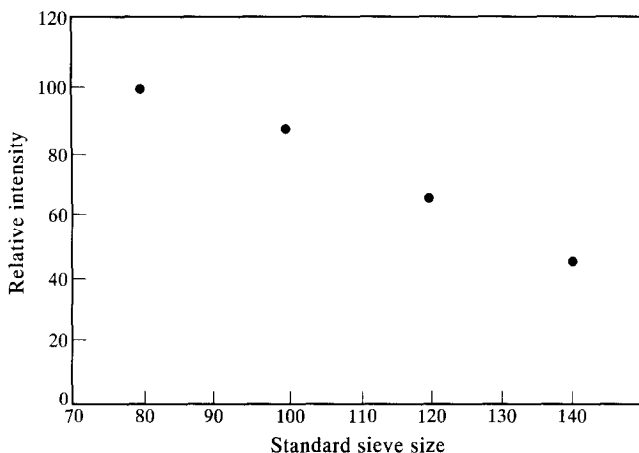
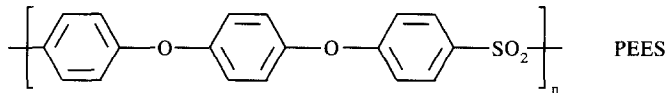
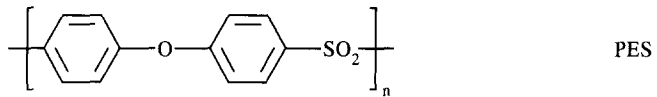


Fig. 26. Raman intensity as a function of particle size for potassium chromate powder. The *x*-axis is the mesh sizes of the standard sieves through which the powder sample passed measured in wires per inch.

correct for the variation of detector response with wavelength, for transmission characteristics of the filters used to remove Rayleigh lines, and for various other instrumental factors. This is conveniently done by measuring the response to a high-temperature black-body source, and comparing this with the theoretical curve.

The quantitative analysis of solids presents significant experimental difficulties. Raman intensity from powdered samples falls as the particle size decreases, as shown in Fig. 26. Also, the number of sample molecules in the laser beam depends on how densely the particles are packed. Unfortunately, these problems hinder the use of external standards for solid samples.

However, the relative band ratios method can be used to extract quantitative data from the spectra for solid samples. Ellis *et al.* have investigated FT Raman spectra of poly(aryl ether sulfone) (PES) and poly(aryl ether ether sulfone) (PEES) and amorphous polymers of the two.⁴⁹ The repeat units for these two homopolymers are as follows:



The authors found clear correlations between the relative band ratios and copolymer compositions (as measured by NMR). This is shown in Fig. 27. The observation could be used to characterize these copolymers in a manufacturing plant.

3.1.2.8. Spectral subtraction – The reproducibility of intensity measurements also facilitates

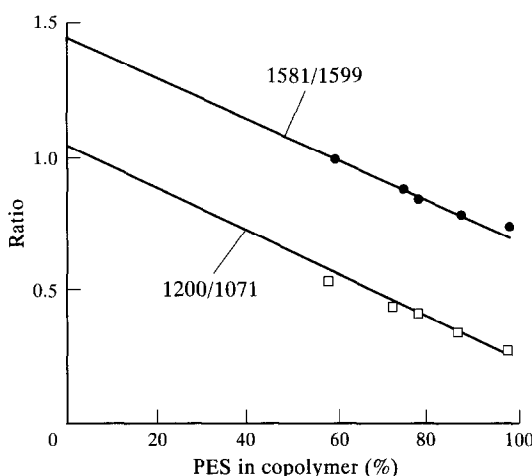


Fig. 27. Band intensity ratios $1581\text{ cm}^{-1}/1599\text{ cm}^{-1}$ and $1200\text{ cm}^{-1}/1071\text{ cm}^{-1}$ for PES/⁵⁰ PEES copolymers as a function of % PES content.⁵⁰

the use of spectral subtraction, already well established as a valuable technique in the characterization of polymers by IR spectroscopy. Walder and Smith have demonstrated the value of FT Raman spectral subtraction techniques using mixtures of the xylem isomers. By subtracting the spectra of the *m*- and *p*-isomers from those of three-component mixtures, they were able to detect the *o*-isomer down to a 1% level and, more generally, concluded that this limit of detection should be achievable for many other compounds.⁵¹

Bourgeois and Church have pointed out that some caution is necessary in the use of spectral subtraction because of small instrumental frequency shifts that may occur. If these are present, then the difference spectrum will have a component that resembles a first-derivative spectrum and this may give rise to a misinterpretation.⁴⁵ This effect can be avoided by calibrating the spectrum via the laser line, a procedure followed by Bourgeois and Church.⁴⁵ Walder and Smith also discuss the optical design factors in FT Raman spectrometers that are involved in trouble-free spectral subtraction.⁵¹ As these factors are appreciated by spectrometer manufacturers, it is reasonable to conclude that the technique will gain wider acceptance.

3.1.3. Resonance Raman spectroscopy

When the exciting laser frequency approaches that of an electronic absorption band of the scattering molecule, certain Raman lines increase in intensity (pre-resonance Raman effect), and are strongly enhanced. When the frequency of the laser radiation coincides with that of an electronic transition (rigorous resonance Raman effect) such that

$$\text{Raman intensity} \propto (\nu_{\text{laser}} - \nu_v)^4 \left(\frac{\nu_{\text{abs}}^2 + \nu_{\text{laser}}^2}{\nu_{\text{abs}}^2 - \nu_{\text{laser}}^2} \right)^2 \quad (17)$$

the enhanced Raman lines may have intensities 10^3 – 10^6 times greater than normal Raman

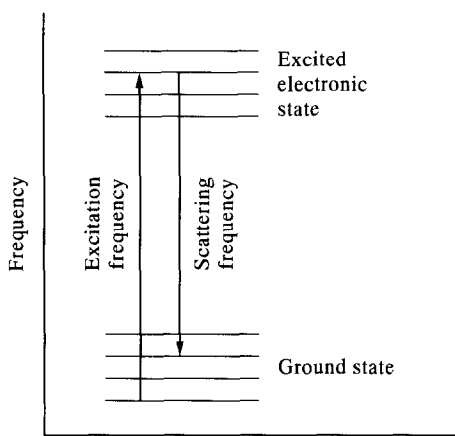


Fig. 28. Resonance Raman effect shown schematically.

intensities. The resonance Raman spectra have lower detection limits (20 ppb level) and are much simpler than normal Raman spectra since only vibrational modes associated with the "chromophore" are enhanced. The advantage of the resonance Raman effect lies in its great sensitivity and selectivity as a probe of chromophore structure.

The resonance Raman effect results from the promotion of an electron into the excited vibronic state, accompanied by immediate relaxation into a vibrational level of the ground state, as shown in the schematic diagram in Fig. 28. This process is not preceded by prior relaxation into the lowest vibrational level of the excited state as in ordinary fluorescence. Consequently, the resonance Raman emission process is essentially instantaneous, and the spectral resolution is good, $10-20 \text{ cm}^{-1}$ (0.3–0.6 nm at 500 nm). A tunable pulsed-UV laser (frequency-doubled Nd:YAG laser) that pumps a dye laser can produce radiation from 217 to 450 nm and will allow for the observation of the resonance Raman effect. Contrary to the high power required for normal Raman and FT Raman spectroscopy, the typical power requirement for resonance Raman spectroscopy is only a few mW. The resonance Raman spectrometer and detectors are the same as for the normal Raman systems.

Exciting higher electronic states sometimes eliminates fluorescence interference and makes resonance Raman spectroscopy an effective method when fluorescence is a problem in the normal Raman experiments.⁵²

Several important reviews on the theoretical and practical aspects of the resonance Raman effect have appeared,⁵³⁻⁵⁶ and many publications have reported the application of resonance Raman spectroscopy in studies of polymeric materials.⁵⁷⁻⁷⁵ The 1064 nm FT Raman spectroscopy exhibits an advantage of obtaining resonant Raman spectra of materials having near-IR absorptions, such as conjugated conducting polymers, charge-transfer complexes, biological pigments, etc. The present review will briefly discuss resonance Raman spectral studies on conjugated conducting polymers.

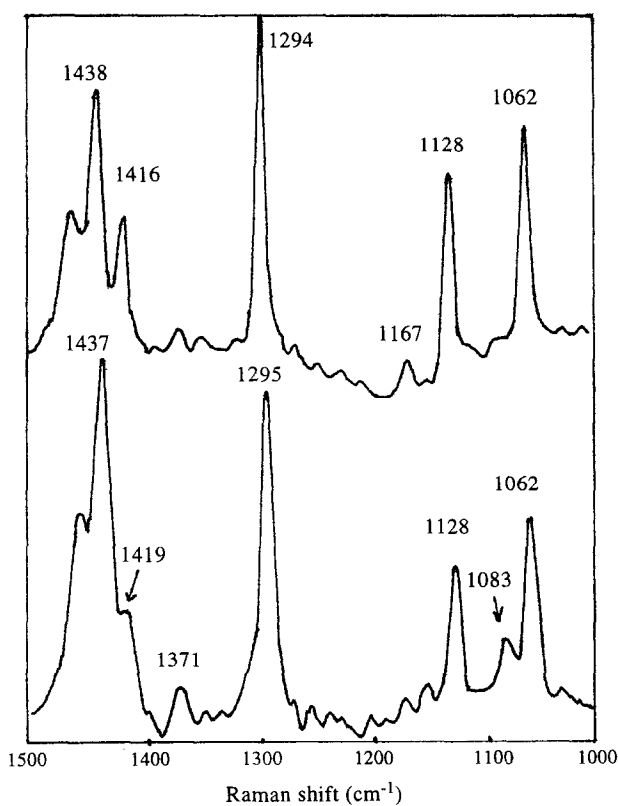


Fig. 29. The FT Raman spectra of low density PE (lower) and annealed high density PE (upper).

3.2. Crystals and tacticity studies

Both Raman and infra-red absorption spectroscopies can give useful information on the tacticity, crystallinity and orientation of a polymer. The spectral differences between syndiotactic and isotactic polypropylene have been documented.⁷⁶ The standard method of determining tacticity is by ¹³C NMR; however, the advantage of the FT Raman method is that it can be applied to specimens without sampling. Broad Raman bands of low peak intensity are characteristic of materials which have a low stereochemical purity, such as atactic samples or those with mixed head-to-head and head-to-tail fragments. The wide range of significantly different chemical species present all have slightly different vibrational frequencies. Highly ordered species give rise to characteristically sharp and hence intense Raman spectral bands compared with those of disordered materials.⁷⁷

The vibrational spectra of crystalline polymers are invariably of high definition since it is only the in-phase modes of the species, characteristic of the crystalline phase, that give the more prominent spectral bands. As crystallinity in the sample falls, for whatever reason, the bandwidth increases and frequently new characteristics appear in the spectrum due to

rotameric species present in the disordered phases. The point is very well established and Fig. 29 shows this for polyethylene.

Methods of obtaining the degree of crystallinity in a polymeric material are well established. A detailed description of a Raman method has been made by Strobl and Hagedorn.⁷⁹ The principle is the same as the methods used in wide-angle X-ray diffraction, NMR and IR. A spectrum is recorded and then resolved into contributions from the ordered and disordered phases. The mass fractions in the different orders can then be determined from the weights of the respective components either directly or after calibration. Strobl and Hagedorn use a three-phase model for partially crystalline polyethylene consisting of an orthorhombic crystalline phase, a melt-like amorphous phase and a disordered, anisotropic phase (the interfacial material). The band intensity of pure crystalline material is estimated from the chain-extended material, and that of the pure amorphous material from the melt. The integrated intensity of band at 1416 cm^{-1} (the A_g component of the CH_2 bending vibration) serves as a measure of the amount of orthorhombic crystalline material present in polyethylene (see Fig. 29). A band at 1083 cm^{-1} is used to estimate the amorphous content. This method has been successfully applied to some other polymers.⁷⁸ FT Raman spectroscopy has recently been applied to determining the crystalline content of poly(aryl ether ketone).⁷⁹ The FT Raman spectrum of Nylon 6 has also been shown to change with crystalline content,⁸⁰ and this may form the basis of a method of measuring its crystallinity.

One point, however, needs to be discussed in relation to this review. In crystalline polymers where the modes are centered in groups unaffected by the degree of order, the spectrum may give very little indication of the presence of crystallinity. Thus, in FT Raman spectra of atactic polystyrene and crystalline isotactic polystyrene, the stereospecific and/or crystalline sensitive bands are markedly weaker. The Raman spectrum of polypropylene is in general characteristically insensitive to order, but in this case the relative intensity of some bands and their widths do vary as the crystallinity and average length of helical runs is altered. These variations have been exploited in polymer morphological studies.⁸¹ To summarize, the

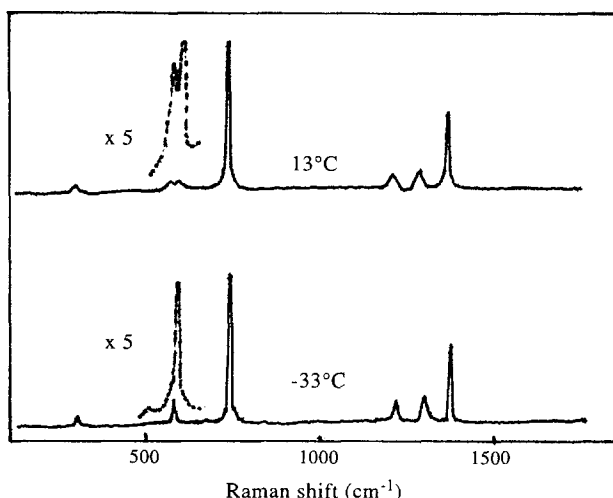


Fig. 30. The FT Raman spectra of polytetrafluoroethylene showing changes in bandwidth and phase changes.⁸⁶

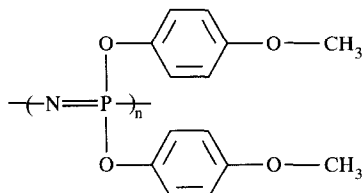
detailed analysis of the weaker features in the vibrational spectra and the bandwidths are indicative of order and can be used for this purpose.⁸²

Changes in crystalline habit as a function of temperature or pressure can be followed using FT Raman spectroscopy. A simple example is polyethylene which contains two chains per unit cell. Each mode of each chain can occur in-phase or out-of-phase with its partner, giving rise to two bands in the Raman spectrum. This is known as correlation splitting,⁸³ and can be monitored as a function of temperature and pressure. FT Raman spectroscopy has been used to study the development of cold crystallization in natural rubber.⁸⁴ A similar study of the crystallization process in chloroprene rubber has also been investigated.³⁴

Polytetrafluoroethylene undergoes a rapid phase transition at 19°C due to a change in its helical pitch from 13/6 to 15/7.⁸⁵ In Fig. 30, it can be noted that the bands near 500 cm⁻¹ change and this is known to be due to this phase change.⁸⁶ However, it is equally clear that the specimen under study is hotter than the temperature actually measured due to adsorption of the near-IR laser.

3.3. Liquid crystalline polymer studies

Liquid crystal structures can often be frozen into the material, facilitating examination of the morphology of the mesophase. However, the poor solubility and elevated transition temperatures can produce difficulties in their study. Among the techniques typically used to characterize thermotropic polymers are X-ray diffraction, differential scanning calorimetry (DSC) and NMR spectroscopy. Vibrational spectroscopy can provide very useful structural information on liquid crystalline polymers and has also been shown to be sensitive to important parameters such as orientation and crystallinity in many systems. IR spectra have been recorded from both main-chain and side-chain liquid crystal polymers, transitional behaviour has been monitored, and IR spectroscopy has been used to determine order parameters. In principle, different liquid crystal polymer phases may also be studied, but in practice this has been limited because of persistent sample fluorescence. Polyphosphazines have been studied successfully.⁸⁵ These materials exhibit thermotropic behaviour which is highly dependent on their thermal histories and the nature and packing of their side chains around the flexible P–N backbone. The general repeat unit of poly(bis-4-methoxy-phenoxy phosphazine) (PBMOPP) is



It has been studied in the crystalline phase and mesophase. A different spectrum between these two states was used to identify band shifts in the aromatic ring breathing mode and the aromatic C–H stretch on crystallization. These shifts reflect the reduction in the mobility of the aromatic ring side chains in the crystalline material. In addition, differences in the relative band intensities of several modes were observed. The C=C stretching mode increases in intensity on crystallization, which is consistent with the view that the arrangement of substituent groups determines the nature of the material.

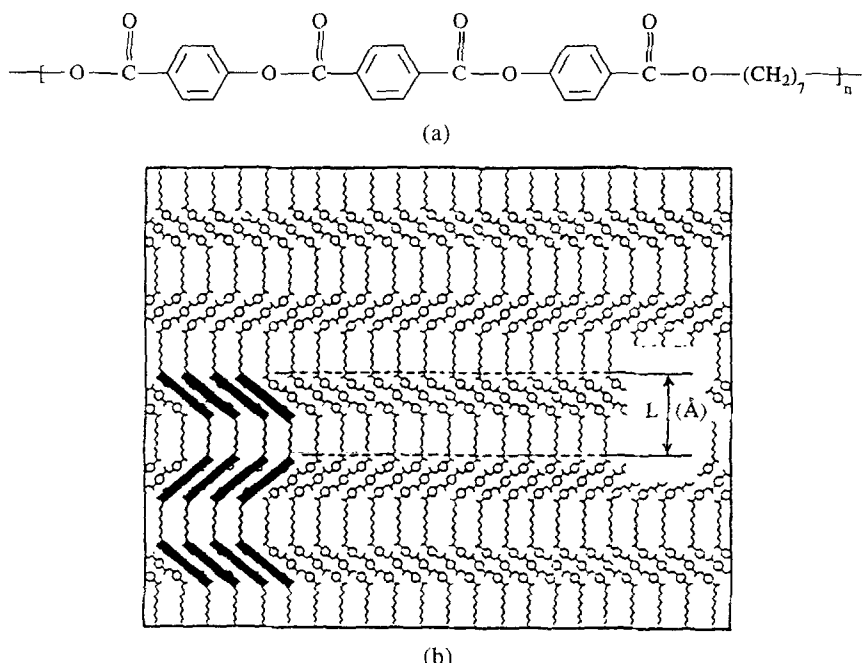


Fig. 31. (a) Structure of PHMTOB and (b) the liquid crystalline, smectic phase.⁸⁷

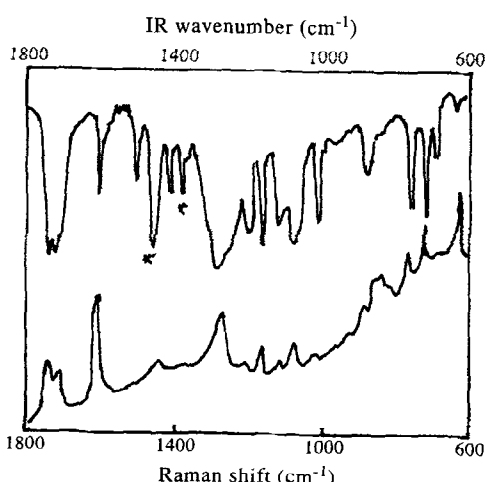


Fig. 32. Vibrational spectra of PHMTOB: FT IR (upper) and FT Raman (lower). * Indicates nujol bands.⁸⁷

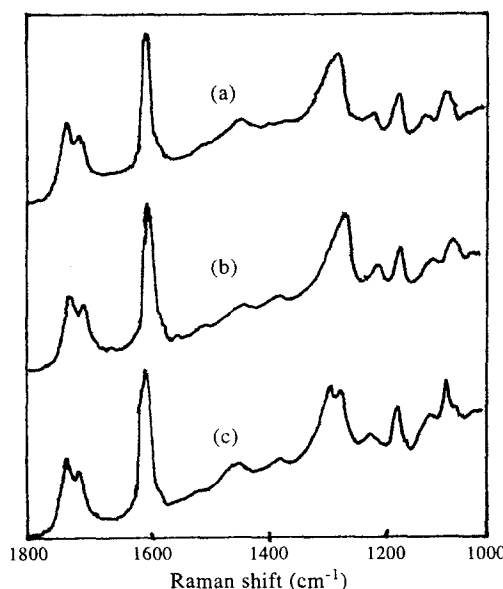


Fig. 33. FT Raman spectra of PHMTOB: (a) the original sample; (b) a sample quenched from the mesophase;⁸⁷ (c) one crystallized from solution.

Ellis *et al.* have identified changes in the FT Raman spectrum of the thermotropic main-chain liquid crystalline polymer, poly(heptamethylene terephthaloyl-bis-4-oxybenzoate) (PHMTOB), as a function of temperature and thermal history.⁸⁶ Main-chain liquid crystalline polymers consist of rigid mesogen units linked by flexible spacers. The structure of PHMTOB is shown in Fig. 31(a). When heated above its crystalline melting point, long-range order persists and, within distinct temperature regions, "liquid crystalline phases" are said to exist. PHMTOB exhibits a layered "smectic" type phase which is shown in Fig. 31(b). Vibrational spectra recorded from the original sample of PHMTOB are presented between 1800 and 600 cm^{-1} in Fig. 32. It can be clearly observed that both the FT IR and FT Raman spectra show many vibrations at corresponding frequencies, and although many modes appear to be strongly coupled, the incidence of a center of symmetry in this polymer is seriously doubted. The FT IR data in Fig. 32 are more complex than the FT Raman data due to a considerable degree of band superimposition. Characteristic frequencies are observed in both techniques. Variations in the FT Raman spectra of PHMTOB with its thermal history were studied using FT IR and FT Raman spectroscopy. In the IR data differences between the original sample and that prepared by crystallization from solution are very slight. In the FT Raman data, many spectral variations between samples with different thermal histories can be observed. Figure 33 shows the FT Raman spectra between 1800 and 1000 cm^{-1} for three samples of PHMTOB: (a) the original material, (b) a sample quenched from the mesophase, and (c) one crystallized from solution. Variations in the FT Raman spectra of PHMTOB with temperature have also been observed.⁸⁷ Spectral changes have been attributed to differences in intermolecular interactions or conformations of the polymer chains between the crystalline, liquid crystalline and amorphous phases.

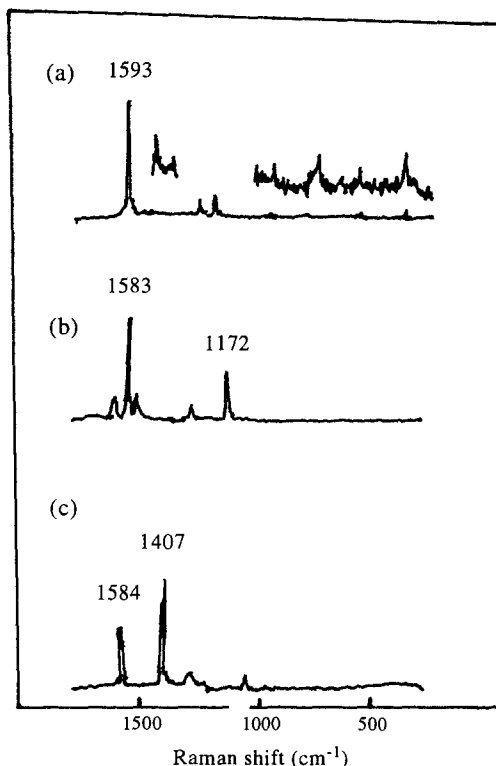


Fig. 34. FT Raman spectra of neutral polymer: (a) PPP; (b) PPV; (c) PTV.

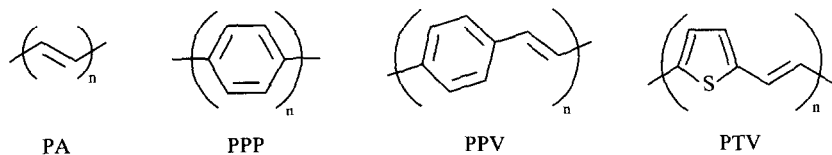
3.4. Conjugated conducting polymers

Since organic polymers are typical insulators, their inability to conduct electricity has been utilized in various applications. However, in response to a growing demand from the optical and electronics industries, many novel conducting polymeric materials have been developed in recent years. Applications of FT Raman in the study of these materials are beginning to appear in the literature. FT Raman is being recognized as an ideal tool, primarily because of the reduced sample fluorescence and adsorption, but also because it is non-destructive and allows samples to be studied *in situ*. It should be noted that this method has another advantage for obtaining resonant Raman spectra having near-IR absorptions, such as doped conducting polymers, charge-transfer complexes, biological pigments, etc.

When electrons are removed (or added to) π -conjugated polymer chains, structural changes supposedly extending over several repeating units occur. These doped-domain structures are classified into polarons, bipolarons and solitons according to their type, and have been extensively discussed in relation to their roles in electric conduction.⁸⁸ Electronic absorptions associated with the doped domains often appear in the region from visible to near IR. Accordingly, near-IR resonant Raman spectroscopy may give a clue to the structural features of the doped domains.

Figure 34 shows the FT Raman spectra of neutral (undoped) poly(1,4-phenylene) (PPP),

poly(1,4-phenylene vinylene) (PPV) and poly(2,5-thienylene vinylene) (PTV).⁸⁹ The chemical repeat units of these conducting polymers are



The Raman spectra obtained have high signal-to-noise ratios in accord with the general trend that molecules with conjugated π -electrons exhibit large Raman scattering cross-sections.

PPP shows intense "fluorescence" backgrounds when visible laser sources are used for Raman excitation; no Raman bands were observed with 488 nm excitation due to a strong background, and only a few bands were observed with 632.8 nm excitation.⁹⁰ However, in the

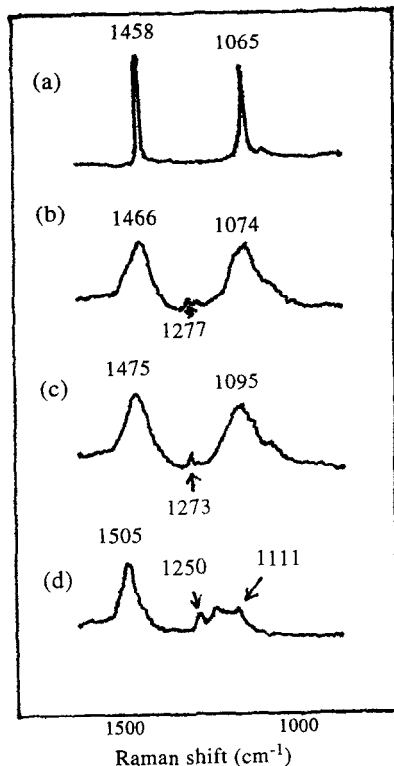


Fig. 35. Dependence of the 1064 nm excited FT Raman spectra of *trans*-polyacetylene upon dopant (Na) concentration: (a) neutral, (b)–(d) Na-doped. Estimated dopant concentrations are 8.5, 9.5 and 14% (full doping), respectively.⁹⁰

1064 nm excited FT Raman spectrum [Fig. 34(a)], no background is observed and the signal-to-noise ratio is high. It has been reported that the ratio of the intensity of the 1223 cm^{-1} band to that of the 1281 cm^{-1} band increases with the number of consecutive phenyl rings.⁹¹ Judging from the observed relative intensity in Fig. 34(a), the chain length in this sample is rather short. In the Raman spectrum of PPP prepared electrochemically, the 1223 cm^{-1} band is much stronger than the 1281 cm^{-1} band.⁹¹ The high quality of the FT Raman spectrum in Fig. 34(a) enables us to observe several weak bands at 1485, 999, 796, 623 and 409 cm^{-1} . On the basis of normal coordinate calculations, the following assignments were made on the assumption that the PPP molecule has D_{2h} symmetry. The bands at 1485, 623 and 409 cm^{-1} are attributed to b_{1g} , the 796 cm^{-1} band to a_{1g} , and the 999 cm^{-1} band to b_{2g} . The strong bands at 1593, 1281 and 1223 cm^{-1} have already been assigned to a_{1g} .^{92,93}

The neutral PPV and PTV samples show broad $\pi^*-\pi$ electron absorption bands centered at about 400 nm and 540 nm, respectively. The wavelength of 1064 nm used in FT Raman measurements is far from these absorptions. Thus their FT Raman spectra in Fig. 34(b) and 34(c) represent off-resonant scattering.

Figure 35 illustrates the dependence of the 1064 nm excited FT Raman spectra of *trans*-polyacetylene (PA) upon dopant (Na) concentration. A neutral PA film has a broad $\pi^*-\pi$ visible absorption centered at about 670 nm. Figure 35(a) represents an off-resonant Raman spectrum. Two strong, sharp bands are observed and a very weak band is observed at 1291 cm^{-1} in Fig. 35(a). The 1291 and 1069 cm^{-1} bands are assigned to mixtures of C–C stretching and CH in-plane bending vibrations. It has been reported that the positions of the 1461 and 1069 cm^{-1} bands are sensitive to the number of *trans*-conjugated C=C bonds.⁹⁴ With increasing conjugation length these bands shift to lower wavenumbers. It is well known that electronic absorptions of conducting polymers change upon doping. As Na-doping proceeds in PA, the visible absorption becomes weak and a very broad absorption appears in the entire near-IR region.⁹⁵ The maximum absorption region is located between 8000 and 6000 cm^{-1} . Thus, the excitation wavelength of 1064 nm is resonant with this near-IR absorption. Remarkable changes can be observed in Fig. 35(b) and (c) recorded from low doping levels of PA. The two strong and sharp bands become very broad, and both these bands shift to higher wavenumbers as the dopant concentration increases. Weak bands are observed at 1277 – 1273 cm^{-1} . At high doping levels, the spectral pattern [Fig. 35(d)] is quite different from those of the neutral and slightly doped samples. A band characteristic of donor-doping is observed at 1250 cm^{-1} with a weak intensity. The strongest band at 1505 cm^{-1} can be assigned to a mode mainly associated with the stretches of CC bonds having double bond features. Therefore, the bond alternation remains in the doped domains, as is the case with neutral PA. It has been reported that an abrupt increase of electrical conductivity occurs at a low dopant concentration ($< 0.5\%$) and that a Pauli susceptibility appears at a higher dopant concentration. It is possible that changes in electrical conductivity and magnetic susceptibility are associated with the two-stage changes in the 1064 nm excited Raman spectra, viz. the first one occurring between Fig. 35(a) and (b), and the second one between Fig. 35(c) and (d).

Near-IR FT Raman spectroscopy seems to have great potential as a tool for detailed structural studies of conducting polymers and doped polymers in particular because they usually exhibit absorptions in the near-IR region. The rigorously resonant or preresonant Raman effect between the near-IR absorptions and near-IR laser lines is expected to selectively enhance the intensities of Raman bands due to vibrations localized in the doped

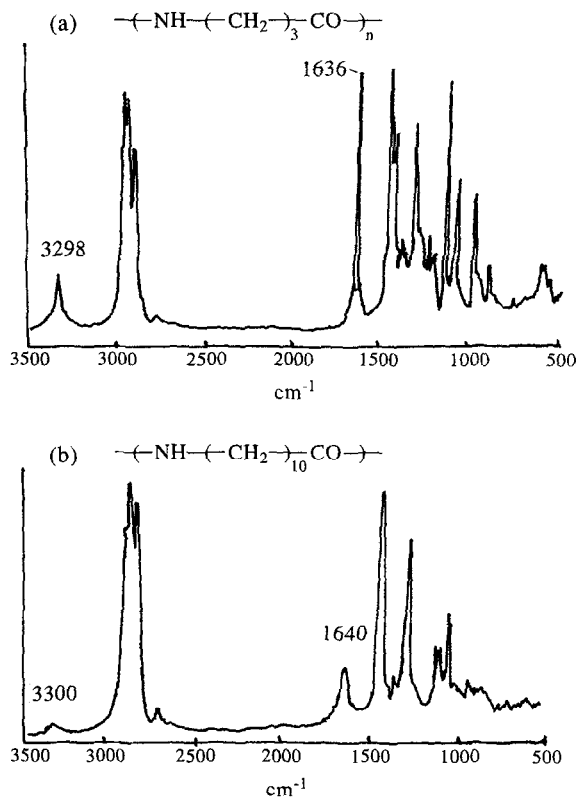


Fig. 36. The FT Raman spectra of (a) Nylon 4 and (b) Nylon 11.⁹⁶

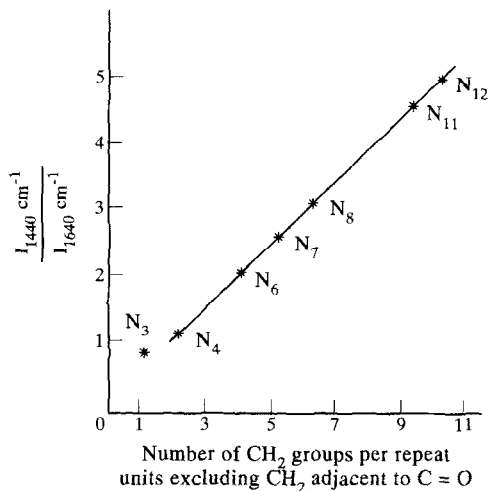


Fig. 37. Plot of the ratio of the relative intensity of the CH_2 bending mode and the amide I mode versus the number of CH_2 groups per unit, excluding CH_2 groups per unit, excluding CH_2 groups adjacent to the carbonyl group, for single number nylons.⁹⁶

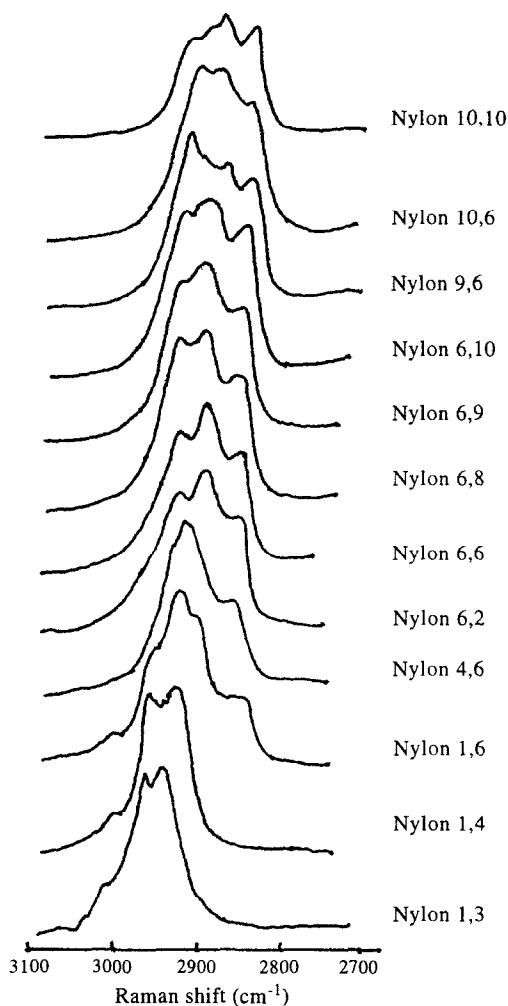


Fig. 38. FT Raman spectra of 12 double number nylons in C–H stretching region.⁹⁷

domains. Therefore, FT Raman spectra observed in this way can be a rich source of information concerning the doped domains.⁸⁹

3.5. Engineering polymers and composites

3.5.1. Nylons

Nylons have gained wide acceptance because they are readily processable by extrusion and molding. Their high strength, toughness and abrasion resistance is also invaluable. Despite their general availability for over four decades, little has been reported on their Raman spectra, primarily because of sample fluorescence.

FT Raman spectroscopy should, therefore, be of great value, and this has proved to be the case. Hendra and co-workers first examined a series of single-numbered nylons, ranging from Nylon 3 to Nylon 12, and obtained good quality FT Raman spectra, as shown in Fig. 36.⁹⁶ Assessed purely on a fingerprint basis, the spectra prove to be very specific and there is no difficulty in identifying any member of the series. When the ratio of the intensity of the methylene bending mode at 1440 cm⁻¹ and the amide I mode at 1640 cm⁻¹ is plotted against the number of methylene groups per repeat unit, excluding the CH₂ group adjacent to the carbonyl group, a straight line is obtained, as shown in Fig. 37. This is useful for analytical purposes. The differences between the spectra of Nylon 4 and Nylon 11, which occur progressively among the intermediate members of the series, relate to the changing relative concentrations of the amide and methylene moieties. The N–H stretching peak at 3300 cm⁻¹ and amide I peak near 1636 cm⁻¹ are relatively more intense in Nylon 4 than in Nylon 11, and one or more weak bands in the vicinity of 1250 cm⁻¹, probably assignable to the amide III vibration, are found with Nylon 4 but are not detectable with Nylon 11. The latter has a spectrum which, to a first approximation, approaches that of polyethylene, the strong peaks being assigned to C–H and C–C vibrations. As expected, the spectrum of Nylon 6,10 and Nylon X,Y samples in general, fit into this pattern.

The FT Raman spectra of 12 double-number nylons in the C–H stretching region are shown in juxtaposition in Fig. 38 and it is evident that there is no difficulty in unambiguous identification of all 12 samples.⁹⁷ Four Nylon copolymers, namely Nylon 6,6/6 with the composition ratios 20:80 and 75:25, and Nylon 6,6/6,10 with the composition ratios 30:70 and 60:40, were also examined.⁹⁷ With each pair there are readily detectable differences in the spectra for the two concentration ratios. The spectra, therefore, are useful for characterizations, although studies on a wider range of copolymers are still required before the scope of this approach can be ascertained.

Hydrogen bonding in nylons is likely to have some influence on their physical properties, and this merits study. Because the forces involved in these intermolecular interactions are weak, their vibrational modes will occur at low frequencies. This poses experimental problems for near-IR FT Raman spectroscopy because of the markedly more intense central Rayleigh line and part of a Rayleigh wing, which must be filtered out. Hansen *et al.* have recently succeeded in measuring a Raman shift as small as 40 cm⁻¹ with an FT Raman spectrometer,⁹⁸ and by using the $R(\bar{\nu})$ representation to present their spectra they have further improved their specificity.⁹⁹ They utilized the $R(\bar{\nu})$ representation of the low-frequency Raman spectrum. This representation is defined in the following way:

$$R(\bar{\gamma}) \propto (\bar{\gamma}_L - \bar{\gamma})^{-4} [1 - \exp(-h\bar{\gamma}c/kt)I(\bar{\gamma})] \quad (18)$$

where $I(\bar{\nu})$ is the intensity in the Raman spectrum at a Raman shift on $\bar{\nu}$ (reciprocal centimetres), h is Planck's constant, k is Boltzmann's constant and T is the absolute temperature. Its use has the effect of diminishing the influence of the Rayleigh line and wing because the Lorentzian part of the Rayleigh wing is converted into a slightly declining plateau. Nylons 6, 6,6 and 12 were examined and all three gave a rather broad peak at about 100 cm⁻¹. This was assigned to modes involved in hydrogen bonding. The authors suggested that the precise form of this peak depends on the specific spatial molecular structure of the nylon.

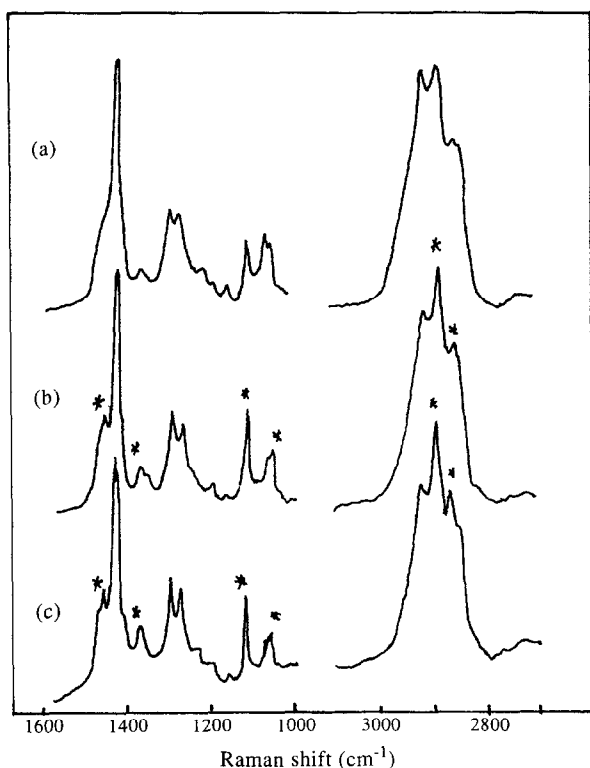


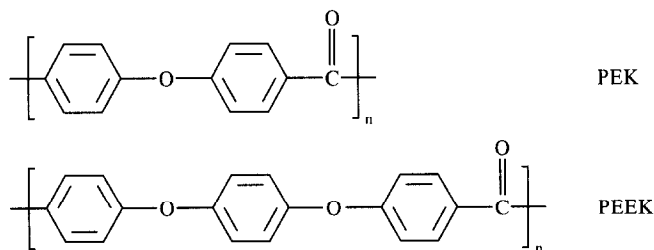
Fig. 39. FT Raman spectra of Nylon 6 (a) before and (b) after annealing, and (c) in powder form. * Denotes crystalline peaks.⁸²

FT Raman spectra have been obtained for Nylon 6 in pellet form, before and after annealing, and in powder form, obtained by dissolution of a pellet and recrystallization from solution. X-ray diffraction measurements on these three materials have shown that the crystalline material present is in the monoclinic α -phase, and there is also some amorphous material whose concentration is lower in the powder and annealed pellet samples. The FT Raman spectra of the three samples are given in Fig. 39 and it is evident that there are several peaks whose intensity varies with sample crystallinity. This may therefore form the basis of a method for measuring crystallinity, although possible complications may occur if β and τ crystalline phases are also present.^{82,100}

Composites of glass-fiber reinforced nylons are now assuming an increasingly important role, and the characterization of such materials is therefore of considerable interest. The Raman spectra of Nylon 6,6 in pellet and fiber forms, and also when present in a glass-fiber reinforced composite were recorded and were found to be in similar forms. Small differences occurred due to changes in crystallinity which result from the processing operations. It is clearly possible to characterize the Nylon 6,6 from the spectrum of the composite, and it is reasonable to surmise that this will be so when other nylons are involved.

3.5.2. Poly(aryl ether ketone) and poly(aryl ether ether ketone)

Poly(aryl ether ketone) (PEK) and poly(aryl ether ether ketone) (PEEK) are semicrystalline polymers with properties that make them attractive for use as high-performance engineering thermoplastics. Predictably, this has led to a search for methods to characterize their morphology. Their chemical repeat units are as follows



In this context, PEEK has attracted more attention and it will be considered first. Both X-ray diffraction¹⁰¹ and IR multiple internal spectroscopy¹⁰² have been used to assess the degree of order and, more recently, Louden has demonstrated the value of Raman spectroscopy.¹⁰³ He has shown that the spectrum changes with changing crystalline/amorphous ratio. There are changes in the position of the carbonyl stretching mode peak near 1650 cm^{-1} , the intensity ratio of the two ring mode peaks near 1600 and 1610 cm^{-1} , and the intensity ratio of peaks at 800 and 810 cm^{-1} . Louden used a dispersive Raman spectrometer and obtained

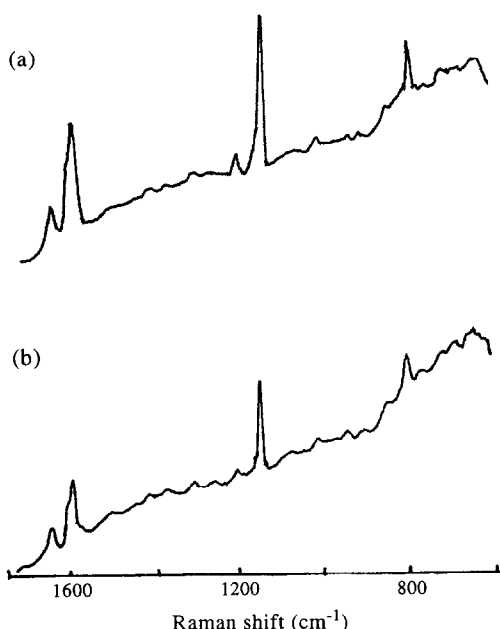


Fig. 40. The Raman spectra of (a) PEEK and (b) PEK composites containing 30% glass fiber.¹⁰⁴

spectra having acceptable quality. However, wider experience has shown that sample fluorescence is frequently a problem, a situation ideally made for the use of the FT Raman technique.

Very recently, Everall *et al.*¹⁰⁴ examined PEEK fibre samples, some of which were uniaxially oriented along the fibre direction. They found that the intensity ratio of the two peaks is also a function of the degree of orientation and its direction relative to the direction of polarization of the laser beam. When the latter is perpendicular to the fiber direction, and therefore the direction of orientation, the intensity of the peak at 1597 cm^{-1} is some 10% greater than when the direction of the polarization is parallel to the fiber direction. Everall therefore suggests that the intensity ratio method should not be used if there is any reason to believe that a degree of orientation is present in the sample being studied. They tentatively suggest that the precise position of the C=O stretching mode may prove to be a more reliable indicator of crystallinity for oriented samples. An FT Raman spectrum of PEK was obtained and its spectral quality was as good as that for PEEK. As with the latter, there is a well-defined doublet in the vicinity of 1600 cm^{-1} and the C=O stretching mode shows clear evidence for the presence of two overlapped peaks, presumably indicative of chain crystallinity subject to the orientation limitations already noted in the case of PEEK.

Both PEEK and PEK are encountered in composites with glass fibers. Figure 40 shows the FT Raman spectra of composites containing PEEK with 30% glass fibers, and PEK with 30% glass fibers. Although there is a rather strong sloping background which becomes more intense for smaller shifts, there is no difficulty in identifying the polymeric component in both cases. This technique both complements and supplements IR specular reflectance, which is particularly useful for the examination of PEEK/carbon and PEK/carbon composites.¹⁰⁵

Recently, a study of the crystallization behaviour of blends consisting of the polymers PEEK and poly(ether imide) (PEI) using FT Raman spectroscopy was reported. The annealing process of PEEK was followed for the virgin polymer and also when it was blended with

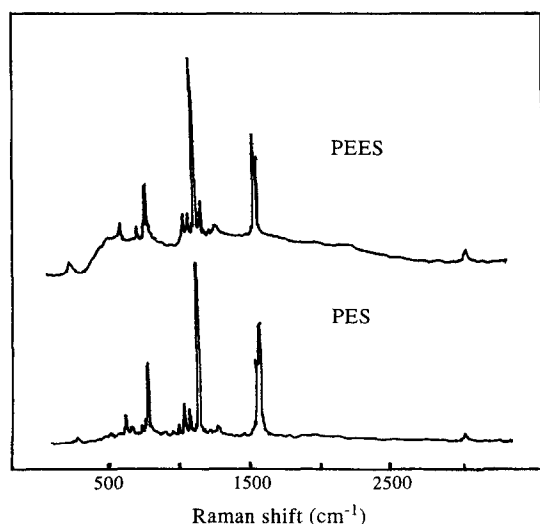


Fig. 41. The Raman spectra of PEES and PES.⁸²

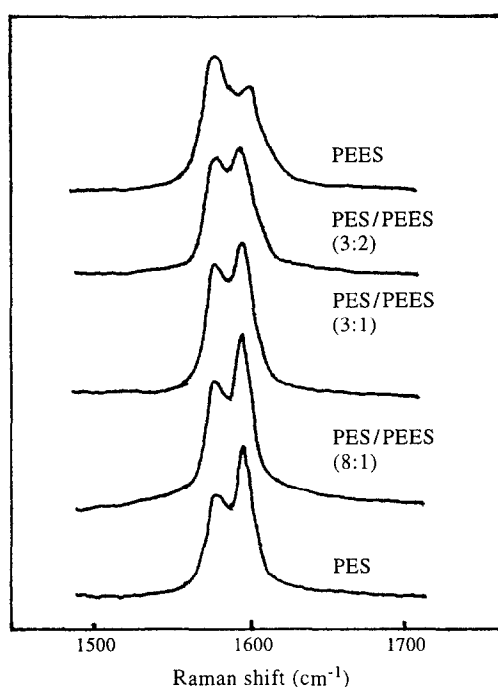


Fig. 42. FT Raman spectra for PES/PEES copolymer.⁸²

PEI. The data presented show that the crystallization process of PEEK is slow in the presence of the PEI, but the final extent of crystallinity is increased. There is also evidence that the presence of PEI induces premelting of the PEEK.^{106,107}

3.5.3. Poly(aryl ether ether sulfone) and poly(aryl ether sulfone)

These two polymers, which are referred to as PEES and PES, respectively, are similar to PEEK and PEK in that they are finding increasing use as high-quality engineering thermoplastics. Hence, it is of interest to ascertain if their Raman spectra are of value for characterization purposes.

Good-quality FT Raman spectra have been obtained without difficulty and are shown in Fig. 41. These spectra are particularly simple, markedly more so than their IR counterparts. There is an intensity inversion of the components of the doublet near 1600 cm^{-1} when the number of ether linkages in the repeat unit increases from one to two. This is particularly useful for analytical purposes as is evident from Fig. 42,⁸² which shows spectra for a series of PES/PEES copolymers over the region $1500\text{--}1700\text{ cm}^{-1}$. These spectra have been used to prepare Fig. 27 (see Section 3.1.1), which gives the intensity ratio I_{1581}/I_{1599} as a function of PES content in the copolymer. Comparable data for two other characteristic bands at 1071 and 1200 cm^{-1} are also shown. Clearly, the measurement of either of these intensity ratios provides a sound analytical method, particularly as these copolymers are substantially amorphous, and therefore not subject to possible spectral changes as the result of the crystallinity changing with copolymer composition.

The C—S—C stretching mode proves to be of particular interest in the Raman spectra of PES and PEES. In the case of the trimethylene polymer, it appears as a doublet in the vicinity of 660 cm^{-1} . With the tetramethylene and higher homologues, the doublet is shifted to 755 and 769 cm^{-1} , due to the conformational effect. Poly(trimethylene sulfide) has an all-*gauche* conformation, whereas the polymers with longer methylene sequences adopt all-*trans* conformations.

3.6. Elastomers

The analysis of elastomers, and natural rubber in particular, using FT Raman spectroscopy serves to illustrate many of the advantages of this technique. The potential of Raman for "real" rubber systems has long been appreciated.¹⁰⁸ However, conventional studies have been severely hampered by sample fluorescence. This is particularly unfortunate as the technique, with its high sensitivity for non-polar species (C=C and C—C) which make up rubber chains and the products of vulcanization, has obvious potential advantages over the complementary technique of IR absorption spectroscopy. Studies on polyisoprene and many synthetic rubbers have been limited to highly purified samples.^{109,110} Most

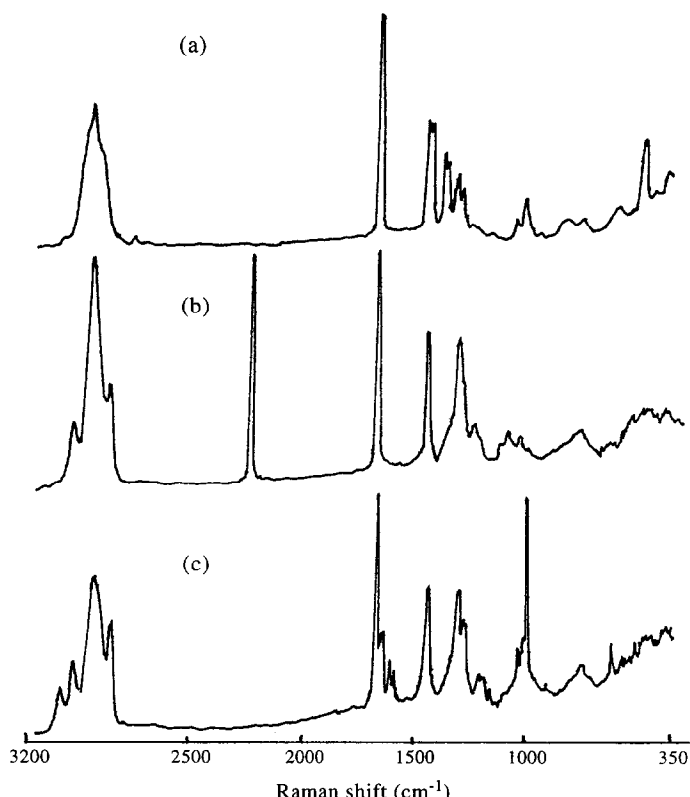


Fig. 43. The Raman spectra of (a) natural rubber, (b) nitrile rubber, and (c) styrene/¹¹¹butadiene rubber.

literature spectra are of relatively poor quality and have only been obtained after solvent extractions and techniques such as "burning out" of the fluorescence by exposing the sample to the laser excitation source for periods of up to 12 h. Near-FT Raman methods have allowed for the study of unmodified samples often taken directly from the bale. This has triggered a re-evaluation of the role of Raman spectroscopy for the evaluation of elastomers.

3.6.1. Raw rubbers

Figure 43 shows the FT Raman spectra of natural rubber and several commercial synthetic elastomers. Natural rubber contains many contaminants (such as proteins and organic matter) and is usually compounded with fillers, anti-degradants and oil for its various applications. Nitrile rubbers (NBR) and styrene–butadiene are also known to have fluorescence problems. However, Fig. 43 shows that by using the FT Raman technique, good-quality spectra can be produced. The styrene and acrylonitrile groups are clearly visible in these spectra. The major feature in the acrylonitrile spectrum is the $\text{C}\equiv\text{N}$ stretching at 2241 cm^{-1} . It is also interesting to note that the butadiene species is predominantly *trans* in the nitrile rubber.¹¹¹

Natural rubber comprises repeating isoprene units in the *cis* configuration. As reported in the literature,¹¹² different grades of rubber give essentially the same FT Raman spectrum, showing the polyisoprene chain, despite their different levels of impurities and visual appearance. Recently, Edwards and co-workers recorded the FT Raman spectra of both *cis*-1,4 and

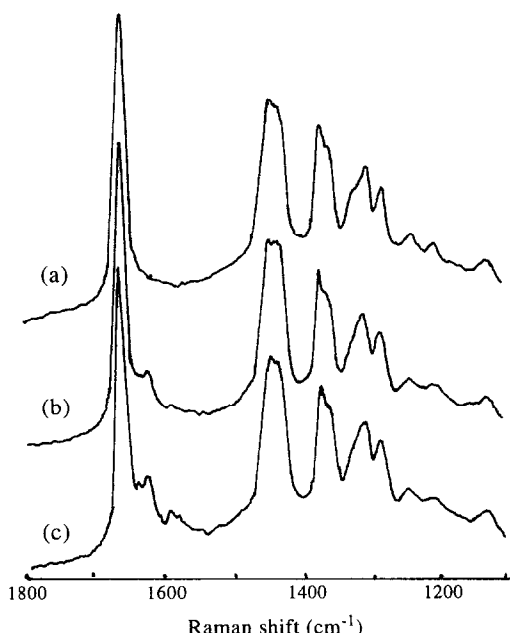


Fig. 44. FT Raman spectra of raw natural rubber (SMRL) vulcanizates prepared with (a) conventional, (b) semi-efficient, and (c) efficient cure systems.¹¹²

trans-1,4 isomers of polyisoprene.¹¹³ They found that the wavenumber positions of the *cis*-1,4 and *trans*-1,4 C=C stretching bands were slightly separated, and that these isomers could also be characterized by bands in the 1400–1250 cm⁻¹ region. In the *trans*-1,4 sample there are three bands in that region at 1384, 1326 and 1280 cm⁻¹, but in the *cis*-1,4 sample there are five bands at 1375, 1364, 1326, 1312 and 1287 cm⁻¹.

3.6.2. *Sulfur-cured elastomers*

Sulfur vulcanization is effected by the reaction of sulfur with an unsaturated polymer chain. Activators and accelerators are used to encourage the production of crosslinks, with a small degree of modification to the polymer chain per crosslink formed. This system of accelerated sulfur crosslinking is used in the vast majority of commercial applications of rubbers.

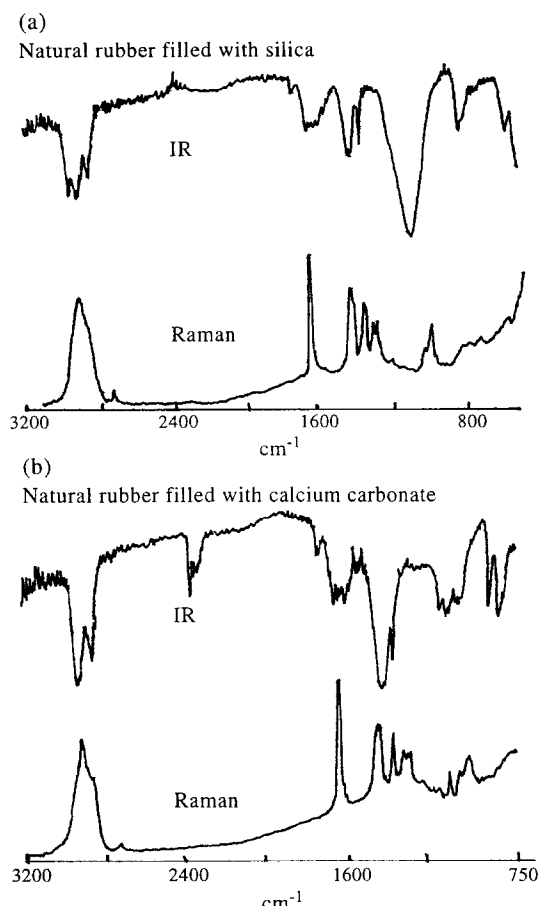


Fig. 45. ATR IR and FT Raman spectra of a natural rubber vulcanizate filled with (a) silica (50% by weight) and (b) calcium carbonate (50%).¹¹⁴

Mechanisms for the process of accelerated sulfur crosslinking have been published. These propose that polysulfidic linkages are initially formed; then, as the cure proceeds, these crosslinks are broken down to form mono- and disulfidic crosslinks. It is also thought that chain modifications, such as isomerization, dehydrogenation, double bond rearrangements and cyclic sulfide formation, increase as the polysulfidic crosslinks are destroyed and are replaced by mono- or disulfidic crosslinks. However, the evidence for this mechanism is only from indirect methods, such as probe molecules and model chemistry. Direct evidence from FT Raman spectroscopy has shown that a greater degree of chain modification is apparent in both the conventional and semi-efficiently cured samples, than in the efficiently cured samples which contain higher levels of accelerator.¹¹² This is illustrated in Fig. 44. Bands at 1623 and 1593 cm⁻¹ have been assigned to conjugated species, indicative of main-chain modifications and the destruction of sulfur crosslinks. The appearance of these bands with time of cure has also been observed.¹¹²

One interesting feature of FT Raman spectra of vulcanized natural rubber systems reported thus far¹¹² is the absence of strong bands in the region 400–600 cm⁻¹. Bands due to S–S stretching vibrations for poly- and disulfidic crosslinks would be expected in this region. The S–S stretch is strongly Raman active and should be apparent even at low concentrations. The fact that no S–S bands are apparent even in the compounded material may indicate that sulfur is no longer in its S₈ configuration after compounding.¹¹⁴

3.6.3. The effect of fillers

The constituents of a commercial vulcanizate can be separated into its major components: (1) elastomer; (2) vulcanizing system; (3) protective agents; (4) reinforcing materials and plasticizers. Reinforcing materials improve the tear and abrasion properties of the rubber as well as increasing the Young's modulus, hysteresis and creep. The most common agents are

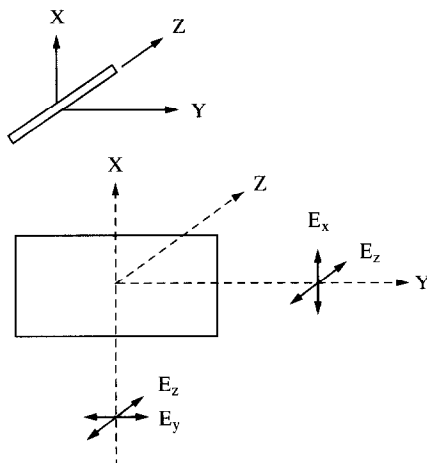


Fig. 46. Coordinate system for the Raman scattering experiment. The laser beam path is along X, with polarization along Y or along Z. The Raman scattering radiation is collected along Y and analyzed either along X or along Z.

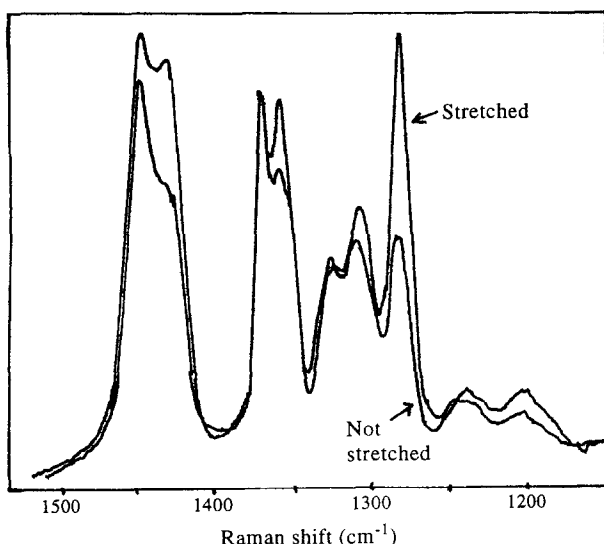


Fig. 47. FT Raman spectra of dicumyl peroxide cured rubber (stretched by 500% and unstretched).

carbon black, silica and calcium carbonate. FT Raman spectra cannot yet be obtained from samples containing carbon black because of the absorption of the excitation source and subsequent heating of the sample. Figure 45 shows the FT Raman and FT ATR-IR spectra of vulcanizates filled with silica and calcium carbonate. Both sets of spectra show that the FT Raman spectra do not suffer from the absorptions present in the infra-red, which are due to the fillers. Polar groups, such as Si–O and C=O, are not strong in the FT Raman. The bands in the Raman spectra due to the fillers are clear and sharp. Note that the filler dominates the IR spectra whereas the C=C stretch at 1665 cm^{-1} is a prominent band in the Raman spectra. This illustrates the complementary nature of Raman and IR spectroscopies, with vibrations giving strong IR absorptions being weak in the Raman spectra and vice versa.

3.6.4. Raman studies of stretched rubber

The Raman scattered radiation has directional properties governed by the symmetry of the corresponding molecular vibrations and the orientations of the molecule relative to the electric vector direction of the exciting beam, as well as the viewing direction of the spectroscopic system. In the usual Raman experiment, the observations are made perpendicular to the direction of the incident beam, which is plane polarized. The depolarization ratio is defined as the intensity ratio of the two polarized components of the scattered light that are parallel and perpendicular to the direction of propagation of the incident light:

$$\rho = I_{\perp}/I_{\parallel} = I_{x(zx)y}/I_{x(zz)y} \quad (19)$$

The symbols outside the parentheses in eqn (19) are the directions of the incident (left) and scattered radiation (right). The symbols inside denote the polarization directions of the

incident (left) and scattered light (right). Theoretically, the depolarization ratio can have values ranging from 0 to 0.75, depending on the nature of the symmetry of the vibrations. Non-symmetric vibrations have ratios of 0.75, while symmetric vibrations have depolarization ratios ranging from 0 to 0.75 depending on the polarizability changes and symmetry of the bonds in the molecule. The coordinate system for the Raman scattering experiment for a fiber is schematically shown in Fig. 46.¹¹⁵

The changes induced by strain crystallization may also be monitored. Figure 47 shows a sample of natural rubber cured with dicumyl peroxide, unstretched and extended to 500%. Large differences in the relative intensities of many of the bands are apparent. Raman scattering arises from changes in the polarizability, a tensor quantity. Hence, if there is any anisotropy in a specimen it can be monitored. Raman spectra of stretched and oriented samples can be recorded with the electric vector of a polarized laser parallel and perpendicular to the stress direction. The scattered light can then be collected through a polarization analyzer, generating still more data on the orientation of the specimen. This subject has been reviewed recently.^{1,2,116} The FT Raman evidence seems to point to the morphology of the stress-induced crystals being different from that of the low-temperature-nucleated random crystals.¹¹⁴

3.7. Paints

FT IR is well established as a useful technique for the study of paints but there are obvious areas where the results obtained are not satisfactory. IR studies of paint films tend to be restricted to reflection techniques because of strong absorption and scattering by pigments. The results of many reflection experiments have, in turn, proved to be difficult to interpret whilst quantitative measurements have been imprecise without the use of complex modeling routines. In addition, many coating materials are water-based and their spectra therefore suffer from strong absorptions in the IR which prevent useful vibrational data from being acquired.

FT Raman spectroscopy has been used to study several systems including the polymerization of water-borne emulsions which form a polymer latex, and the curing and weathering reactions that occur in alkyd resins.¹¹⁷ Because of chemical and environmental concerns, polymer latices are becoming increasingly important. They can be produced by emulsion polymerization which allows the particle size and morphology to be controlled. The mechanism of these reactions is not well understood and studying them using IR spectroscopy has always been hampered by the presence of water. Attempts at ATR IR studies were also misleading because the latex tended to deposit on the ATR crystal. FT Raman is a non-contact technique and results suggest that very dilute suspensions, down to well below 1% w/w solid, can be studied in favorable cases. Cells with small pathlength are used to study these emulsions in order to limit water self-absorption.

The degradation reactions which occur whilst paints and coatings are in service are commercially important. The photodegradation of a number of systems has been studied using FT IR, although the results obtained are generally of poor quality.¹¹⁸ In addition, TiO₂, which of course limits FT IR studies, is also thought to play an important part in the degradation reactions. It is postulated that even though it offers some protection from photodegradation by absorbing and scattering radiation, TiO₂ also acts as an oxidation catalyst in photolysis reactions. ATR can provide some useful results from weathered systems, but penetration of

the IR radiation is limited to a depth of about $2\text{ }\mu\text{m}$, and therefore it tends only to give information on those reactions which occur at or very close to the surface early in the process. In contrast, FT Raman spectroscopy probes the bulk sample. Recently, FT Raman spectra have been compared with those obtained from ATR from unpigmented, red and white acrylic polyurethane coatings used on phosphated steel panels for motor vehicles.¹¹⁷ The differences in the FT Raman spectra caused by weathering are small and unfortunately close to the noise limit. However, as instrumentation is constantly improving, more information will undoubtedly become available on these systems.

Some abrasion- and chemical-resistant paints and coatings are based on epoxy resins which are also used as adhesives and sealing agents. FT Raman studies have been carried out on the curing reactions which occur in some of these materials.¹¹⁹

3.8. *The study of gels*

One of the areas in which vibrational spectroscopy can make a contribution to our understanding of synthetic polymer structure is in the investigation of solute–solvent interactions. The study of PVC gels is just such an investigation. Gels of poly(vinyl chloride) (PVC) in solvents such as nitrobenzene or dioxane melt at temperatures around 70°C . The nature of the structure producing and stabilizing the network of the gel is not clear, most of the investigations to date having concentrated on solids produced by evaporating off the solvent. Jawhari¹²⁰ has investigated this problem by measuring NMR, IR and Raman spectra of the gels at a series of temperatures below, through and above the gel–sol transition, and complemented these with measurements on ΔH and density. He concludes, mainly based on the comparison of NMR and Raman data, that the structural change at the transition is almost exclusively relaxational and the structural network is very loose but capable of suppressing transitional motion in the gel phase.

3.9. *Thin polymer films*

Thin polymer films—which, for the present review, may be defined as having thicknesses less than about $5\text{ }\mu\text{m}$ —pose problems for Raman spectroscopy because of their very small scattering volumes, and hence low scattering intensities with conventional optical systems. Since films of both polymers and composites are becoming more important, this has prompted studies to overcome the problem.

Recently, an enhanced Raman effect has been reported for thin layers of some organic compounds adsorbed on a silver electrode in an electrolytic cell or on a roughened silver plate.^{121–125} Enhancement has also been observed for thin-layered structures by inelastic electron tunneling spectra.¹²⁶ Although these techniques have excited considerable interest and enthusiasm, the observed intensity enhancements appear to be limited to a few metals. It has long been an experimental challenge to the vibrational spectroscopist to record a Raman spectrum from ultrathin polymer films. A total reflection coupling method was described by Cipriani *et al.* and used to record acceptable Raman spectra of the CH stretching vibrations in barium stearate layers.¹²⁷ Other techniques utilize the creation of a stationary electric field from reflection at the surface of a metal substrate but suffer from inherently weak signals in the observed Raman spectra.¹²⁸ It should be noted that considerable success has been

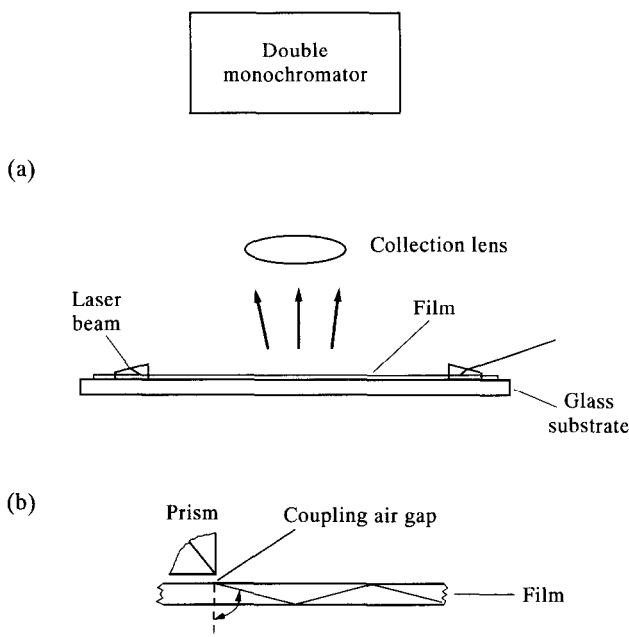


Fig. 48. (a) Instrumental arrangement for recording a Raman spectrum. (b) Laser beam coupled into a thin polymer film and undergoing multiple reflection.¹³³

obtained using infra-red reflection absorption spectroscopy where films measuring 1.0 to 1.5 nm in thickness have been examined.¹²⁹ Raman spectroscopy of ultrathin films (about 1 μm) have been successfully obtained using integrated optics.¹³⁰ Figure 48 illustrates the instrument with integrated optics and the laser beam coupled into a thin polymer film and undergoing multiple reflection. The incoming laser beam is coupled to the guide using high-index glass prisms. The prism is clamped against the film and an evanescent field traverses the coupling air gap (about 50.0 nm) and couples the light to the thin film. The thin film will conduct only for certain coupling angles, i.e. k vector values, which are solutions of the eigenvalue equation for the various modes. In these cases the beam will propagate inside the film as shown in Fig. 48(b).

The Raman spectrum of polystyrene obtained from a thin film (thickness = $1.165 \pm 0.001 \mu\text{m}$) with the guided wave technique has been compared with a normal Raman spectrum obtained from a sample in a capillary.¹³⁰ The TE spectrum (electric vector of laser is parallel to film surface and perpendicular to the plane of incidence) obtained from the thin film has a significantly higher signal-to-noise ratio and has no apparent contributions from the substrate. The improved sensitivity of this method over standard scattering geometries illustrates the potential capabilities for obtaining Raman spectra from minute amounts of material in a bilayered film arrangement. The integrated optical method for thin film studies is also called the "optical-wave-guiding technique".

Diacetylenes have received considerable attention because of their ability to form highly oriented polymers by photochemical polymerization in the solid state to form a "Langmuir-

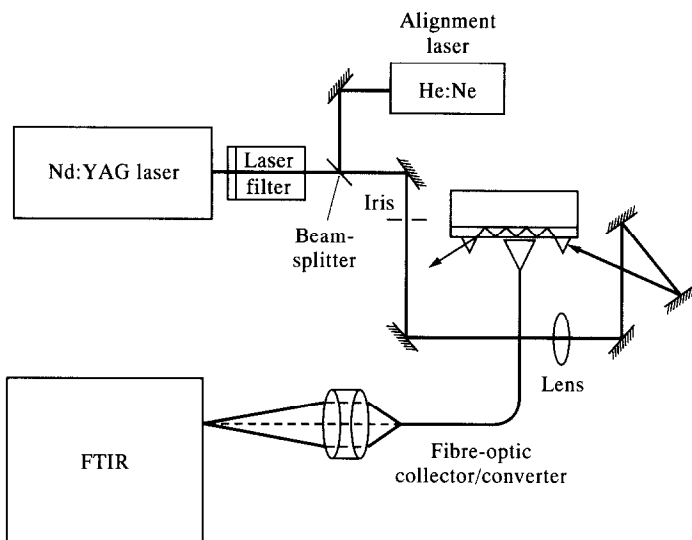
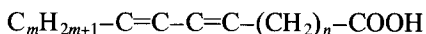


Fig. 49. Experimental arrangement used in experiments carried out by Rabolt *et al.*¹³⁵

Blodget film".^{131,132} One special group of diacetylenes has the general formula:



These amphiphilic diacetylenes form monolayer or multilayer Langmuir–Blodget (LB) films. These films are initially blue and non-fluorescent but subsequently transform to a red form that is highly fluorescent. The exact nature of this transformation is proposed to be due to the reduction of π -electron conjugation in the red form. The structural analysis and the formation of both blue and red forms in LB films have been reported by Prasad and co-workers by use of the Raman optical-wave-guide technique.¹³³ The irradiation of diacetylene films was carried out before and after the spectroscopic measurement.

Rabolt and co-workers¹³⁴ coupled their asymmetric slab waveguide to a conventional dispersive Raman spectrometer. As the laser beam traverses the film, it spreads out into an approximately rectangular pattern which is easily focused on to the entrance slit of the spectrometer. There is a critical thickness below which propagation does not occur. In the case of polystyrene and 488 nm radiation, it is about 1 μm . Although the authors obtained very satisfactory results, the technique should not be regarded as routine.

Predictably, the other problem is sample fluorescence. This has led Rabolt and co-workers¹³⁴ to explore the possibilities of an integrated system involving an FT Raman spectrometer. Changes are required for the fundamental problem relating to the fact that the refractive index difference between the polymer film and the substrate decreases with increasing wavelength, and is markedly smaller at 1064 nm than at 488 nm. This problem is not particularly acute with the relatively high refractive index of polystyrene, but is more so with poly(vinyl alcohol) and even more so with cellulose acetate. There is a need for the use of lower refractive index substrates that meet the other requirements of the technique. The

rectangular image from the exit of the waveguide is not well matched to the circular Jacquinot stop of the interferometer. However, coupling is possible via a fiber optics system. The end adjacent to the film has a rectangular cross-section and the other end is circular, so the shape of the collected scattered radiation beam changes to the required form as it traverses the fiber optics bundle. A lens then matches the exit size to that of the entrance to the spectrometer.¹³⁴

Submicrometre-thick films, including organic films, molecular composites and polymer laminates, can be studied using FT Raman in conjunction with waveguide technology.¹³⁴ Figure 49 shows the experimental arrangement used to obtain spectra from thin polymer films. When the conditions for total internal reflectance are satisfied, an evanescent wave traverses the quartz substrate and energy moves into the thin film.¹³⁵ This excites the Raman scatter, which in this case is collected by a fiber-optic probe. Of particular interest because of their non-linear optical properties are "guest/host" films. These consist of highly oriented conjugated chromophores in a thin film polymer matrix, e.g. naphthalene or 2-nitro-5-(*N*-methyl-*N*-octadecylamino) benzoic acid in a cellulose acetate matrix. Visible studies of these types of material are limited because of fluorescence and very extensive sample heating, leading to degradation.

3.10. Polymerization kinetics studies

Despite the problems involved in making quantitative measurements with dispersive Raman spectrometers, various workers have undertaken what may, broadly, be classified as kinetic studies. Most addition polymerizations involve the loss of C=C and, as C=C stretching gives a strong peak in the Raman spectrum, the quantification of polymerization reactions accounts for most of the reported kinetic studies.¹³⁶

In view of the ease with which quantitative measurements may be made with FT Raman spectrometers, kinetic studies should become relatively commonplace, and the limited work to date supports this view. Williams and Mason¹³⁷ have followed the polymerization of methyl methacrylate at 65°C, with azobisisobutyronitrile as the initiator. Their plot of conversion as a function of time shows clearly an induction period when polymerization proceeds rather slowly, followed by a much faster reaction. These workers also studied the polymerization of styrene by monitoring the decrease in the intensity of C=C stretching at 1640 cm⁻¹ and, in the light of their results, suggest that such monitoring should be possible *in situ* and on-line using fiber optics.

The polymerizations of three commercial acrylate monomers, butyl acrylate, hydroxypropyl methacrylate and lauryl methacrylate, have been examined.¹³⁸ The effects of reaction temperature, monomer addition and the presence of oxygen were all determined, and were shown to have a significant effect on the polymerization rate, particularly for butyl acrylate.

Epoxy resins are widely used in elastic, abrasion-resistant and chemical-resistant paints and coatings, and as adhesives and sealing agents. Although the curing processes of such resins are well understood on a purely empirical basis, there is a need for methods that will provide a more detailed understanding of the chemical reactions that occur, and the way that the kinetics of the curing process are influenced by parameters such as temperature. IR spectroscopy has already been utilized for this purpose, but Raman spectroscopy should prove to be superior because of the simplicity of the sampling requirements. Agbenyega *et al.* have followed the curing of Araldite epoxy resin using FT Raman spectroscopy.¹³⁹ They used the intensity of a peak at 1257 cm⁻¹ specific for the stretching of the aromatic oxygen aliphatic unit, which decreases as the reaction proceeds, ratioing it against the

intensity of an invariant peak at 1608 cm^{-1} , which characterizes the aromatic ring moiety. In the plot of this intensity ratio versus reaction time, one can find that the cure was complete in about 10 h.

De Bakker and co-workers¹⁴⁰ were able to obtain good-quality spectra for the tetraglycidyl-4,4'-diaminodiphenyl methane/diaminodiphenyl sulfone system over the entire cure cycle. They normalized the intensities of the peaks used to monitor the reaction against that of a peak which is invariant with time. The Raman results were compared with those obtained by near-IR transmission spectroscopy. There was good agreement during the early part of the reaction, but less agreement during the autocatalytic stage. This may be because the reaction is not completely homogeneous with respect to sample volume, and the FT Raman technique is probing the surface layer only. They found evidence to suggest that an impurity cyclization reaction may occur, the decrease in intensity of a peak at 1614 cm^{-1} being attributed to the formation of a cyclic hydroquinoline by-product.

4. FT RAMAN SPECTRA OF BIOLOGICAL MATERIALS

Vibrational spectra can provide useful information about the chemical compositions as well as the secondary and tertiary structures of large biological molecules. For example, some evidence for the basic amino acid sequence and its three-dimensional structure is available from the IR and Raman spectra of proteins. It has been shown that many of the building blocks of life—proteins, polypeptides, nucleic acids and saccharides—can be isolated and studied using conventional and resonance Raman techniques. However, impurities and the chromophores present in biological samples often fluoresce and some can degrade or denature when irradiated at visible wavelengths, preventing useful data from being acquired. FT Raman spectroscopy using near-IR excitation should in principle prove particularly useful for studying systems where laser-induced decomposition and fluorescence have hampered previous studies.

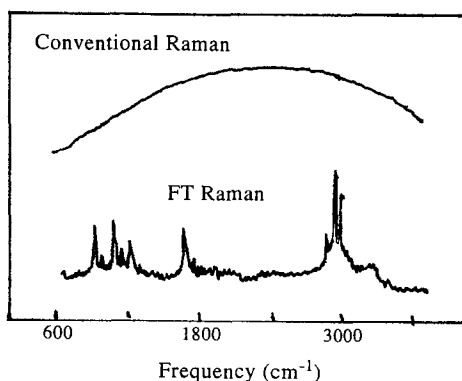


Fig. 50. Comparison of conventional and FT Raman spectra of PLA-10 (powered sample).¹⁴⁴

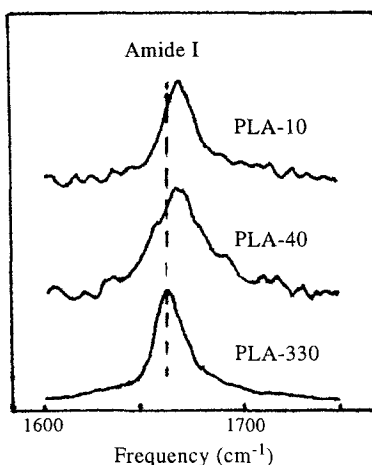


Fig. 51. Amide I region of PLA-10, PLA-40 and PLA-330.¹⁴⁴

4.1. *Polypeptides and proteins*

4.1.1. *Polypeptides*

The importance of α -helical and β -sheet structures on the function of both fibrous and globular proteins is well established. What is less well known is the interrelated role of primary and secondary structures and how these influence the tertiary structure responsible for protein function. Energy calculations do not yet have the sophistication to resolve this puzzle, but some progress is being made at the experimental forefront particularly with the advent of FT Raman spectroscopy.

Polypeptides have been studied by a number of different research groups^{141–144} but the general conclusion is clear. Isolated amino acids and crystalline homopolypeptides give FT Raman spectra of excellent quality. A typical example is illustrated in Fig. 50 where a conventional Raman spectrum of a poly(L-alanine) oligomer containing 10 peptide units (PLA-10) is compared with the spectrum obtained by using the FT Raman technique.¹⁴⁴ The fluorescent background observable in the former due to the presence of an impurity resulting from the synthetic procedure completely obscures the Raman bands. In contrast, with the use of FT IR with laser excitation at 1064 nm, no such background is present and a number of medium-to-strong Raman bands can be easily observed.

In an attempt to understand the role of the peptide sequence length on secondary structure, a series of different (10, 40 and 330) poly(L-alanine) oligomers have been studied with the FT Raman technique. Estimates of the secondary structure content of proteins and polypeptides, both in the crystal and solutions, from an analysis of the amide I ($C=O$ stretch) band have been shown to be reliable and sensitive to small changes.¹⁴⁵ Typically the amide I band for β -sheet structures is found in the 1666–1669 cm^{-1} region, while that for the α -helix is usually found at 1655 cm^{-1} .¹⁴⁶ As shown in Fig. 51, the amide I band in PLA-10 is found close to 1668 cm^{-1} , indicating that it exists in the β structure in the solid state. In contrast, the

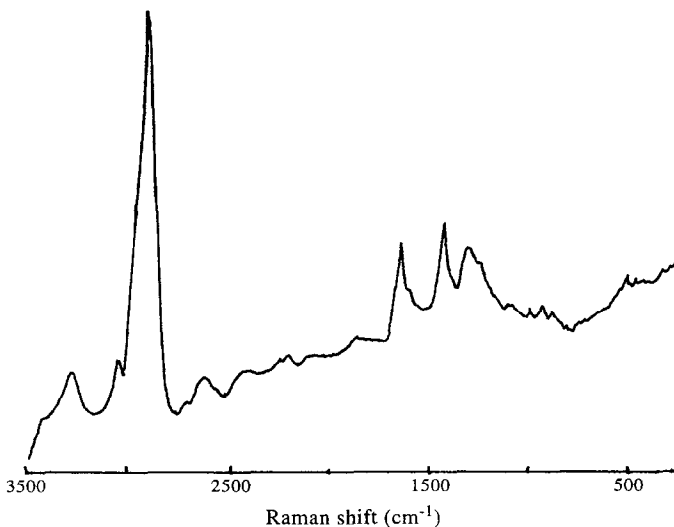


Fig. 52. FT Raman spectrum of human nail. Uncorrected data.¹⁴¹

spectrum of PLA-40 reveals that the amide I band has shifted considerably to lower frequency, suggesting that PLA-40 contains a significant amount of α -helical structure. This becomes clear in the PLA-330 spectrum where amide I is found at 1655 cm⁻¹; it is known from X-ray measurements that polypeptides which exist in the α -helical conformation have amide I bands at this position. This result is confirmed by far-IR studies.

4.1.2. Keratin

FT Raman spectroscopy using near-IR excitation has also been used to study heteropolypeptides, i.e. proteins. The spectra obtained tend to contain many overlapping bands which makes assignments difficult and limits their analytical usefulness. These materials are inevitably of low crystallinity and are often highly hydrogen-bonded. Consequently, spectral bands tend to be relatively broad. However, some information on the composition and structure of these materials is available. Naturally occurring proteins, such as the globular protein bovine serum albumin, have been investigated.¹⁴³ Although the amide I and III modes can be identified, the spectrum is very complex and band assignments are difficult. However, deconvolution routines and chemometric methods may assist in this process.

Figure 52 shows the FT Raman spectrum of human nail which contains the protein keratin.¹⁴¹ Keratin is composed of α -helical polypeptide chains which are linked by the disulfide bridges of cystine molecules. This polymer is also found in hair, birds' feathers and horses' hooves. When hair is "permmed", the disulfide bridges are first reduced, the hair is formed into the desired shape and then they are reformed in an oxidizing reaction. A novel application of FT Raman spectroscopy could be to monitor this procedure using the disappearance and return of the peaks near 490 cm⁻¹ associated with the S-S stretch.³⁴

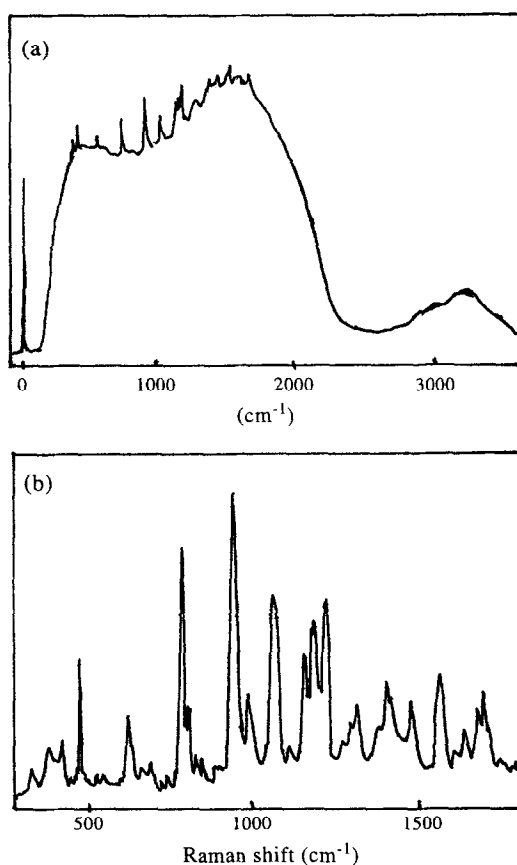


Fig. 53. (a) FT Raman spectrum of chromatophore membrane fragments of *Rsp. rubrum*.¹⁴⁷
 (b) Vibrational region 250–1800 cm⁻¹ of (a) with baseline subtracted.

4.1.3. Photosynthetic proteins

Early events of the photosynthetic process, occurring in specialized membranes, include: (1) absorption of light by specialized antenna pigments (carotenoids and chlorophyll pigments); (2) singlet–singlet energy transfer among these antenna pigments towards the central protein of the photosynthetic reaction; and (3) trapping of the singlet excitation resulting in charge separation where an electron migrates to successive acceptors. This electron migration results in the establishment of an electrochemical gradient in the photosynthetic membrane. Knowledge of the pigment–protein interactions which tune the properties of the chlorophyll pigments is of particular importance in the understanding of the primary events in photosynthesis. Resonance Raman spectroscopy has proven to be a powerful tool in the study of these interactions,¹⁴⁷ because of its selectivity in enhancing vibrational modes of specific chromophores, with distinctive electronic absorption bands, in the protein. FT Raman spectroscopy can be used as a non-damaging tool to study photosynthetic proteins and to obtain a

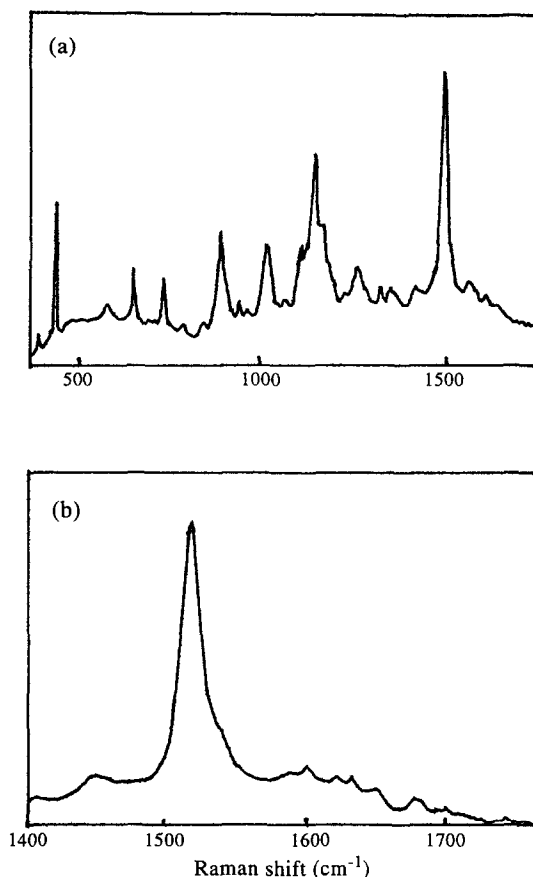


Fig. 54. FT resonance Raman spectrum of the B800-850 antenna complex from *Rb. sphaeroides*, carotenoid-containing 2.4.1 strain.¹⁴⁷

wealth of vibrational data at physiological temperatures. By exciting at 1064 nm, in many cases one may circumvent the problem of spurious fluorescence because this excitation is usually at energies lower than the radiative states of most molecules. Also, the 1064 nm excitation should not initiate photochemistry in most biological systems.^{148,149} Aqueous samples, however, may suffer from heating effects (and possibly degradation) if excessive laser power is used since water exhibits a sizeable absorption at 1064 nm.¹⁵⁰

Mattioli *et al.*¹⁴⁷ presented the FT Raman spectra of two antenna complexes which are highly fluorescent in the lowest-lying excited electronic singlet state of bacteriochlorophyll (BChl) molecules: a core antenna protein, the B880 complex from *Rhodospirillum (Rsp.) rubrum*, carotenoidless strain (G9); and a peripheric antenna protein, the B800-850 complex from *Rhodobacter (Rb.) sphaeroides* 2.4.1, which contains a spheroidene carotenoid molecule as well as three BChl α molecules. These spectra are compared with those obtained at Soret resonance at 30 K.

Figure 53 shows the FT resonance Raman (FT RR) spectrum of chromatophore membrane fragments from *Rsp. rubrum* in which both RCs and B880 proteins are present. The latter, however, outnumber the RCs by an order of magnitude.¹⁵¹ The absorption spectrum of this preparation indicates that the 880 nm absorbing BChl α species of the B880 antenna proteins is the overwhelmingly dominant chromophore. The spectrum in Fig. 53 agrees well with that published elsewhere¹⁵² and, comparing it with that of RCs from *Rb. sphaeroides* R 26,¹⁵³ indicates that, as expected, there is no evidence of RC contributions.

Figure 54 shows the FT RR spectrum of the B800-850 antenna complex from *Rb. sphaeroides* 2.4.1. The "minimal unit" of the B800-850 antenna complex contains three BChl α molecules and two carotenoid molecules.¹⁵⁴ Its FT RR spectrum also does not show any evidence of interference from protein modes. This spectrum is dominated by carotenoid modes at 1518, 1286 and 1154 cm⁻¹ which clearly indicate all-trans configuration.¹⁵⁵ The apparent lack of structure of the 1518 cm⁻¹ band suggests that the two carotenoids in the minimal unit probably assume the same configuration. Despite the fact that the lowest allowed absorption transition of spheroidene is observed at 500 nm and those of the BChl α molecules are found at 800 and 850 nm, the carotenoid modes are preresonantly enhanced to a greater extent than those of BChl α . Under similar resonance conditions, it has been estimated that the RR cross-section of the β -carotene molecule is about 50 times greater than that of a chlorophyll molecule.¹⁵⁶

FT Raman spectroscopy can readily yield direct vibrational information concerning the reduced or resting primary electron donor in bacterial photosynthetic RCs containing BChl α via a significant preresonance enhancement with this species using 1064 nm excitation. Also, for the first time, Mattioli *et al.* have obtained a resonance Raman spectrum of P in its cation radical state which sheds light on the electronic structure of this species.¹⁴⁷ This information will no doubt be useful in probing the asymmetric functioning of these RCs.

FT Raman spectroscopy should also be applicable for the study of most chlorophyll-containing photosynthetic systems and 1064 nm excitation should result in significant preresonance enhancements of these chromophores in their lowest-lying excited electronic singlet states. This is particularly important for studying the vibrational structure of the primary donor in the photosynthetic RCs of bacteria and of higher plants because P exhibits the lowest-lying electronic absorption in the purified RC and should therefore exhibit the greatest degree of preresonance enhancement.

4.2. Plant materials

4.2.1. Wood tissues

Plants are made of two broad groups of cells: the first is responsible for performing all of the metabolic activities, and the second group is metabolically inactive and functions either as a mechanical support or as a conductor of fluids through the plant. The presence of a cell wall is one of the characteristics by which a plant cell is distinguished from an animal cell. Two of the most important chemical constituents of all plant cell walls are cellulose (polysaccharide) and lignin (a complex, highly ramified polymer of phenylpropane residues). Traditional methods for investigating molecular structures in plant cell walls require prior isolation of the components, which is frequently destructive to morphology.

Raman spectroscopy has been used to provide *in situ* structural information of cellulose

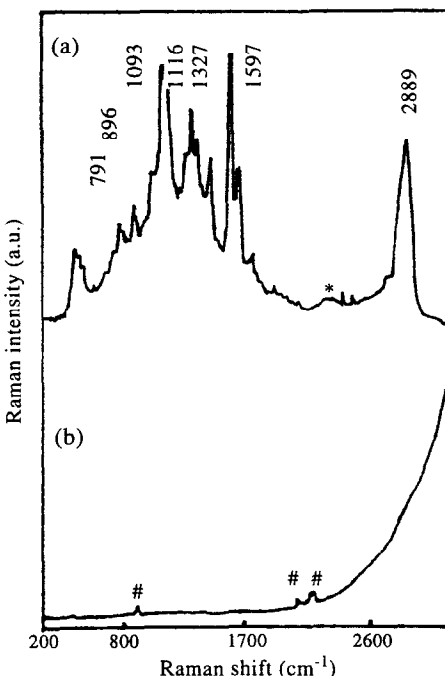


Fig. 55. Comparison of near-IR and visible Raman spectra of native birchwood tissues. (a) FT Raman spectrum excited at $1.064\text{ }\mu\text{m}$, 200 scans, 1.0 W . (b) Conventional Raman spectrum excited at 647.1 nm , laser power = 10 mW , scan rate = $2.0\text{ cm}^{-1}/\text{s}$, band pass = 4.0 cm^{-1} , # represents plasma lines, and * indicates an artifact.¹⁵⁸

fibers and wood tissues.¹⁵⁷ However, for complex native wood samples, a rather unorthodox method involving immersion of the sample in deuterated water was employed to reduce the fluorescence background, and long data acquisition times (up to 8 h) were needed to obtain a resolved Raman spectrum.¹⁵⁸ As illustrated in Fig. 55(b), the fluorescence background from a typical wood sample completely masks the weak Raman signals even with 647.1 nm excitation, but a FT Raman spectrum free from fluorescence can be obtained in less than 5 min.

Raman studies of model cellulose and lignin compounds reveal that the Raman lines of the spectrum [Fig. 55(a)] at 2889 and 1093 cm^{-1} originate solely from cellulose vibrations, and the 1656 and 1597 cm^{-1} lines are solely attributable to lignin modes, while overlapping bands of cellulose and lignin are detected at 1455 , 1373 , 1327 , 1267 , 1116 , 1038 , 896 and 791 cm^{-1} .^{158,159}

Goral and Zichy extended their study of wood samples, comparing the spectra they obtained with those from certain wood products, such as Xerox paper and tissue paper.¹⁴¹ The spectra of these woody materials were also compared with the spectra of cotton fibers. Wood contains between 40 and 50% cellulose whilst cotton fibers are essentially pure cellulose. Kenton and Rubinovitz also describe the application of FT Raman spectroscopy to wood and other forest products.¹⁶⁰ The results of a feasibility study for recording spectra from coatings on paper were also presented. A number of different paper samples were

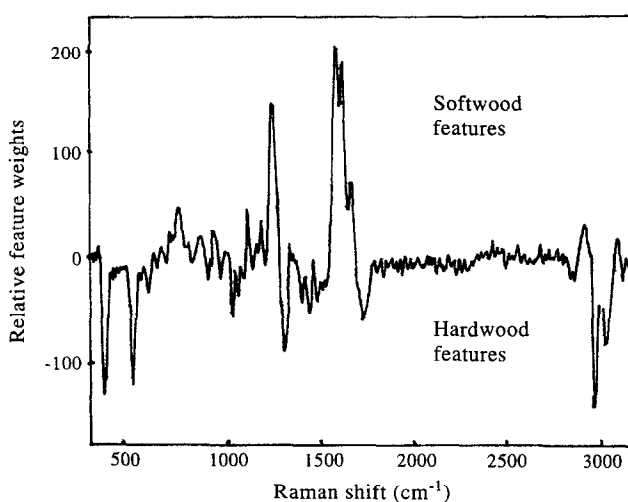


Fig. 56. Feature spectrum generated from 8 cm⁻¹ resolution spectra.¹⁶¹

studied. In one case, spectra were recorded from filter paper which had been partially covered with red ink. By subtracting the spectrum of clean white paper from that of paper impregnated with the dye, a spectrum of the pure ink was obtained. A spectrum was also obtained from a high-quality paper sample. Bands were identified due to fillers, titanium oxide and clay, and the adhesives, poly(vinyl acetate) and poly(styrene–butadiene).

Very recently, Griffiths and co-workers reported the coupling of FT Raman spectroscopy and neural computing for spectral feature extraction and the classification of woods.¹⁶¹ It was demonstrated that fluorescence rejection is accomplished only for the lighter colored woods and that fluorescence was found to be severe for 10 of the 71 woods studied in their work, even using excitation at 1064 nm. They further found that hardwoods were no more or less susceptible to sample heating than softwoods. Feed-forward neutral networks were used to extract the principal features of wood spectra and to classify spectra as either temperate hardwoods or temperate softwoods. Neutral networks were constructed using zero and two processing elements in the hidden layer. It was shown that neutral networks with two hidden processing elements perform near optimally, since each hidden layer processing element may function as either a hardwood or softwood feature detector.

Feature spectra were obtained from fully trained feed-forward neutral networks by application of a systems engineering technique known as sensitivity analysis. A sensitivity measure or spectral feature may be calculated as the partial derivative of a neutral network's output with respect to its inputs.¹⁶² Neutral networks with no hidden layer processing elements were unable to learn adequately how to distinguish hardwoods from softwoods. This was clearly evident from the neutral-network-generated feature spectrum where the signal-to-noise ratio was approximately equal to 4:1. Neutral networks constructed with two hidden layer processing elements performed significantly better, yielding a signal-to-noise ratio of about 25:1. The small learning coefficient and momentum values indicate that the hardwood versus softwood pattern recognition task is moderately difficult, as is observed by the similarity of the spectra. Figure 56 shows a feature spectrum produced from sensitivity

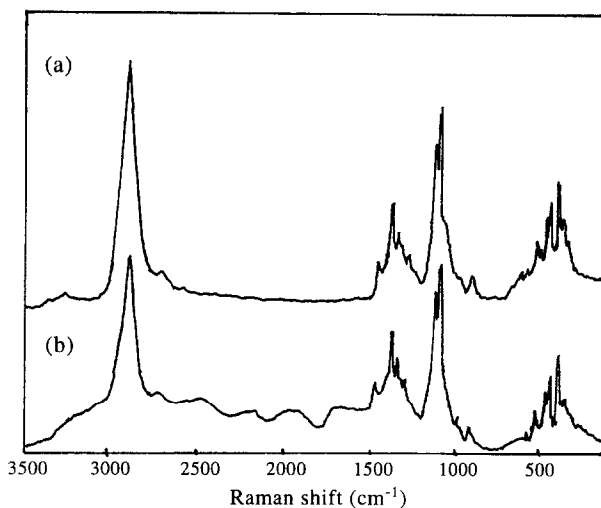


Fig. 57. FT Raman spectra of (a) natural cotton ball and (b) surgical bandage.¹⁶³

analysis of a neutral network trained on the Raman spectra of 56 good-quality spectra at 8 cm⁻¹ resolution. The positive-going features are characteristics of softwoods whilst the negative-going features are characteristics of hardwoods.¹⁶¹ This work represents the first time that FT Raman spectroscopy and neutral network technology have been coupled for spectral feature extraction and classification.¹⁶¹

4.2.2. Cotton

Cotton is unique in nature in that cellulose amounts to as much as 90% of the dry weight of the fibers. The morphological structure of the cotton boll is very complex and consists of primary and secondary fiber walls containing cuticles and fibrils. Cellulose is a polydisperse polymer of high molecular weight, typically 6×10^5 – 1.5×10^6 , comprised of long chains of α -D-glucose units joined by β -1,4-glycosidic links; the anhydroglucopyranose units are in a chair conformation which, with the β -1,4-linkages, confers a rigidity on cellulose that is not present in starch amylose with α -glycosidic links between the 1,4-anhydroglucose units. There have been several vibrational spectroscopic studies of cellulose and related materials but molecular assignments are generally incomplete. Edwards and co-workers reported the FT Raman spectra of cellulose in its natural fibrous state (American cotton boll) and as a woven fabric (surgical bandage), as shown in Fig. 57.¹⁶³ Considering the spectra of the monosaccharides (α -D-glucose), disaccharides (cellobiose, sucrose, maltose) and polysaccharides (cellulose, starch, dextran), they proposed descriptions of vibrational modes for the majority of the observed bands.¹⁶³

The FT Raman spectra obtained for natural cotton and bandage samples are identical as clearly shown in Fig. 57(a) and (b) and this indicates that minimal chemical modification has taken place for the preparation of the fabric studied here.

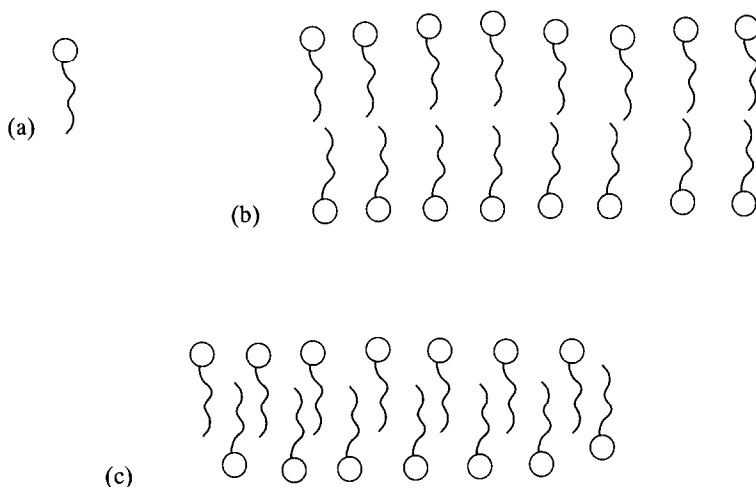


Fig. 58. Stylized diagram of (a) a lipid molecular, (b) a bilayer assembly and (c) an interdigititated model membrane.³⁴

4.3. Membranes

Membranes are an important component of all mammalian cells and are composed of lipid molecules arranged in lyotropic liquid crystalline phases. A lipid molecule contains two properties: a hydrophilic head and a hydrophobic tail, usually a long alkyl chain. A typical ordered bilayer packing geometry for these molecules is shown in Fig. 58(b). Membranes mediate the passage of materials in and out of cells. Of interest to researchers are the packing and dynamic properties of the lipid molecules which aggregate to form membranes, and their interactions with materials such as antibiotics and other drugs. In particular, information is required on the process of interdigitation which causes a degree in the bilayer thickness of model membrane systems and an ordering of the lipid chain. The resulting packing geometry is shown in Fig. 58(c).³⁴ Model lipid systems have been studied in both the gel and liquid crystalline phase using FT Raman spectroscopy.^{164,165} Real membranes, such as bovine synaptic plasma membrane, have also been studied, although the procedure should not be considered as routine.¹⁶⁶ The sample was cooled to prevent heating and it was necessary to accumulate data for more than 2 h to achieve a spectrum with an adequate signal-to-noise ratio.

FT Raman spectroscopy has also been applied to the study of a dipalmitoylphosphatidylcholine model membrane system and its interaction with the polyene antibiotics, amphotericin A and B, and nystatin.¹⁶⁴ These drugs are known to be active against fungal infections; however, the mechanism of the interaction at a molecular level is not understood. The effect of cholesterol on the interaction between the antibiotic and both the bilayer and multilamellar structures was also investigated. By analyzing the C–H stretching region, the ratio of the intensities of the symmetric in-plane methyl stretch at 2850 cm^{-1} and the asymmetric out-of-plane stretch at 2880 cm^{-1} was used to monitor the packing properties of the membrane system as the antibiotics were added. The ratio $2850\text{ cm}^{-1}/2880\text{ cm}^{-1}$

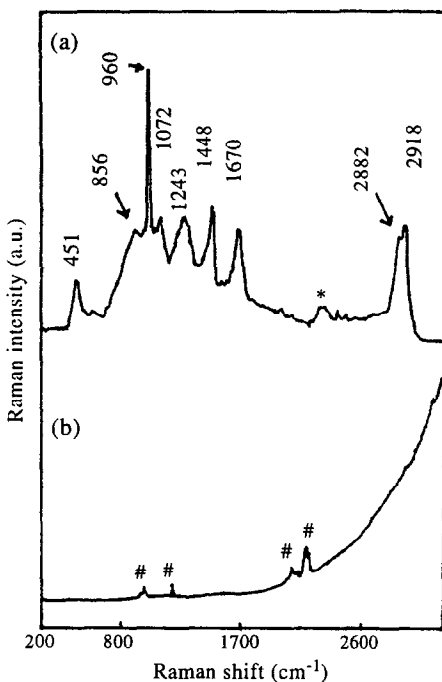


Fig. 59. Comparison of near-IR and visible-excited Raman spectra of a chicken leg bone. (a) FT Raman spectrum with $1.064\text{ }\mu\text{m}$ excitation (300 scans, 1.0 W), and (b) conventional Raman spectrum with 647.1 nm excitation. Laser power = 10 mW , integration time = 1.0 s , scan rate = $2.0\text{ cm}^{-1}/\text{s}$, band pass = 4.0 cm^{-1} , # represents plasma lines, and * indicates an artifact.¹⁵⁸

decreased, indicating a significant ordering of the chains, as the drugs were added. Cholesterol did not appear to influence the packing and/or ordering of the membrane. These observations were interpreted by Levin and co-workers^{165,166} in terms of the mechanism of formation and the structure of the lipid membrane which was thought to have undergone an interdigititation process.

4.4. Biomedical applications

4.4.1. Bone tissue

Bone derives its characteristics of firmness, rigidity and elasticity from the unique composition and organization of its matrix. Its basic structural unit is the osteon, which consists of organized lamellae of collagen that have become embedded with crystals of inorganic salts, principally of calcium and phosphate. These salts, deposited as flat crystal plates of hydroxyapatite, constitute about 70% of the bone matrix. Laser Raman spectroscopy can be employed as a non-destructive technique to provide structural information on the organic and inorganic components of an intact bone as well as to probe structural changes associated

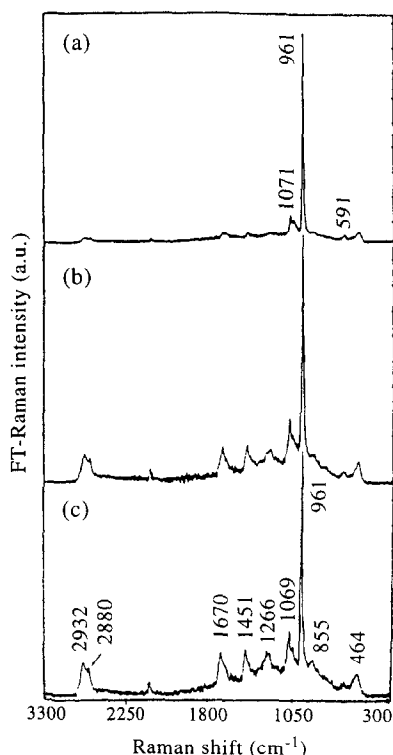


Fig. 60. FT Raman spectra obtained from a typical human tooth at several locations: (a) enamel, (b) dentine, and (c) root.¹⁵⁸

with normal bone mineralization or pathological development. However, visible Raman studies of bone tissue have been severely hampered by sample fluorescence. Yu *et al.* have obtained FT Raman spectra from chicken leg bone of excellent quality.¹⁵⁸ They illustrated the problem of fluorescence by comparing the FT Raman spectrum with one recorded using krypton 647.1 nm excitation. This diagram has been reproduced as Fig. 59. The basic structural unit of bone is an osteon composite consisting of inorganic salts embedded in organized lamellae of collagen. Over 70% of bone is comprised of the calcium phosphate, hydroxyapatite. FT Raman could be used to monitor the changes associated with normal bone mineralization and identify those which occur as the result of disease.

4.4.2. Teeth

Two sets of teeth, the milk and the permanent teeth, are acquired by human beings at different periods in life. Each tooth normally consists of three parts: the crown, which projects above the gum; the root, which is entirely concealed within the alveolus; and the neck, the constricted portion between the crown and the root. The exposed portion of the crown is covered with enamel, a thin crusta petrosa. The dental substance under the enamel is dentine, which forms the larger portion of the tooth. To better understand caries formation and to

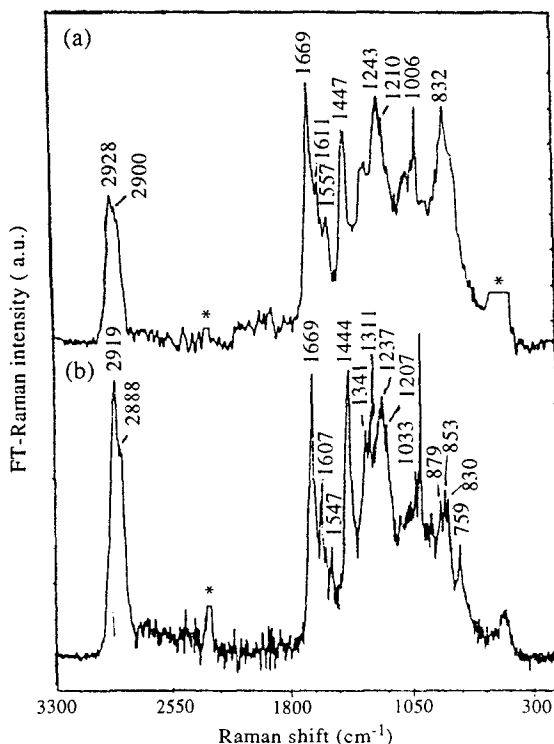


Fig. 61. FT Raman spectra of normal human lenses in intact and lyophilized forms: (a) intact human lens of an 82-year-old, and (b) lyophilized human lens of an 82-year-old.¹⁵⁸

improve oral hygiene, human tooth enamel and dentine have been extensively investigated using an array of physical techniques. Figure 60 displays fluorescence-free FT Raman spectra obtained for a human tooth at three different locations, i.e. the enamel, the dentine and the root.¹⁵⁸ The enamel spectrum is dominated by bands which can be attributed to the mineral apatite (1071 , 961 and 591 cm^{-1}). The dentine and root spectra indicate the presence of a much larger proportion of organic material. The C–H stretching bands at 2932 and 2880 cm^{-1} are more intense, and amide I and III bands at 1670 and 1243 cm^{-1} respectively have been identified. These bands correlate with those found in the FT Raman spectra of bone, indicating a similar protein conformation in the two materials.

4.4.3. Ocular lenses

The ocular lens is a highly organized, transparent, avascular organ suspended by zonular fibers between the aqueous humor and the anterior face of the vitreous body. Surrounded by an elastic capsule, the lens is composed of *ca.* 33% by weight of structural proteins (α -, β -, and τ -crystallins)—higher than that of any other organ in the body. Such a high protein content is essential for the lens to focus light, which enters the eye through the pupil, on the retina. The

physicochemical arrangement of the lens proteins is of great importance to lens transparency; the presence of a lenticular opacity (cataract) due to any aberration may lead to blurred vision or even complete blindness. The most common type of cataract found in the human eye is senile cataracts which most frequently afflict older people and may be hereditary or acquired. Raman spectroscopy has been extensively employed as a non-invasive technique to investigate the lens' normal and pathological processes at the molecular level. The determination of the lens crystalline conformation *in situ*, visual axial profiles of important chemical constituents, and *in vivo* assessment of precataractous lenses have all come from the application of Raman spectroscopy to lens research. However, conventional Raman spectra become increasingly difficult to record as the eye ages, because of the appearance of various fluorophors in the lens. These fluorophors may be of a photochemical, metabolic or pathological origin. Techniques to limit the effects of sample fluorescence, such as time-resolved studies, surface enhanced Raman scattering, resonance and non-linear Raman and photobleaching have all been attempted with varying success. Yu and co-workers have studied a large variety of eyes and have cataloged the results such that they have been able to distinguish those processes which occur naturally in the lens because of ageing from those associated with disease, in this case the development of lenticular opacity (cataracts). Differences between the FT Raman spectra relating to the formation of cataracts have been interpreted in terms of changes in certain protein conformations. The ease of use of the FT Raman technique should enable libraries of eye spectra to be accumulated and other abnormalities which occur in the lens, such as lipid peroxidation and protein glycation, to be quantified and studied.¹⁶⁷

Figure 61 shows FT Raman spectra obtained from the nucleus region of an intact 82-year-old human lens and a lyophilized 82-year-old human lens. The detailed spectral features important for studying lens aging and cataract formation are revealed in Fig. 61(b): amide I (1669 cm^{-1}), amide III (1237 cm^{-1}), tyrosine modes (830 , 853 and 1207 cm^{-1}), and tryptophan modes (759 , 879 and 1547 cm^{-1}). Spectral differences observed between the spectra in Fig. 61 are apparently attributable to microenvironmental and structural changes of the lens proteins between the intact and the lyophilized state.¹⁶⁷ The near-IR FT Raman technique makes possible the spectroscopic investigation of the pathological processes in human lenses, such as senile cataract formation, lipid peroxidation and protein glycation. These important processes are not amenable to studies by the conventional Raman method due to the presence of fluorescent materials.

FT Raman spectroscopy also allows for the study of brunescent human eyes, which absorb visible radiation, as well as pigmented animal lenses. Certain diurnal animals, such as squirrels and chipmunks, have highly pigmented lenses in order to protect the retina from UV-induced damage and to enhance the sharpness of their vision by reducing chromatic aberrations in the lens, particularly from shorter wavelength light. These pigments have prevented previous Raman studies. In addition to the study of lenses, pathological developments in other parts of the eye may also be investigated using FT Raman methods. Preliminary spectra have been observed from human and chicken eye sclera.¹⁶⁷ The sclerotic membrane is the hard firm opaque coating outside the iris which forms the white of the eye. A comparison of the two spectra indicates that chicken sclera contain a band at 963 cm^{-1} absent in that of humans. This band has been attributed to the symmetric P–O stretch in the inorganic salt apatite, which is commonly found in bones and teeth.

4.4.4. Skin

The absorption of materials through human skin is an important process which is currently receiving attention in biomedical science, particularly in the field of drug delivery. However, there are many problems associated with studies on human skin caused by difficulties in supply and standardization of post mortem or surgical samples for percutaneous absorption experiments. For this reason *in vitro* animal skins have been utilized for these studies. In recent years, those of snakes and the hairless mouse have been exploited.¹⁶⁸

Biomedically and chemically, the use of shed aquamate epidermis as a model membrane for human skin has several advantages, one of the most important being a plentiful supply obtained by natural shedding from the animal without killing it.¹⁶⁹ Another useful feature of shed snake skin, unlike that removed surgically from human cadavers, is the absence of biohazards. Barry and co-workers reported their research results of FT Raman microscopic and FT IR studies of the shed skin of the American black rat snake, which has been used in permeability barrier tests for chemically enhanced drug delivery, as well as simple drug diffusion studies.^{168,170}

Snake epidermis has a complex structure based on a hinge and scale construction. Based on the Raman and IR spectroscopic studies, Barry and his co-workers believe that the hinges consist primarily of flexible β -keratin and that the scales contain keratin folds with entrapped pigmentation. Beneath the keratin layer are regions of lipid lamellae. It seems that the biomedical applications are important at the molecular level for the assessment and evaluation of the effect of drug permeation and chemical treatment of skin for drug delivery enhancement.¹⁷⁰

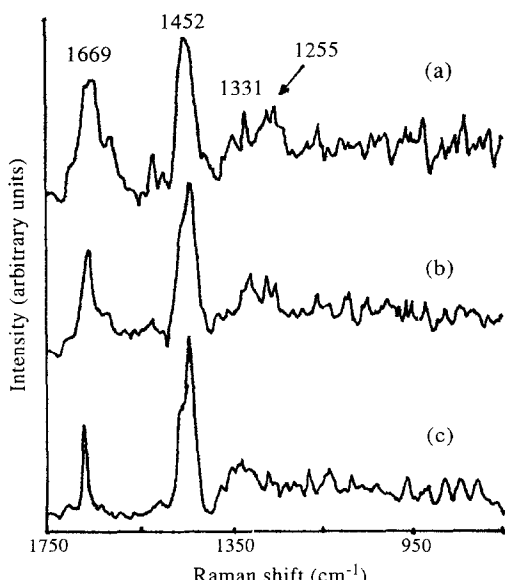


Fig. 62. FT Raman spectra of human aorta: (a) normal artery, (b) atheromatous plaque, and (c) solid cholesterol.¹⁷¹

4.4.5. Arteries

Many people die each year because of heart attacks, nearly all attributable to coronary atherosclerosis. Several treatments for atherosclerosis are available, but no reliable method exists to determine how each patient will react to the particular therapy chosen. The *in situ* biopsy of blood vessels is difficult and thus detailed information on the state of the diseased vessel is limited. It has been demonstrated that FT Raman spectroscopy can provide information on the molecular level changes which result due to atherosclerosis in the human aorta. Rava *et al.* have carried out an FT Raman study of healthy and diseased human arteries, as shown in Fig. 62.¹⁷¹ In normal human aortas, two bands at 1669 and 1452 cm⁻¹ dominate the spectrum and can be assigned to protein amide I and C—H in-plane bending vibrations, respectively. Weaker bands are also observed between 1250 and 1350 cm⁻¹. Non-calcified atherosclerotic lesions with a large amount of necrotic debris below the tissue surface show a relative increase in the intensity of the 1452 cm⁻¹ band. In atherosclerotic aortas which contain calcified deposits several hundred micrometres below the tissue surface, a strong 961 cm⁻¹ band is observed due to the symmetric stretch of phosphate groups in the calcified salts. Changes in the spectrum associated with an initial build-up of cholesterol in the inner layer of the aorta (the intima) can also be identified. Other differences between the spectra of healthy and atherosclerotic tissue are attributed to the accumulation of calcium and the formation of calcium hydroxyapatite crystals in the tissue below the surface. This is thought to occur in the advanced stages of the disease. Information on the increased levels of cholesterol and calcium should eventually enable physicians to prescribe the correct treatment for each patient.

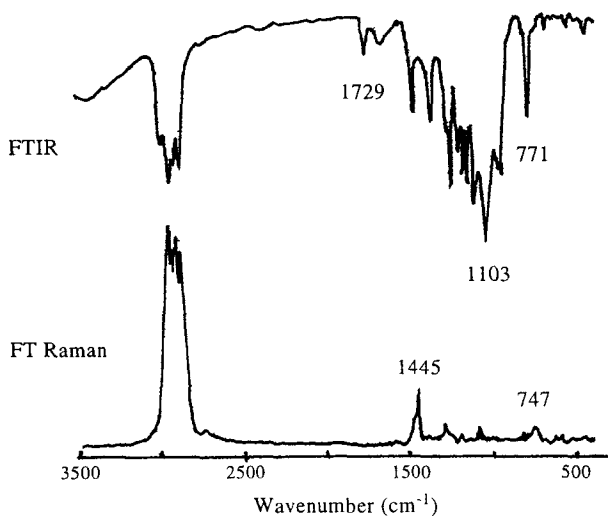


Fig. 63. Comparison of the FT IR spectrum and FT Raman spectrum of polymer IB, pentane 1,5 diol.¹⁷⁵

4.5. Biodegradable polymers

Biodegradable polymers such as polyanhydrides, polyesters and poly(ortho esters) have received substantial interest in the field of pharmaceutical science for the controlled release of drugs in clinical applications.¹⁷² These polymers contain a biodegradable functional group within the repeat unit which facilitates programmable degradation kinetics that can dictate the release of any drug over a specific period of time.¹⁷³ Poly(ortho esters) exhibit pH-sensitive degradation involving chain scission in an acidic environment. The addition of basic salts or acidic functionalities within the polymer structure is known to influence the local pH within the polymer matrix and hence may be employed to retard or promote the degradation rate as necessary. Consequently, a considerable body of work has demonstrated that the formulation of the polymer may be manipulated, allowing precise programming of the degradation kinetics. This degradation process is surface mediated and whilst, studies on the interfacial chemistry of the biomedical poly(ortho esters) have been reported recently, little information is available on the bulk solid-state vibrational spectroscopy of such systems. Recently, Tudor and co-workers examined polyanhydrides and their subsequent hydrolytic degradation, and a range of poly(ortho esters) homopolymers and copolymers using near FT Raman spectroscopy.^{174,175} Figure 63 shows FT IR and FT Raman spectra of a poly(ortho ester) (Polymer IB, pentane-1,5-diol). They demonstrated the potential application of FT Raman spectroscopy for the analysis of a range of complex orthoesters. While the technique is sensitive to changes in the methylene groups within the orthoester structure, the ether bonds arising from the diol and orthoester unit, which are relatively poor Raman scatterers and which are readily observed within the FT IR spectra, were undetected. However, FT Raman was shown to be sensitive to the nature of the diol employed. Semiquantitative relationships were obtained for the homopolymers as a function of the methylene number in the diol and the phenyl content in the copolymers. Such studies contribute to an increasing body of work which suggests that peak ratios can reflect bulk composition in a semiquantitative manner.

4.6. Foodstuffs

The examination of food products is challenging to the analyst. In many cases, “wet chemical” tests remain the only way to characterize certain products. For example, the unsaturation level in a fat-containing food is measured by titration with iodine to give an “iodine number”. Sadeghi-Jorabchi *et al.* have demonstrated that FT Raman spectroscopy can be used to give a quantitative measure of the level of unsaturation and also the ratio of *cis* to *trans* isomers.¹⁷⁶ Dispersive Raman spectra of oils and fats are highly fluorescent. FT IR spectra of a number of oils and fats have been recorded and the weak 1660 cm⁻¹ peak due to the C=C stretching mode was used to determine the degree of unsaturation in the sample. This method is unreliable for the case of margarines which contain water and therefore suffer from a strong absorption at 1660 cm⁻¹ due to the O–H bending vibration. FT IR spectra can yield an estimation of the concentration of the *trans* isomer, but no independent measure of the *cis* isomer content is possible.

The derivation of oils and fats to methyl esters followed by analysis using gas chromatography (GC) is the standard method of estimating the fatty acid composition of lipids and of also determining the degree of unsaturation as well as the ratio of *cis* to *trans* isomers. Results available from the technique have been compared with those derived from FT Raman

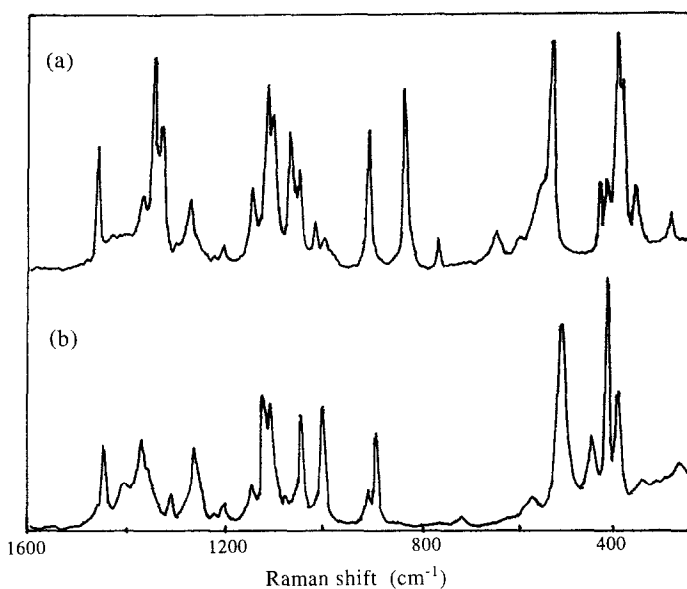


Fig. 64. FT Raman spectra of (a) α - and (b) β -D-glucose.¹⁴¹

studies.¹⁷⁶ It has been noted from GC studies that hydrogenation, a process involved in converting an oil into a margarine, causes not only a decrease in the total degree of unsaturation, but also a decrease in the ratio of the *cis* polyunsaturate to *cis* monounsaturate content, with a concurrent increase in the concentration of *trans* monoenes. The results are confirmed by FT Raman studies. The band ratio of C=C stretching (band area recorded between 1700 and 1601 cm^{-1}) to the C=O stretching (band area between 1790 and 1713 cm^{-1}) decreases with the total level of unsaturation in the sample. The band recorded at 1265 cm^{-1} correlates with the concentration of the *cis* isomer in the sample. The decrease in the ratio of the *cis* polysaturation to *cis* monosaturation is reflected in the shift in the *cis* C=C stretching band from 1657 to 1655 cm^{-1} . The appearance of a shoulder at 1666 cm^{-1} indicates the increase in the *trans* isomer content on hydrogenation. Problems are encountered, however, in reliably measuring the *trans* content at low concentrations, i.e. below 20%. The correlation between the GC results and those obtained using the FT Raman method was excellent for the standard lipid samples and mixtures; however, it is suggested that real systems will benefit from the application of sophisticated multicomponent analysis routines, such as CIRCOM, which are now becoming available to assist particularly with the estimation of the isomer content.³⁴

Carbohydrates are an important group of compounds which include mono-, di-, and polysaccharides, starch, glycogen, and cellulose. Raman analysis of these compounds, and in particular naturally occurring saccharides, has traditionally been limited because of the problems associated with a weak signal and sample fluorescence. Goral and Zichy have studied a number of carbohydrates using FT Raman spectroscopy.¹⁴¹ Comparing the spectrum of α -D-glucose with that of β -D-glucose in Fig. 64, it is most surprising that the spectra contain so many differences. Intuitively one would expect the spectra to be very similar

because the two compounds have almost identical structures. However, large spectral changes as a result of minor structural changes are a general observation for saccharides. Thus, FT Raman spectroscopy appears to have great potential for use as a routine analytical technique for studying these compounds.

5. FT SURFACE-ENHANCED RAMAN SCATTERING (SERS)

5.1. *SERS spectra of polymers*

The observation of enormously enhanced cross-sections (up to 10^6) for Raman scattering from molecules adsorbed on metal surfaces is one of the most important discoveries in the field of surface science in the past few years.¹⁷⁷⁻¹⁸⁴ Surface-enhanced Raman scattering (SERS) was first observed for pyridine monolayers adsorbed onto electrochemically roughened silver electrodes.¹⁷⁷ Since then, there has been tremendous interest in this subject. Most of the research reported in the early studies was devoted to understanding the mechanisms responsible for SERS and, although many theories have been presented, it seems likely that most SERS is associated with two mechanisms. One of these is related to relatively long-range electromagnetic resonances within metallic substrates which enhance the electric field at the surface. The other is related to the formation of so-called charge-transfer complexes between adsorbed molecules and the substrate which causes a distortion of the polarizability of the molecules. The charge-transfer mechanism is associated with defect sites¹⁸⁵ or sites of atomic-scale roughness that cover 3% of the surface of an SERS-active substrate.¹⁸⁶

Despite the enormous interest in understanding the mechanism of SERS, only recently has there been intense interest in the development of practically useful sample systems for the identification and characterization of adsorbed species. This tendency seems to reveal that it is worthwhile to initiate analytical or catalytic studies on SERS-active surfaces even without a complete understanding of the SERS process. For a suitably prepared silver surface, SERS amplifies the Raman cross-sections by a factor of more than 10^6 .¹⁷⁸ The SERS effect has been observed for an increasing number of metals. Within the group of coinage metals, the enhancement drops in the order Ag > Au > Cu. SERS has a significant potential for use in surface reactions and mechanistic studies of heterogeneous catalysis.¹⁸⁷

Although several different mechanisms for the SERS effect have been proposed, a general agreement was reached that the surfaces of metals need to be roughened properly in order to get excellent enhancements. Silver substrates on which the SERS effect is observed most intensively include colloidal silver, silver island films (Ag/CaF₂), silver films deposited on quartz or Teflon particles, roughened electrodes,¹⁸⁸⁻¹⁹⁰ and chemically reduced silver films on glass slides.¹⁹¹ In each case, the metal can be prepared independently of the sample. The sample can be mixed with a suspension of colloid or coated particles, or spotted on a plate containing silver island films. Colloidal silver, gold and copper have been the most widely employed, possibly because their preparation requires no specialized apparatus. With respect to the aforementioned substrates, it has been difficult to obtain reproducible enhancements that are stable for long periods of time under elevated temperatures. These problems hinder widespread acceptance of SERS as a technique for the mechanistic investigations of polymer–metal interfaces.

Recently, a simple substrate preparation involving etching of the metals with nitric acid

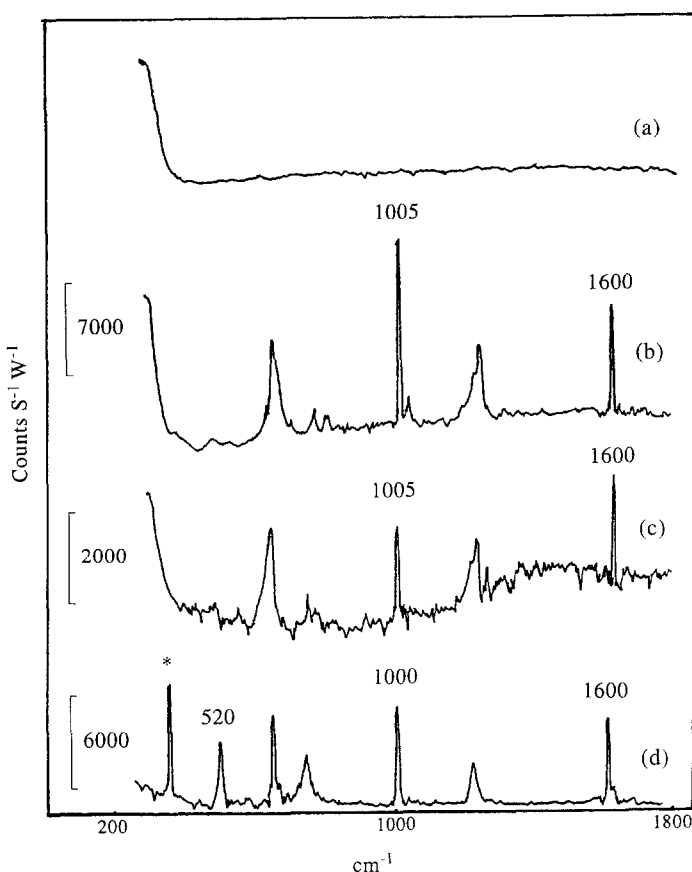


Fig. 65. (a) SERS spectrum of nitric acid etched silver without adsorba. (b) SERS spectrum of benzyl on HNO_3 etched silver. (c) SERS spectrum of benzyl disulfide on Ag/CaF_2 substrate. (d) Normal Raman spectrum of benzyl disulfide in chloroform solution (0.5 M); * indicates the bands of chloroform.

was reported by Xue and others.^{187,192-196} They demonstrated that the chemical etching method has the potential to be developed into an analytical tool for a routinely preparable substrate system suitable for SERS studies. In order to establish the versatility of this sampling technique, Raman measurements were undertaken after the sample substrates had been exposed to different environmental conditions.¹⁹⁷

In order to find the enhancement factor for Raman scattering from the nitric-acid-etched surfaces, a series of SERS spectra was recorded for adsorbed benzyl disulfide.¹⁹⁸ The etching procedure is quite simple. A 0.025 mm thick silver foil was immersed into vigorously agitated 4 M HNO_3 at ambient temperatures for a few minutes until the foil had a milky surface. This procedure created a sponge-type surface with abundant roughness on a 10–100 nm scale as shown by scanning electron micrographs. After etching, the foil was thoroughly rinsed with distilled water and dried in air. The roughened foil was then ready for sample doping.

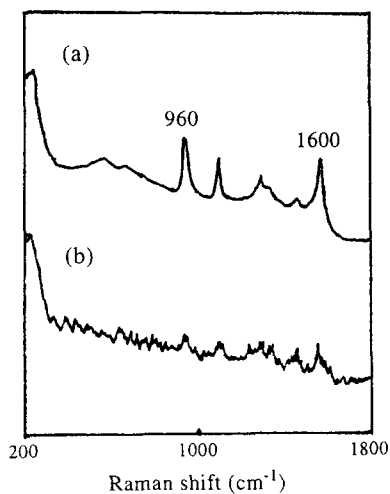


Fig. 66. SERS spectra of poly(4-vinyl pyridine) after heating at 130°C for 12 h: (a) on HNO₃-etched Ag foil; (b) on a vacuum-deposited Ag/CaF₂ substrate.²⁰²

For etching copper foil, a 2 M nitric acid solution was used as the etching medium. Figure 65(a) shows a Raman spectrum recorded from an etched silver foil without any adsorbate, where no significant peaks could be observed. An excellent SERS spectrum was obtained from the monolayer benzyl disulfide on an etched surface as shown in Fig. 65(b). For comparison, the SERS spectrum on Ag/CaF₂ substrate is in Fig. 65(c). A normal Raman spectrum of benzyl disulfide was recorded from its chloroform solution (0.5 M concentration) and is shown in Fig. 65(d).

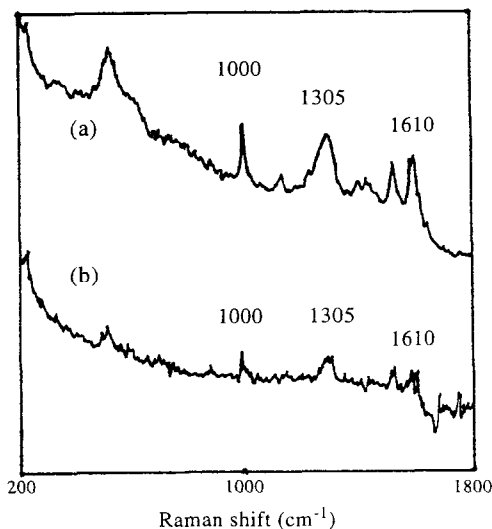


Fig. 67. SERS spectra of polybenzimidazole on metals after heating at 130°C for 8 h: (a) on HNO₃-etched Cu foil; (b) on vacuum deposited Ag/CaF₂ substrate.²⁰⁴

All Raman spectra in Fig. 65 were recorded with a SPEX-1403 Raman spectrometer. The incident laser excitation wavelength was 647.1 nm from a Kr⁺ laser source, with an output of 40–200 mW. A back-scattering collection geometry in air was used. The Raman band intensities are reported in counts s⁻¹ W⁻¹ to account for the different laser powers and integration times. In order to ensure that there is no laser-induced change in the SERS spectra, the foil was spun during the spectrum measurement.

The Raman line at 520 cm⁻¹, due to the S–S stretch, exists in the normal Raman spectrum in the chloroform solution [Fig. 65(d)], but disappeared in the SERS spectrum [Fig. 65(b) and (c)], indicating the breakage of the S–S bond. This is consistent with the previous finding that disulfides, on coinage metal surfaces, split and form R–S–metal surface bonds.¹⁹⁹ The enhancement factor for the sharp ring mode at 100 cm⁻¹ was estimated by comparing the SERS intensity and surface coverage to those in solution. Following the procedure in another reference,²⁰⁰ Xue *et al.* obtained an enhancement per molecule of 1.4×10^6 on a nitric-acid-etched silver foil and an enhancement factor of 4.5×10^5 on the vacuum-deposited Ag/CaF₂ substrate. The signal-to-noise ratio of the SERS spectrum in Fig. 65(b) is obviously larger than that in Fig. 65(c), confirming that the nitric-acid-roughened silver foil exhibits a stronger enhancement than Ag/CaF₂.

It is important for the substrates to remain stable after reasonably long times or after heating in order to apply SERS as an analytical tool for catalytic studies. Figures 66 and 67 compare the thermal stabilities of the surface enhancement factors of polymers on metals. After heating, the nitric-acid-roughened silver or copper foil could still produce good SERS spectra for polymer samples, while the vacuum-deposited silver island film lost almost all of its enhancement. The good enhancement factor and high stability of the nitric-acid-etched metal foils indicate that SERS has a good potential for use as a general analytical tool for the study of the adsorbed materials under various conditions.

In the field of polymer characterization a few SERS spectra have been reported.^{201–208} Lee and Meisel recorded SERS spectra of poly(vinyl pyridine) adsorbed onto silver and gold colloids.²⁰³ They observed the strong band characteristic of the symmetric ring breathing vibration at 1014 cm⁻¹ in the SERS spectrum. There was no indication of a band near 1025 cm⁻¹ which is usually attributed to a pyridinium ion or to pyridine chemisorbed at Lewis acid sites, and it was concluded that poly(vinyl pyridine) was physisorbed by bonding through the π system and with the pyridine rings parallel to the substrate. Boerio and Tsai reported the SERS spectrum from poly(4-vinyl pyridine) adsorbed onto silver island films.²⁰¹ Strong bands were observed near 1613, 1219 and 1020 cm⁻¹ in the SERS spectra and were assigned to vibrational modes $\nu_{(8a)}$, $\nu_{(9a)}$ and $\nu_{(1)}$, respectively. Moskovits showed that the most intense lines in the Raman spectra of compounds adsorbed at metal surfaces corresponded to modes belonging to the same symmetry species as α_{zz} , where z is perpendicular to the surface should be especially intense in the spectra. For pyridine moieties with C_{2v} symmetry adsorbed with their twofold axes perpendicular to the surface, modes $\nu_{(8a)}$, $\nu_{(9a)}$ and $\nu_{(1)}$ belong to the symmetry species A₁, as does α_{zz} , and involve motions mostly perpendicular to the surface. Therefore, it was reasonable to conclude that the pyridine rings were adsorbed through the nitrogen atoms with a vertical conformation. The ring-breathing mode $\nu_{(1)}$ shifted from near 997 cm⁻¹ in the Raman spectrum of poly(vinyl pyridine) to 1020 cm⁻¹ in the SERS spectra, due to coordination of pyridine rings or to formation of pyridinium ions, providing additional evidence that the pyridine rings were adsorbed through the nitrogen atoms.

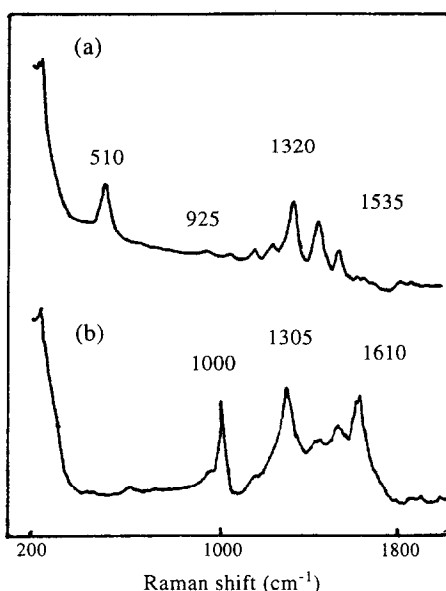


Fig. 68. SERS study of the orientation transition of polybenzimidazole on silver: (a) before heating; (b) after heating at 130°C for 6 h.²⁰⁴

Very recently, Xue *et al.* recorded SERS spectra of polymers on nitric-acid-etched silver foils. They found that different sampling techniques resulted in different molecular orientations. As a dilute solution, 0.04% of poly(vinyl pyridine) was spread onto a silver foil and the solvent was evaporated slowly. The ring of pyridine was observed to reside down flat on the surface. If the foil was dipped into a hot solution of the polymer, the SERS spectra indicated that the ring was standing up on the surface. Xue also reported that two molecular orientation states of poly(L-histidine) could be observed in SERS spectra from the solutions of different solvents.²⁰⁹ The orientation transition of polybenzimidazole was observed by SERS. Fig. 68(a) shows an SERS spectrum of polybenzimidazole applied onto a roughened silver foil by a “spread-casting” method. After heating the sample at 130°C for 6 h, an SERS spectrum was recorded again, and as shown in Fig. 68(b). In the Raman spectra of heterocyclic compounds, the bands at 1000 and 1600 cm⁻¹ are due to in-plane ring bending and stretching modes, respectively, and the band at 510 cm⁻¹ is due to out-of-plane vibration involving a changing dipole moment which is perpendicular to the plane of the molecule. In contrast, the change of dipole moment accompanying an in-plane vibration is parallel to the plane of the molecule. In the SERS spectrum of Fig. 68(a) the out-of-plane vibration of the ring at 510 cm⁻¹ is enhanced, but the in-plane vibrations are very weak, indicating that the rings of the polybenzimidazole chain are lying down flat on the surface. In the SERS spectrum of Fig. 68(b), the in-plane vibrations of the ring at 100 and 1600 cm⁻¹ are intensified, but the out-of-plane vibration at 510 cm⁻¹ is absent. On the bases of surface selection rules, it was proposed that the aromatic ring of the polybenzimidazole chains were standing up on the surface after heating the sample. Based on the spectral changes in Fig. 68,

the flat bonding geometry of the aromatic ring (π -bonded to the surface) translated to a bonding through the nitrogen lone pair (N -bonded through π -donation); as a result, the rings are standing up. However, the SERS study did not find any evidence that the "standing" ring could translate to the flat binding geometry, suggesting that the N -bonded geometry is more stable than the π -bonded orientation.

Suh and Michaelin have observed SERS spectra of acrylamide and polyacrylamide adsorbed onto silver colloid particles.²⁰⁴ The CH stretching vibration modes were at considerably lower frequencies for acrylamide adsorbed onto silver colloid particles than for the monomer in aqueous solutions, indicating that acrylamide polymerized on the surface of the silver particles. Differences were also observed in SERS spectra of acrylamide polymerized on colloidal particles and of polyarylamide adsorbed onto the particles, perhaps because of the different surface geometries of the two samples of polymer.

One of the problems associated with SERS of polymers has concerned the appearance of strong bands near 1375 and 1575 cm^{-1} . These bands were first observed by Otto in SERS spectra of cyanide ions adsorbed at silver electrodes and attributed to the formation of surface carbonate.²⁰⁵ Tsang used Auger electron spectroscopy to show that SERS samples for which the bands near 1375 and 1575 cm^{-1} were observed

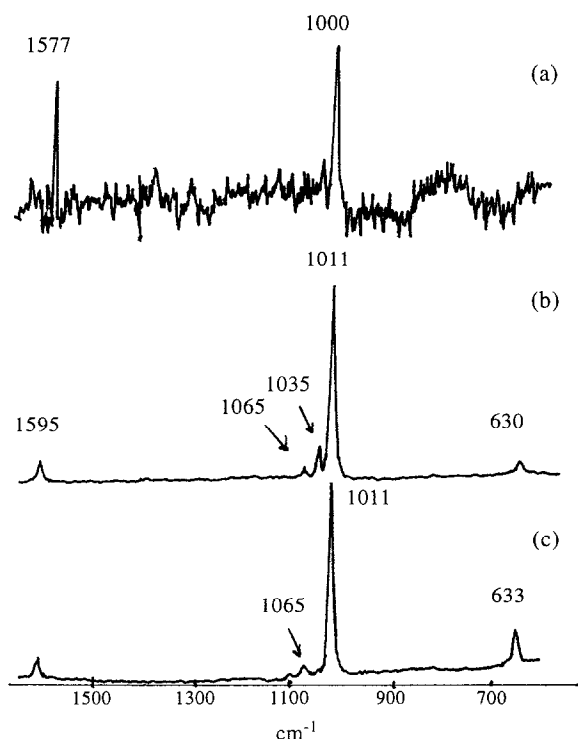


Fig. 69. FT near IR SERS spectra of 0.5 M pyridine in 0.1 M KCl solution adsorbed on to (a) platinum, (b) gold and (c) copper electrode.³⁴

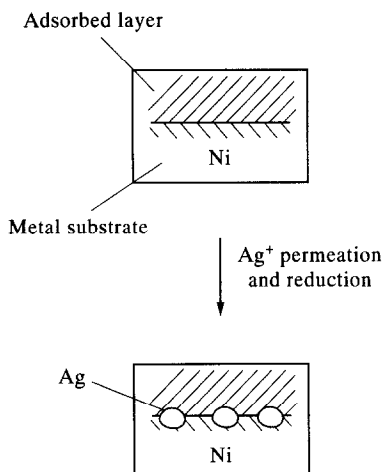


Fig. 70. Schematic diagram of doping silver particles in the nickel/adsorption interfacial region by Ag^+ permeation and displacement reaction.²¹²

contained too little oxygen to be due to carbonates and attributed the bands instead to amorphous carbon formed on SERS-active substrates by the decomposition of organic compounds.²⁰⁶

Boerio and co-workers showed that decomposition of polymers during SERS experiments, apparently due to oxidation catalyzed by the metal substrate, could be reduced if the polymer film was overcoated with a thin film of a second polymer having a small cross-section for Raman scattering.^{207,208}

5.2. Near-infrared FT Raman SERS studies

There are several good reasons for attempting to excite SERS spectra with a near infra-red laser. Theories describing the mechanism of SERS enhancement are not yet fully comprehensive. Hence, observation of SERS and the measurement of SERS enhancement factors in the near-IR provide useful experimental data with which to compare to theoretical predictions. Also, in electrode studies using a visible laser, species adsorbed onto the electrode have been shown to be both generated and removed by laser radiation. As the photon energy in the IR is reduced, photochemical changes are less likely to be induced by the laser. SERS spectra frequently appear over an intense background which varies in intensity with the number of ORCs used in preparing the SERS surface. Again, by moving to near-IR excitation, this background might well be reduced, thus improving the signal-to-noise ratio in the spectra.

The first near-IR FT Raman spectra obtained showing the SERS effect were reported by three independent groups in 1988 and all used electrodes as SERS substrates. Chase and Parkinson²¹⁰ studied pyridine on silver and gold, while Angel *et al.*²¹¹ studied pyridine on copper and gold, and Crookell *et al.*¹⁹⁷ studied pyridine on silver, copper and gold. All three groups used FT Raman systems with an Nd:YAG laser. The SERS spectrum of pyridine adsorbed onto an electrode surface has been extensively investigated with visible excitation

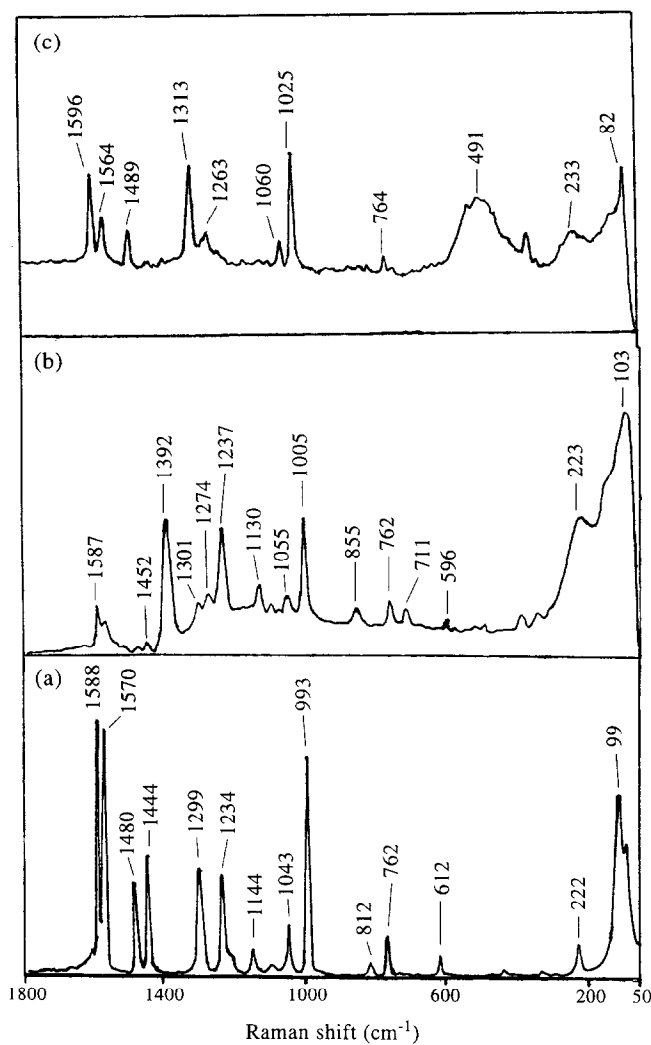


Fig. 71. (a) FT Raman spectrum by BPY recorded after 16 scans. (b) FT SERS spectrum of BPY on silver recorded after 100 scans. (c) FT SERS of BPY on Ni subjected to doping with silver (after 100 scans).²¹³

and was the obvious place to start a near-IR FT Raman study. The SERS effect operates very effectively with 1064 nm excitation, with an estimated enhancement factor of 10^6 on silver electrodes.²¹¹ The enhancement factors for pyridine on other metals are expected to be smaller. Figure 69 shows the spectra of pyridine adsorbed onto different metal electrodes. Pyridine has C_{2v} symmetry and thus all its vibrations are Raman active. The strongest bands in the SERS spectra are centered around 1000 cm^{-1} and are due to ring breathing motions of the pyridine molecule. Lewis-coordinated pyridine is not found on copper and gold electrodes, as it is on silver, at any pH, as shown by the absence of a band at 1025 cm^{-1} . Also, Fig. 69

shows that it is possible to record weak but observable SERS spectra from platinum in the near infra-red.

The development of strategies for producing SERS spectra on transition metals other than the main SERS-active metals (Ag, Au, Cu) is of importance in revealing complex interactions between species at various surfaces or interfaces, since many catalytic processes or electrochemical reactions occur on non-coinage metals. Very recently, Xue and Dong^{212,213} reported the application of FT Raman spectroscopy to chemisorption on nickel, which was supposed to be a poor substrate for producing SERS. The FT SERS spectrum was observed on nickel surfaces prepared by doping with silver particles in the chemisorbed layer. As shown in Fig. 70, the silver particles formed by a displacement reaction after Ag^+ ion permeation will probe the bonding and structure of the adsorbed layer originally formed on HNO_3 -etched nickel.²¹² If the silver particles are produced by a direct displacement reaction of Ag^+ on nickel before exposure to adsorbate sample, the SERS experiment can hardly discriminate the adsorption on nickel from that on reduced silver when foreign compounds are deposited. In contrast, the silver doping method described here allows one to recognize the adsorption on nickel by comparison with the SERS spectra from silver. Figure 71 shows the FT Raman spectra of 2,2'-bipyridine (BPY) on nitric-acid-etched silver [Fig. 71(b)] and on nickel-doped silver particles [Fig. 71(c)] along with a normal Raman spectrum of BPY in the solid state [Fig. 71(a)].²¹³ BPY on silver electrodes or silver sols was studied extensively. It has been

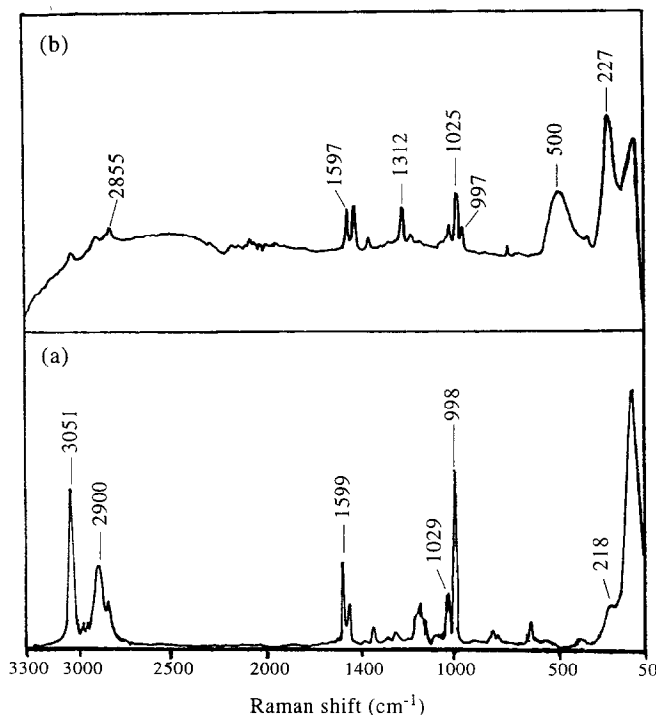


Fig. 72. (a) FT Raman spectrum of a-PS recorded after 200 scans. (b) FT SERS spectrum of a-PS on Ni subjected to doping with silver (100 scans).²¹³

shown that the Raman-active ring breathing mode located at 993 cm^{-1} is sensitive to its chemical environment. The FT SERS of BPY on HNO_3 -etched silver foil [Fig. 71(b)] shows that this band shifted to 1005 cm^{-1} . Should the binding of BPY be through at least one of the nitrogen atom's lone pairs, there would be an enhanced probability that binding will occur through both nitrogen atoms. This would result in a frequency shift of ring modes in the SERS spectrum. In fact, no appreciable frequency shift is observed for ring modes other than the ring breathing mode. The FT SERS spectrum of BPY on silver indicates weak signal intensities of the 1587 , 1570 , 1452 and 1301 cm^{-1} bands due to ring in-plane deformation, or in-plane CH bending modes, when compared with their counterparts at 1587 , 1570 , 1444 and 1299 cm^{-1} in Fig. 71(a), respectively. The strong 1480 cm^{-1} band in Fig. 71(a) is completely lost in Fig. 71(b). It is remarkable that the 855 and 223 cm^{-1} bands attributed to CH out-of-plane wagging and ring out-of-plane deformation, respectively, are retained in Fig. 71(b). The appearance of a strong band at 1392 and 1274 cm^{-1} in the SERS spectrum implies that the presence of the surface has led to a reduction in symmetry and made these Raman-inactive vibration modes (a_u and b_u modes) SERS-active. We propose that the BPY rings are oriented parallel to the surface if the SERS selection rule based on electromagnetic theory is applied. The most notable feature in the FT SERS spectrum of BPY on nickel with doped silver [Fig. 71(c)] is the complete loss of the 1444 cm^{-1} band seen in Fig. 71(a). In addition, the in-plane ring modes between 1600 and 700 cm^{-1} in Fig. 71(c) appear very strong and have shifted considerably. Therefore, the SERS spectrum reveals an adsorption configuration on nickel, showing that BPY interacts uniquely with the surface via σ donation from both 2-position nitrogens, in a standing-up chelating fashion. The bands observed at 233 and 491 cm^{-1} are assigned to Ni–N stretching and Ni–O stretching of nickel oxide, respectively. In particular, we would like to mention that the signal intensity of the 1025 cm^{-1} band in Fig. 71(c) is about one-fifth that of its counterpart in Fig. 71(b), indicating that enhancement on nickel is weaker than that on silver.

The FT SERS technique for probing the adsorption layer on nickel can be extended to polymeric coatings. Figure 72(a) shows the FT Raman spectrum of atactic polystyrene (a-PS). The 3051 , 2900 , 1599 and 998 cm^{-1} bands are ascribed to phenyl ring CH stretching, backbone CH stretching, ring stretching and ring breathing, respectively. The FT SERS spectrum of a-PS adsorbed on nickel followed by doping with silver, shown in Fig. 72(b), illustrates the Ni–O band at 500 cm^{-1} . The strong broad band near 227 cm^{-1} , corresponding to the 218 cm^{-1} band in Fig. 72(a), is attributed to ring-C _{α} out-of-plane bending. The ring breathing at 997 cm^{-1} and ring in-plane deformation at 618 cm^{-1} are very weak in Fig. 72(b), indicating that phenyl rings are oriented parallel to the surface.²¹³

The SERS effect has been demonstrated to work well using 1064 nm exciting radiation, and excellent quality spectra have been obtained using FT Raman instrumentation. Experiments on electrodes, colloids and HNO_3 -etched metals have been very successful, and it will presumably be only a matter of time before this technique is applied to studies of polymer coatings or polymer/metal interfaces. One very clear advantage which FT Raman SERS experiments have over their conventional visible counterparts is speed. The SERS spectra are so strong that very acceptable spectra can be obtained with just a few scans of the interferometer, taking much less than 30 s , whereas comparable measurements using a scanning monochromator require many minutes. This has a number of important implications. Firstly, it is possible to perform electrode kinetics experiments if the reaction is not too fast. Secondly, it has been often observed that photochemical degradation reactions occur for polymer coatings on metals with visible lasers.

With FT Raman, not only is the photon energy lower but the measurement time is very much less, so this problem can be largely eliminated. To date all of the FT Raman SERS spectra obtained have been excited using an Nd:YAG laser. As the SERS enhancement is a function of excitation wavelength, an FT Raman spectrometer fitted with a tunable near-IR laser would make a very powerful tool in SERS research, and would allow spectra to be obtained from the surfaces of metals other than Cu, Ag and Au.

6. CONCLUDING REMARKS

This review was intended to show how laser Raman spectroscopy has increasingly contributed to the elucidation of polymeric structure since the introduction of the near infra-red laser excited Fourier transform Raman technique. In a number of studies to date, recent developments in FT Raman spectroscopy, the near-IR resonance Raman effect, and FT surface-enhanced Raman scattering have made it possible to record fluorescence-free spectra from synthetic polymers and biomaterials and have brought about tremendous enhancements in Raman intensity, generating much excitement both in the academic community and in the industrial laboratory.

However, there will be a great need for further developments in instrumentation, such as laser sources, filters and detectors, to improve sensitivity.

There is an inherent drawback in reviewing such a vast amount of literature that it is nearly impossible to attain completeness. The reader is therefore reminded at the end of this review that emphasis has been placed primarily on applications of, and recent developments in, FT Raman spectroscopy rather than in particular theoretical details.

ACKNOWLEDGEMENTS

The author would like to express his thanks to all his co-workers for their fruitful and kind collaborations. He is very grateful to Professor Otto Vogl, Polytechnic University, Brooklyn, NY, USA and Professor Fu Sie, Institute of Chemistry, Academia Sinica, Beijing, People's Republic of China for their recommendations.

REFERENCES

1. J. L. Koenig, *Spectroscopy of Polymers*, American Chemical Society, Washington, DC (1992).
2. G. Xue, *Prog. Polym. Sci.*, **19**, 317–388 (1994).
3. G. W. Chantry, H. A. Gebbie and C. Hilsum, *Nature*, **203**, 1052 (1964).
4. D. B. Chase, and T. Hirschfeld, *Appl. Spectrosc.*, **40**, 133 (1986).
5. D. B. Chase, *J. Am. Chem. Soc.*, **108**, 7485 (1986).
6. V. M. Hallmark, C. G. Zimba, J. D. Swalen and F. Rabolt, *Spectrosc.*, **2**, 40 (1987).
7. D. B. Chase, *J. Am. Chem. Soc.*, **108**, 7485 (1986).
8. S. F. Parker, K. P. J. Williams, P. J. Hendra and A. J. Turner, *Appl. Spectrosc.*, **42**, 796 (1988).
9. C. G. Zimba, V. M. Hallmark, J. D. Swalen and J. F. Rabolt, *Appl. Spectrosc.*, **41**, 721 (1987).
10. B. Chase, *Anal. Chem.*, **59**, 881A (1987).
11. F. J. Purcell, *Spectrosc.*, **4** (2), 24 (1989).
12. F. J. Bergin and H. F. Shurvell, *Appl. Spectrosc.*, **43**, 516 (1989).
13. S. Nie, L. G. Marzilli and N.-T. Yu, *J. Am. Chem. Soc.*, **111**, 9256 (1989).
14. E. N. Lewis, V. F. Kalasinsky and I. W. Levin, *Appl. Spectrosc.*, **42**, 1188 (1988).
15. D. S. Schwab and R. L. McCreery, *Anal. Chem.*, **56**, 2199 (1984).

16. D. L. Gerrard, *Chem. Br.*, **20**, 728 (1984).
17. F. J. Bergin and H. F. Shurvell, *Appl. Spectrosc.*, **43** (3), 516 (1989).
18. P. B. Fellgett, *Infrared Phys.*, **24**, 95 (1984).
19. P. B. Fellgett, *J. Opt. Soc.*, **67**, 419 (1977).
20. R. H. Norton and R. Beer, *J. Opt. Soc.*, **66**, 259 (1976).
21. R. J. Anderson and P. R. Griffiths, *Anal. Chem.*, **47**, 2339 (1975).
22. S. F. Parker, *Spectrochim. Acta*, **50A** (11), 1841 (1994).
23. S. F. Parker, Y. Patel, P. B. Tooke and K. P. J. Williams, *Spectrochim. Acta*, **47A**, 1171 (1991).
24. P. J. Hendra, P. Le Barazer and A. Crookell, *J. Raman Spectrosc.*, **20**, 35 (1989).
25. P.R. Griffiths and J. A. de Haseth, *Fourier Transform Infrared Spectroscopy*, Wiley Interscience, New York (1986).
26. S. F. Parker, N. Cotton and V. Patel, *Spectrochim. Acta*, **49A**, 657 (1993).
27. R. J. Bell, *Introductory Fourier Transform Spectroscopy*, Academic Press, London (1972).
28. L. Mertz, *Infrared Phys.*, **7**, 17 (1967).
29. M. L. Forman, W. H. Steele and G. A. Vanasse, *J. Opt. Soc. Am.*, **56**, 59 (1966).
30. J. Chamberlain, *The Principles of Interferometric Spectroscopy*, Wiley Interscience, Chichester (1979).
31. J. W. Cooley and J. W. Tukey, *Math. Comput.*, **19**, 297 (1965).
32. E. O. Brigham, *The Fast Fourier Transform*, Prentice Hall, New Jersey (1974).
33. P. R. Griffiths, *Chemical Infrared Fourier Transform Spectroscopy*, Wiley, New York (1974).
34. P. Hendra, C. Jones and G. Warnes, *Fourier Transfrom Raman Spectroscopy Instrumentation and Chemical Applications*, Ellis Horwood, New York (1991).
35. D. J. Cutler, H. M. Mould and B. Bennett, *J. Raman Spectrosc.*, **23**, 367 (1991).
36. C. J. Petty, G. M. Warnes, P. J. Hendra and M. Judkins, *Spectrochim. Acta*, **47A**, 1179 (1991).
37. T. Hirschfeld and B. Chase, *Appl. Spectrosc.*, **40**, 133 (1986).
38. H. Graener and A. Laubereau, *Opt. Commun.*, **54**, 141 (1985).
39. R. Signer and J. Weiler, *Helv. Chim. Acta*, **15**, 649 (1932).
40. J. L. Koenig, *Appl. Spectrosc. Rev.*, **4**, 233 (1971).
41. D. L. Gerrard and W. F. Maddams, *App. Spectrosc. Rev.*, **22**, 251 (1986).
42. B. Schrader, *Angew. Chem. Int. Edn*, **12**, 884 (1973).
43. K. P. J. Williams and S. M. Mason, *Spectrochim. Acta*, **46A**, 187 (1990).
44. G. Ellis, P. J. Hendra, C. M. Hodges, T. Jawhari, C. H. Jones, P. Le Barazer, C. Passingham, I. A. M. Royaud, A. Sanchez-Blasquez and G. M. Warnes, *The Analyst*, **114**, 1061 (1989).
45. D. Bourgeois and S. P. Church, *Spectrochim. Acta*, **46A**, 295 (1990).
46. D. J. Cutler, *Spectrochim. Acta*, **46A**, 131 (1990).
47. K. P. J. Williams and S. M. Mason, *Spectrochim. Acta*, **46A**, 187 (1990).
48. D. K. Veirs, J. W. Ager and G. M. Rosenblatt, *Proc. 12th Conf. Raman Spectrosc.*, p. 898, Wiley, New York (1990).
49. J. K. Agbenyega, G. Ellis, P. J. Hendra, W. F. Maddams, C. Passingham and H. A. Willis, *Spectrochim. Acta*, **46A**, 197 (1990).
50. J. G. Grasselli, M. K. Snavely and B. J. Bulkin, *Chemical Applications of Raman Spectroscopy*, Wiley, New York (1981).
51. F. T. Walder and M. J. Smith, *Spectrochim. Acta*, **47A**, 1201 (1991).
52. J. M. Dudik, C. R. Johnson and S. A. Asher, *J. Phys. Chem.*, **89**, 3805 (1985).
53. T. G. Spiro, in *Chemical and Biochemical Applications of Lasers* (C.B. Moore, Ed.), Academic Press, New York (1974).
54. R. J. H. Clark and R. E. Hester (Eds), *Advances in Infrared and Raman Spectroscopy*, Vol. 1, Heyden, London (1975).
55. E. J. Zeman, K. T. Carron, G. C. Schatz and R. P. van Duyne, *J. Chem. Phys.*, **87** (7), 4189 (1987).
56. D. A. Weitz, S. Garoff, J. I. Gersten and A. Nitzan, *J. Chem. Phys.*, **78** (9), 5324 (1983).
57. R. J. Young, *China-UK Bilateral Conference on Polymer Science*, Beijing, China, 15-19 April 1992.
58. R. J. Young and P. P. Ang, in *Interfacial Phenomena in Composites Materials '91* (I. Verpoest and F. R. Jones, Eds), Butterworth-Heinemann Ltd, Oxford (1991).
59. W. F. Lewis and D. N. Batchelder, *Chem. Phys. Lett.*, **60**, 232 (1979).

60. C. Galiotis, Ph.D. Thesis, University of London (1982).
61. D. N. Batchelder and D. Bloor, in *Advances in Infrared and Raman Spectroscopy* (R. J. H. Clark and R. E. Hester, Eds), Vol. II, Wiley Heydon, Chichester (1983).
62. C. Galiotis, R. J. Young, P. H. J. Young and D. N. Batchelder, *J. Mater. Sci.*, **19**, 3640 (1984).
63. I. M. Robinson, R. J. Young, C. Galiotis and D. N. Batchelder, *J. Mater. Sci.*, **22**, 3642 (1987).
64. D. Hull, *An Introduction to Composite Materials*, Cambridge University Press, Cambridge (1981).
65. I. M. Robinson, C. Galiotis, D. N. Batchelder and R. J. Young, *J. Mater. Sci.*, **26**, 2293 (1991).
66. M. Takayanagi, in *High Modulus Polymers and Composites* (C. L. Choy, Ed.), The Chinese University Press, Hong Kong (1985).
67. W. F. Hwang, D. R. Wiff, C. L. Benner and T. E. Helminiak, *J. Macromol. Sci., Phys.*, **B22**, 231 (1983).
68. S. J. Krause, T. Haddock, G. E. Price, P. G. Lenhert, J. F. O'Brien, T. E. Helminiak and W. W. Adams, *J. Polym. Sci., Polym. Phys. Edn.*, **B24**, (1986, 1991).
69. S. J. Krause, T. B. Haddock, G. E. Price and W. W. Adams, *Polymer*, **29**, 195 (1988).
70. R. J. Young, R. J. Day and P. P. Ang, *Polym. Commun.*, **31**, 47 (1990).
71. D. N. Batchelder and D. Bloor, *J. Polym. Sci., Polym. Phys. Edn.*, **17**, 569 (1979).
72. S. van der Zwaag, M. G. Northolt, R. J. Young, I. M. Robinson, C. Galiotis and D. N. Batchelder, *Polym. Commun.*, **28**, 276 (1987).
73. I. M. Robinson, R. J. Day, M. Zakikhani and R. J. Young, *Polymer*, **28**, 1833 (1987).
74. C. Galiotis, I. M. Robinson, D. N. Batchelder and R. J. Young, in *Engineering Application of New Composites* (S. A. Paipetis and G. C. Papanicolaou, Eds), Omega Scientific, Wallingford, UK (1988).
75. R. J. Young, R. J. Day and P. P. Ang, *Polym. Commun.*, **31**, 47 (1990).
76. G. V. Fraser, P. J. Hendra, D. S. Watson, M. J. Gall, H. A. Willis and M. E. A. Cudby, *Spectrochim. Acta*, **29A**, 1525 (1973).
77. H. W. Siesler and K. Holland-Monitz, *Infrared and Raman Spectroscopy of Polymers*, Marcel Dekker, New York (1980).
78. D. L. Gerrard and W. F. Maddams, *Appl. Spectrosc. Rev.*, **22**, 251 (1986).
79. G. R. Strobl and W. Hagedorn, *J. Polym. Sci., Polym. Phys. Edn.*, **16**, 1181 (1978).
80. W. F. Maddams and I. A. M. Royaud, *Spectrochim. Acta*, **46A**, 747 (1990).
81. L. A. Hanna, P. J. Hendra, H. A. Willis, V. Zichy, M. E. A. Cudby and W. Maddams, *Polymer*, **29**, 180 (1988).
82. J. K. Agbenyega, G. Ellis, P. J. Hendra, W. F. Maddams, C. Passingham, H. A. Willis and J. Chalmera, *Spectrochim. Acta*, **46A**, 197 (1990).
83. D. I. Bower and W. F. Maddams, *The Vibratioal Spectroscopy of Polymers*, Cambridge Solid State Science Series, Cambridge University Press, Cambridge (1989).
84. C. H. Jone and P. J. Hendra, *Proc. European Symp. Polym. Spectrosc. Cologne*, (1990).
85. J. L. Koenig and F. J. Boerio, *J. Chem. Phys.*, **50**, 2829 (1969).
86. G. Ellis, C. Marco, M. A. Gomez, J. G. Fatou and R. C. Haddon, *Polym. Bull.*, **25**, 351 (1991).
87. G. Ellis, J. Lorente, C. Marco, M. A. Gomez, J. G. Fatou and P. J. Hendra, *Spectrochim. Acta*, **47A**, 1353 (1991).
88. A. J. Heeger, S. Kivalson, J. R. Schrieffer and W. P. Su, *Rev. Mod. Phys.*, **60**, 781 (1988).
89. Y. Furukawa, H. Ohta, A. Sakamoto and M. Tasumi, *Spectrochim. Acta*, **47A**, 1367 (1991).
90. S. Krichene, S. Lefrant, G. Froyer, F. Maurice and Y. Pelous, *J. Phys. Colloq.*, **44**, C3–733 (1983).
91. S. Lefrant, J. P. Buisson and H. Eckardt, *Synth. Met.*, **37**, 91 (1990).
92. G. Zannoni and G. Zerbi, *J. Chem. Phys.*, **82**, 31 (1985).
93. S. Krichene, J. P. Buisson and S. Lefrant, *Synth. Met.*, **17**, 589 (1987).
94. I. Harada, Y. Furukawa, M. Tasumi, H. Shirakawa and S. Ikeda, *J. Chem. Phys.*, **73**, 4746 (1980).
95. T. C. Chung, F. Moraes, J. D. Flood and A. J. Heeger, *Phys. Rev.*, **B29**, 2341 (1984).
96. P. J. Hendra, W. F. Maddams, I. A. M. Royaud, H. A. Willis and V. Zichy, *Spectrochim. Acta*, **46A**, 747 (1990).
97. W. F. Maddams and I. A. M. Royaud, *Spectrochim. Acta*, **47A**, 1327 (1991).
98. S. B. Hansen, D. H. Christensen and O. F. Nielsen, *Spectrochim. Acta*, **49A**, 769 (1993).

99. J. M. Espinosa, D. H. Christensen, G. O. Sørensen and O. F. Nielson, *Spectrochim. Acta*, **47A**, 1423 (1991).
100. P. Schmidt and P. J. Hendra, *Spectrochim. Acta*, **50A**, 1999 (1994).
101. D. J. Blundell and B. N. Osborn, *Polymer*, **24**, 953 (1983).
102. J. M. Chalmers, W. F. Gaskin and M. W. Machenzie, *Polym. Bull.*, **11**, 433 (1990).
103. J. D. Louden, *Polym. Commun.*, **27**, 82 (1988).
104. N. J. Everall, J. Lumsden, J. M. Chalmers and N. Mason, *Spectrochim. Acta*, **47A**, 1305 (1991).
105. B. J. Briscoe, B. H. Stuart and S. Rostami, *Spectrochim. Acta*, **49A**, 753 (1993).
106. S. B. Hansen, D. H. Christensen and O. F. Nielsen, *Spectrochim. Acta*, **49A**, 769 (1993).
107. B. H. Stuart and B. J. Briscoe, *Spectrochim. Acta*, **50A**, 2005 (1994).
108. K. Kurosaki, *Int. Polym. Sci. Technol.*, **15**, 601 (1988).
109. S. W. Cornell and J. L. Koenig, *Macromolecules*, **2**, 540 (1968).
110. S. W. Cornell and J. L. Koenig, *Macromolecules*, **2**, 546 (1969).
111. K. D. O. Jackson, M. J. R. Loadman, C. H. Jones and G. Ellis, *Spectrochim. Acta*, **46A**, 217 (1990).
112. T. Hirschfeld and B. Chase, *Appl. Spectrosc.*, **40**, 133 (1986).
113. S. J. Bunce, H. G. M. Edwards, A. F. Johnson, I. R. Lewis and P. H. Turner, *Spectrochim. Acta*, **49A**, 775 (1993).
114. P. J. Hendra and K. D. O. Jackson, *Spectrochim. Acta*, **50A**, 1987 (1994).
115. N. W. Schlotter and J. F. Rabolt, *Polymer*, **25**, 146 (1984).
116. D. Bower and W. Maddams, *Vibrational Spectra of Polymers*, Cambridge University Press, Cambridge (1992).
117. G. Ellis, M. Claybourn and S. E. Richard, *Spectrochim. Acta*, **46A**, 227 (1990).
118. L. M. Briggs, D. R. Banes and R. O. Cater, *Int. Eng. Chem. Res.*, **26**, 667 (1987).
119. J. K. Agbenyega, G. Ellis, P. J. Hendra, W. F. Maddams, C. Passingham, H. A. Willis and J. Chalmers, *Spectrochim. Acta*, **46A**, 197 (1990).
120. T. Jawhari, Ph.D. Thesis, University of Southampton, (1989).
121. M. Fleishman, P. J. Hendra and A. J. McQuillian, *Chem. Phys. Lett.*, **26**, 163 (1974).
122. R. P. van Duyne, *J. Phys. Colloq.*, **C5-38 (11)**, 2393 (1977).
123. D. L. Jeanmarie and R. P. van Duyne, *J. Electroanal. Chem.*, **84**, 1 (1977).
124. F. J. Boerio, W. H. Tsai, P. P. Hong and G. Montaudo, *Macromolecules*, **22**, 3955 (1989).
125. G. Xue, J. Din and M. Zhang, *Chinese Sci. Bull.*, **36 (16)**, 1339 (1991).
126. J. C. Tsang and J. Kirtley, *Solid State Commun.*, **36**, 617 (1979).
127. J. Cipriani R. Racine, R. Dupeyrat, H. Hasmonay, M. Dupeyrat, Y. Levy and C. Imbert, *Opt. Commun.*, **11**, 70 (1974).
128. M. L. Howe, K. L. Watters and R. G. Greenler, *J. Phys. Chem.*, **80**, 582 (1976).
129. D. L. Allara, A. Baca and C. A. Pyrde, *Macromolecules*, **11**, 1215 (1978).
130. J. F. Rabolt, R. Santo and J. D. Swalen, *Appl. Spectrosc.*, **33 (6)**, 549 (1979).
131. D. Bloor, R. Chance and M. Nighars, *Polydiacetylenes*, Proceedings of a NATO Conference, Boston, MA (1984).
132. B. Tieke and J. Weiss, *J. Colloid Interface Sci.*, **101**, 128 (1984).
133. R. Burzynski, P. N. Prasad, J. Biegajski and D. A. Cadenhead, *Macromolecules*, **19**, 1059 (1986).
134. C. G. Zimba, S. Turrell, J. P. Swalen, V. M. Hallmark and J. F. Rabolt, *J. Phys. Chem.*, **94**, 939 (1990).
135. R. Iwamoto, M. Miya, K. Ohta and S. Mima, *J. Chem. Phys.*, **74**, 4780 (1981).
136. D. L. Gerrard and W. F. Maddams, *Appl. Spectrosc.*, **22**, 251 (1986).
137. K. P. J. Williams and S. M. Mason, *Spectrochim. Acta*, **46A**, 187 (1990).
138. J. Clarkson, S. M. Mason and K. P. J. Williams, *Spectrochim. Acta*, **47A**, 227 (1991).
139. J. K. Agbenyega, G. E. Ellis, P. J. Hendra, W. F. Maddams, C. Passingham, H. A. Willis and J. Chalmers, *Spectrochim. Acta*, **46A**, 295 (1990).
140. C. J. de Bakker, G. A. George, N. A. St John and P. M. Fredericks, *Spectrochim. Acta*, **49A**, 739 (1993).
141. J. Goral and V. Zichy, *Spectrochim. Acta*, **46A**, 253 (1990).
142. D. Gani, P. J. Hendra, W. F. Maddams, C. Passingham, I. A. M. Royaud, H. A. Willis and V. Zichy, *Analyst*, **1990**, **115**, 1313.

143. P. J. Hendra, C. Passingham and I. A. M. Royaud, *Proc. Twelfth Int. Conf. on Raman Spectroscopy*, Columbia, South Carolina (J. R. During and J. F. Sullivan, Eds), p. 678, Wiley, New York (1990).
144. V. Hallmark and J. F. Rabolt, *Macromolecules*, **22**, 500 (1989).
145. R. W. Williams, J. O. McIntyre, B. P. Gaber and S. J. Fleischer, *Biol. Chem.*, **261**, 14520 (1986).
146. B. Fanconi, *Biopolymers*, **12**, 2759 (1971).
147. T. A. Mattioli, A. Hoffmann, D. G. Sockalingum, B. Schrader, B. Robert and M. Lutz, *Spectrochim. Acta*, **49A**, 785 (1993).
148. P. J. Hendra, *Spectrochim. Acta*, **47A**, 1135 (1991).
149. J. Sawatzki, R. Fischer, H. Scheer and F. Siebert, *Proc. Nat. Acad. Sci. U.S.A.*, **87**, 5903 (1990).
150. B. Schrader, A. Hoffmann and S. Keller, *Spectrochim. Acta*, **47A**, 1135 (1991).
151. C. N. Hunter, R. van Grondelle and J. D. Olsen, *TIBS*, **14**, 72 (1989).
152. B. Robert and M. Lutz, *Biochim. Biophys. Acta*, **307**, 10 (1985).
153. T. A. Mattioli, A. Hoffmann, B. Robert, B. Schrader and M. Lutz, *Biochemistry*, **30**, 4648 (1991).
154. J. Cogdell and J. P. Thornber, *FEBS Lett.*, **122**, 1 (1980).
155. K. Iwata, H. Hayashi and M. Tasumi, *Biochim. Biophys. Acta*, **810**, 269 (1985).
156. M. Lutz, in *Advances in Infrared and Raman Spectroscopy* (R.J.H. Clark and R.E. Hester, Eds), Vol. 1, p. 211, Wiley, New York (1984).
157. R. H. Atalla, *J. Wood Chem. Technol.*, **7**, 115 (1987).
158. S. N. Katrina, L. Bergbauer, J. J. Ho, J. F. R. Kuck Jr. and N. Yu, *Spectrosc.*, **24**, 24 (1990).
159. R. G. Messerschmidt and D. B. Chase, *Appl. Spectrosc.*, **43**, 11 (1989).
160. R. C. Kenton and R. L. Rubinovitz, *Appl. Spectrosc.*, **44**, 1377 (1990).
161. I. R. Lewis, N. W. Daniel Jr, N. C. Chaffin and P. R. Griffiths, *Spectrochim. Acta*, **50A**, 1943 (1994).
162. K. W. Thornton, in *Systems and Control Encyclopedia*, (M.G. Singh, Ed.), Pergamon Press, New York (1987).
163. H. G. M. Edwards, D. W. Farwell and A. C. Williams, *Spectrochim. Acta*, **50A**, 807 (1994).
164. I. W. Levin and E. N. Lewis, *Anal. Chem.*, **62**, 1101 (1990).
165. I. W. Levin and E. N. Lewis, *SPIE (Fourier Transform Spectroscopy)*, **1145**, 602 (1989).
166. E. N. Lewis, M. T. Devin and I. W. Levin, *SPIE (Fourier Transform Spectroscopy)*, **1145**, 99 (1989).
167. S. Nie, K. L. Bergbauer, J. F. R. Kuck Jr and N. T. Yu, *Exp. Eye Res.*, **51**, 619 (1990).
168. P. C. Rigg and B. W. Barry, *J. Invest. Dermatol.*, **94**, 235 (1990).
169. J. B. Robert, *J. Toxicol. Cut Ocular Toxicol.*, **5**, 319 (1986).
170. B. W. Barry, A. C. Williams and H. G. M. Edwards, *Spectrochim. Acta*, **49A**, 801 (1993).
171. R. P. Rava, J. J. Baraga and M. S. Feld, *Spectrochim. Acta*, **47A**, 509 (1991).
172. S. Y. Ng, D. U. H. Penhale and J. Heller, *Macromol. Syn.*, **11**, 23 (1992).
173. J. Heller, *J. Control. Rel.*, **2**, 167 (1985).
174. A. M. Tudor, C. Jones and G. Warnes, *Fourier Transform Raman Spectroscopy, Instrumentation and Chemical Applications*, Ellis Horwood, Chichester (1991).
175. A. M. Tudor, C. D. Melia, M. C. Davies, S. J. Church and J. Heller, *Spectrochim. Acta*, **49A**, 759 (1993).
176. H. Sadeghi-Jorabchi, P. J. Hendra, R. H. Wilson and P. S. Belton, *JAOCs*, **67**, 483 (1990).
177. M. Fleishman, P. J. Hendra and A. J. McQuillan, *Chem. Phys. Lett.*, **26**, 163 (1974).
178. R. P. van Duyne, *J. Phys. Colloq.*, **C5-38 (11)**, 2393 (1977).
179. D. L. Jeanmarie and R. P. van Duyne, *J. Electroanal. Chem.*, **84**, 1 (1977).
180. F. J. Boerio, W. H. Tsai, P. P. Hong and G. Montaudo, *Macromolecules*, **22**, 3955 (1989).
181. G. Xue, J. Din and M. Zhang, *Chinese Sci. Bull.*, **36 (16)**, 1339 (1991).
182. R. K. Chang and T. E. Furtak (Eds), *Surface Enhanced Raman Scattering*, Plenum, New York (1982).
183. R. P. Albrecht and J. A. Creighton, *J. Am. Chem. Soc.*, **99**, 5215 (1977).
184. R. P. van Duyne, in *Chemical and Biochemical Applications of Lasers* (C. B. Moore, Ed.), Vol. 4, pp. 101-105, Academic Press, New York (1979).
185. T. E. Furtak and D. Roy, *Phys. Rev. Lett.*, **50**, 1301 (1983).
186. C. Pettenkofer, J. Eickmans, U. Erturk and A. Otto, *Surf. Sci.*, **151**, 9 (1985).
187. G. Xue and J. Dong, *Anal. Chem.*, **63 (20)**, 2393 (1991).

188. T. Vo-Dinh, M. Hiromoto, G. Begun and R. Moody, *Anal. Chem.*, **56**, 1667 (1984).
189. J. P. Goudenned, G. Begun and E. Arakawa, *Chem. Phys. Lett.*, **92**, 197 (1982).
190. M. Meier, A. Wokaun and T. Vo-Dinh, *J. Chem. Phys.*, **89**, 1843 (1985).
191. D. W. Boo, W. S. Oh, M. S. Kim, K. Kim and H. Lee, *Chem. Phys. Lett.*, **120** (3), 301 (1985).
192. G. Xue, J. Dong and M. Zhang, *Appl. Spectrosc.*, **45** (15), 756 (1991).
193. G. Xue, Y. Lu and J. Gao, *Polymer*, **35** (14), 3127 (1994).
194. G. Xue, Y. Lu and J. Zhang, *Macromolecules*, **27**, 809 (1994).
195. S. K. Miller, A. Baiker, M. Meier and A. Wokaun, *J. Chem. Soc., Faraday Trans.*, **80**, 1305 (1984).
196. K. T. Caron, G. Xue and M. L. Lewis, *Langmuir*, **7**, 2 (1991).
197. S. Garoff, R. B. Stephens, C. D. Hanson and G. K. Sorenson, *Opt. Commun.*, **41**, 257 (1982).
198. A. Crookell, M. Fleischmann, M. Hanniet and P. J. Hendra, *Chem. Phys. Lett.*, **149** (2), 123 (1988).
199. C. J. Sandroff and D. R. Herschhach, *J. Phys. Chem.*, **86**, 3277 (1982).
200. D. A. Weitz and S. Garoff, *J. Chem. Phys.*, **78**, 5324 (1983).
201. F. J. Boerio and W. H. Tsai, *J. Polym. Sci. Part B, Polym. Phys.*, **27**, 1017 (1989).
202. D. L. Allara, C. A. Murray and S. Bodoff, in *Physicochemical Aspects of Polymer Surfaces* (K. L. Mittal, Ed.), Vol. 1, p. 33, Plenum Press, New York (1983).
203. P. C. Lee and D. Meisel, *Chem. Phys. Lett.*, **99**, 262 (1983).
204. J. S. Suh and K. H. Michaelian, *J. Raman Spectrosc.*, **18**, 409 (1987).
205. A. Otto, *Surf. Sci.*, **57**, L392 (1978).
206. J. C. Tsang, J. E. Demuth, P. N. Sanda and J. R. Kirtley, *Chem. Phys. Lett.*, **76**, 54 (1980).
207. P. G. Roth and F. J. Boerio, *J. Polym. Sci. Part B, Polym. Phys.*, **25**, 1923 (1987).
208. R. S. Venkatachalam, F. J. Boerio, P. G. Roth and W. H. Tsai, *J. Polym. Sci. Part B, Polym. Phys.*, **26**, 2447 (1988).
209. G. Xue, J. Dong and J. Zhang, *Macromolecules*, **24**, 4195 (1991).
210. D. B. Chase and B. A. Parkinson, *Appl. Spectrosc.*, **42** (7), 1186 (1988).
211. S. M. Angel, L. F. Katz, D. D. Archibald, L. T. Lin and D. E. Honigs, *Appl. Spectrosc.*, **42** (8), 1327 (1988).
212. J. Dong, Z. Sheng and G. Xue, *Chem. Phys. Lett.*, **231**, 183 (1994).
213. J. Dong, Z. Sheng and G. Xue, *Spectrochim. Acta.*, **51A**, 1031 (1995).